THE CRYSTAL STRUCTURE OF ZUNYITE

Thesis by

W. Barclay Ray

In Partial Fulfillment of the Requirements

For the Degree of

Doctor of Philosophy

California Institute of Technology

Pasadena, California

1956

ACKNOWLEDGMENTS

It is a pleasure to thank Professor Linus Pauling for providing the opportunity to carry out this study under his guidance, and for his interest and help in the progress of the work. I am grateful to Dr. E. W. Hughes for instruction and assistance in X-ray crystallography, and for supervision of the detailed procedure of structural refinement. The Division of Geologic Sciences has kindly allowed this study to be carried out under Professor Pauling's direction. I am indebted to the Corning Glass Works Foundation for the Corning Glass Works Foundation Fellowship under which I have carried out this study. I wish to thank Mr. William C. Miller for valuable help in the preparation of illustrations for this thesis, and Mr. Ronald L. Shreve for untiring aid in editing the manuscript.

ABSTRACT

Zunyite, a rare aluminosilicate mineral of composition $(OH, F)_{18}Al_{13}Si_5O_{20}Cl$, has an unusual structure built up of Si_5O_{16} groups of linked silicon tetrahedra and aluminium-oxygen groups of linked octahedra. The structure proposed by Pauling is verified and refined by X-ray methods, using 163 (hkO) reflections from single-crystal photographs with Mo Kα radiation. Refinement of positional parameters is carried out by the least-squares method, with inclusion of off-diagonal terms in the normal equation matrix because of overlap of oxygen atoms in the (100) projection. Refinement of isotropic temperature parameters for separate atoms is carried out with the use of difference syntheses, by methods differing somewhat from published ones. A general discussion of isotropic temperature factor refinement from differerence syntheses is given. One stage of least-squares refinement using 410 (hhl) reflections is carried out, for comparison with the (hkO) refinement. The corresponding accuracy of interatomic distances is $\pm$ 0.02 Å. A large apparent temperature factor discrepancy between the two refinements is attributed to a deviation in the contrast of one of the X-ray photographs. The refined structure differs from the trial structure in distortion of coordination polyhedra, as found in other similar structures. The arrangement of protons in the structure is proposed from structural arguments, and the proposed arrangement requires the inclusion of at least two fluorine atoms per stoichiometric molecule.

TABLE OF CONTENTS

I. INTRODUCTION

The study of crystals by means of X-rays has introduced new order and understanding into mineralogy. Before X-rays were used, minerals could be described only by variable and sometimes intangible physical properties, and could be classified only on the basis of uncertain and frequently disputed chemical formulae, whose relationships to the physical properties were at best conjectural. This was especially true in the mineralogy and chemistry of silicates, whose complex structures allow a great variety of substitutions of one element by others. The X-ray techniques introduced by W. H. and W. L. Bragg, with their discovery in 1913 of the diamond and rock salt structures, were developed and strengthened by application to crystals of simple composition in the early days of X-ray crystallography, and then, beginning in the 1920's, were turned upon the complicated silicate structures. From this study came the idea that the silicate minerals group themselves naturally into several large classes, according to the broad plans of their structure, and that the structural plan of a silicate mineral largely determines its properties and hence its role in chemical processes - an idea that has been widely and fruitfully applied in geology.

Aberrant from the large and well-known classes of silicate minerals are a few rare species of relatively little geologic interest but of definite significance crystallographically, because of the unusual features of their structures. One of these is the aluminosilicate mineral zunyite, whose structure is of a type

unknown for any other substance. This unusual structure was proposed by Pauling in 1933. Professor Pauling showed that the proposed structure accounted well for the size of the unit cell and the intensities of X-ray reflections from crystals of the mineral; but the X-ray diffraction techniques available at the time were not capable of subjecting so complicated a structure to a systematic study that would prove beyond any reasonable doubt that its atoms were arranged in the proposed way, and that could use the X-ray data to determine the most probable atomic positions. Although the crystallographic world has not hesitated in general to accept results of the stochastic method of discovering crystal structures, some skepticism about the zunyite structure has prevailed, due perhaps to the complexity of the proposed structure and to the fact that Professor Pauling proposed not only the structure for the mineral but also its chemical formula, which was also in dispute. W. L. Bragg may have regarded the structure as speculative, for he did not include it in his celebrated book The Atomic Structure of Minerals.

During the last fifteen years powerful new methods have been developed for the study of complicated crystal structures. In view of the unique features of the proposed structure, it has been desirable to reinvestigate zunyite to see whether the structure can be established according to modern crystallographic standards. This thesis presents the results of such a study. The correctness of the atomic arrangement proposed by Professor Pauling has been verified, and all atoms in the crystal, with the exception of hydrogen, have been located to within a probable

accuracy of a hundredth of an Ångström.

Although, therefore, this thesis presents no essentially new facts about the atomic arrangement in silicate minerals, the results of this study have made it possible to consider the unusual zunyite structure in a detailed way that was not possible before its verification and refinement. At the present stage of progress in research in the field of silicate structural chemistry, most of the problems of greatest interest concern structural details in substances whose general atomic arrangement is already known, and interpretation of these details in terms of the physical and chemical properties of the materials and their possible application to geologic and other problems. The recent intensive work on the structures of the feldspars is a good example of this.

In keeping with the spirit of this attack on structural problems, we have endeavored to carry the present study as far toward interpretation of the geologic role of zunyite as known data permit, although, of course, our main concern has been strictly structural. The very rarity of zunyite is indication of the special geologic setting of its occurrences, and of the very special conditions in the earth which must have produced it. Our study has made it possible, we believe, to outline these conditions with considerable confidence.

But the bulk of this thesis will be devoted to derivation and interpretation of accurate atomic positions. After surveying briefly the development of ideas on the composition and structure of zunyite, we will present the X-ray data used in this investigation, and then turn to the procedure of testing and refining the proposed structure by means of least squares and difference synthesis methods.

It will be shown that the atomic parameters obtained can be relied on to ± 0.001, and interatomic distances to ± 0.02 Å. By use of the refined distances, a number of features of interest in the structure can be considered in detail, and in particular a satisfactory arrangement of the protons in the structure can be postulated.

II. HISTORICAL SKETCH

Zunyite was discovered in ores of the Zuñi Mine, on Anvil Mountain, near Silverton, San Juan County, Colorado. It was first described by W. F. Hillebrand in 1883 as occurring as hard, small, clear, isotropic, perfectly developed tetrahedral crystals imbedded in a matrix of another previously unknown mineral, the sulfarsenide of lead, guitermanite. Hillebrand had available only two small samples of the fresh zunyite-guitermanite rock, although he had in addition a quantity of cloudy to opaque white, porcelain-like, partially altered crystals. He analyzed the crystals chemically, but was obliged to use the partially altered material for his analyses. The analyses are given in Appendix I, together with all other published analyses of zunyite. Hillebrand assigned the empirical formula $R_{18}Al_{16}Si_6(0, F_2, Cl_2)_{45}$, where R was to include the supposedly isomorphous substituents H, Na, and K.

S. L. Penfield discovered zunyite at the Charter Oak Mine, five miles from the Zuñi Mine, in 1852. Writing of his analyses, he stated (1893, p. 398): "The agreement between the author's and Mr. Hillebrand's analyses is very satisfactory. Especially the percentages of chlorine, fluorine, and hydroxyl, which are regarded as isomorphous, are very close and yet there seems to be no definite proportion in which these constituents are related to one another."

Opinion on the composition of zunyite underwent several changes after Hillebrand's original formulation. This development is summarized by L. T. Nel (1930, p. 215):

"Hillebrand's original empirical formula was modified by P. Groth in 1889 as $(SiO_4)_3Al_2[Al(OH,F,Cl)_2]_6$, representing a basic orthosilicate analogous to the garnet formula. B. Gossner and F. Mussgnug in 1926, insisting on a ratio Si:Al = 1:3 gave as alternate formula

$$SiO_2 \cdot AlOF \cdot 2AlO_2H \text{ or } SiO_2 \cdot AlF(OH)_2 \cdot 2AlO_2H$$

and

$$2SiO_2 \cdot 2AlOF \cdot 3AlO_2H \cdot Al(OH)_3,$$

while later, in order to conform with the results given by X-ray analysis, Gossner again readjusted the formula to

$$3SiO_2 \cdot 3AlO(F,Cl) \cdot 4AlO_2H \cdot 2Al(OH)_3 .$$

J. McCrae (1929), who analyzed crystals of zunyite discovered by L. T. Nel at Postmasburg, South Africa, wrote:

"The formula assigned to zunyite is $Al_6(OH,F,Cl)_{12}(SiO_4)_3$. The amount of chlorine in the specimens (say, 2.5%) shows that whereas a halogen-free zunyite might be formulated as $4Al(OH)_3 \cdot 2Al_2O_3 \cdot 3SiO_2$, the specimens contain chlorine replacing hydroxyl to the extent expressed by the (doubled) formula

$$AlCl(OH)_2 \cdot 2AlF_2OH \cdot 5Al(OH)_3 \cdot 4Al_2O_3 \cdot 6SiO_2,$$

but in the South African specimen hydroxyl has been replaced only to an extent approximately represented by the (quadrupled) formula

$$2AlCl(OH)_2 \cdot AlF(OH)_2 \cdot 13Al(OH)_3 \cdot 8Al_2O_3 \cdot 12SiO_2 .$$

B. Gossner (1927) was the first to study zunyite by means of X-rays. He made powder photographs using iron and also copper radiation and determined the size of the (cubic) unit cell as a_o = 13.80 X.U. and 13.97 $\pm$ .04 X.U. for the respective radiations. On the basis of the chemical study of Gossner and Mussgnug (1926) he accepted the formula

$$SiO_2 \cdot AlO \cdot \left(\tfrac{15}{19}F + \tfrac{4}{19}Cl\right) \cdot 2AlO(OH) \cdot \tfrac{12}{19}H_2O$$

and, from the measured density, 2.878 gm cm^{-3}, found six molecules of this composition in the unit cell. He assigned the point-group symmetry T_d. From oscillation photographs about [100],

[110], and [111] as oscillation axes he derived a mean value $a_o = 13.93$ X.U., based on the layer-line spacings. On the photograph around [110] all odd layer lines were absent, due to extinction of all reflections with mixed indices. This indicated face-centering, which could not, however, be in harmony with the number of molecules found in the unit cell. Gossner therefore dismissed the systematic extinction evidence and assigned the mineral to space-group $T_d^1 - P\bar{4}3m$, stating that among all space groups isomorphous with T_d, only in T_d^1 could plausible atomic positions be found. He commented (1927, S. B. p. 468) as follows:

> "(1) Das falsche Verhältnis der Translationen (T_{100}: T_{110}: $T_{111} = 1: \frac{1}{2}\sqrt{2}: \sqrt{3}$ anstatt $1:\sqrt{2}:\sqrt{3}$ fur T_d^1) läßt sich vielleicht so erklären, dass durch das sehr ähnliche Beugungsvermögen von Si and Al für die Röntgenuntersuchung eine zu kleine Translation T_{110} vorgetauscht wird."

This was the state of affairs when Pauling (1933) undertook the study of zunyite. Pauling confirmed the point-group symmetry T_d found by Gossner but assigned the crystals to space group T_d^2 - F $\bar{4}$ 3 m, regarding the face-centering translations as significant. He then reviewed published analyses of the mineral by calculating the number of atoms of Si, Al, OH, F, and Cl present in the fundamental unit (one fourth of the unit cell), using a density $\rho = 2.89$ gm cm^{-3} and using the value $a_o = 13.82$ X.U. found by him from an oscillation photograph. By assuming that fluorine could substitute for hydroxyl in the structure but not for chlorine, and that aluminium could be expected to replace silicon to some extent, he arrived at the provisional formula $(OH,F)_{18}$ Al_{13} Si_5 O_{20} Cl.

The choice of this formula was an excellent demonstration of the value of X-ray study in deciding compositional questions. The size of the cell determined the number of atoms in the fundamental unit, and this restricted the Al:Si ratio. Because the number of silicon atoms was calculated consistently at about 4.6 for all analyses (see Appendix II) there had to be at least 5 silicon-type positions in the structure, with therefore some substitution of aluminium for silicon. Finally, the recognition of the distinct structural roles of Cl and F, contrary to previous investigations, allowed a satisfactory assignment of anion composition and a (partial) explanation for Penfield's observation, p. 5, on the OH, F, and Cl content.

With this formula, with a knowledge of the space group and cell dimensions, and using the coordination theory of ionic crystals and the electrostatic valence rule (Pauling, 1939, p. 378-384) Pauling was able to formulate a detailed atomic arrangement for zunyite. This arrangement is the trial structure used in the present investigation, and we present Pauling's derivation and description of it in Chapter 3.

Pauling then measured the intensities of 72 X-ray reflections on oscillation photographs of zunyite made with Mo Kα radiation. Using the proposed structure he calculated intensities to be expected for these reflections, applying Lorentz and polarization corrections but no temperature factor. The calculated values agreed well with the observed values. All strong reflections were accounted for, and there was general agreement between calculated and observed values for moderate and weak

reflections. The overall agreement may be judged from the value of the mean discrepancy

$$R_1' = \frac{\sum_g |I_o - I_c|}{\sum_g I_o}$$

(the sum being over all observed reflections), which for Pauling's data (1933, p. 450) is 0.29. Considering the fact that Lipson and Cochran (1953, p. 147) regard a value of 0.4 for the residual

$$R_1 = \frac{\sum ||F_o| - |F_c||}{\sum |F_o|}$$

as indicating that a proposed structure is probably correct, and realizing that $I = |F|^2$, it is clear that Pauling's structure is promising.

III. THE TRIAL STRUCTURE

Pauling's discussion (1933, pp. 446-448) of his derivation of the trial structure is illuminating, and because it provides an excellent description of this structure, we reproduce it here:

> " Let us first assume that there are six equivalent silicon atoms in the fundamental unit, that is, 24 or more in the unit cube. (a) If there are 24 equivalent and distinct tetrahedra, the 24 Si occupy 24a or 24b (in Wyckoff's notation). No value of the parameter prevents infraction of the condition $O\text{-}O \geqslant 2.4$ Å, eliminating this possibility. (b) If the 24 equivalent silicon tetrahedra share corners, these corners lie on three-fold axes, which makes $O^{=}$ common to three silicon tetrahedra, contradicting assumption 3.
>
> The only remaining positions for 20 or 24 silicon atoms are 16a plus one or two of the positions 4b, 4c, 4d, and 4e. Agreement with the electrostatic valence rule with silicon tetrahedra in 4b (or c, d, e) is reached only when the corners are shared with other tetrahedra. The crystals must consequently contain groups of five tetrahedra such as shown in Fig. 1.
>
> The formula suggests that the unit contains four groups of twelve octahedra, with point-group symmetry T_d (positions 4b, c, d, e). Such groups, shown in Fig. 2, occur in spinel. A framework might be constructed by sharing the tetrahedral groups of Fig. 1 with these, the three oxygen atoms labeled A in Fig. 2 forming the base of a tetrahedron. The chemical formula and the electrostatic valence rule require, however, that the atoms labeled B be shared with similar octahedra in a neighboring group, and it is found that this sharing is not geometrically possible.
>
> If the groups of three octahedra be inverted, the group of twelve shown in Fig. 3, also with point-group symmetry T_d, is obtained. When four such groups are placed in the positions 4b, it is found that the corners B of one group (at 0 0 0 , say) can be shared with the corners B' of an adjacent group (at $\frac{1}{2}$ 0 $\frac{1}{2}$), and that such sharing for regular octahedra with Al-O = 1.89 Å leads to a value of 13.82 Å for a_o, in exact agreement with the observed value. Moreover, the groups of five tetrahedra can be placed in position 4d, and tetrahedron corners shared with corners A with only a slight distortion (of a few hundredths of an Angström). This agreement in dimensions makes it highly probable that this is the framework of zunyite.

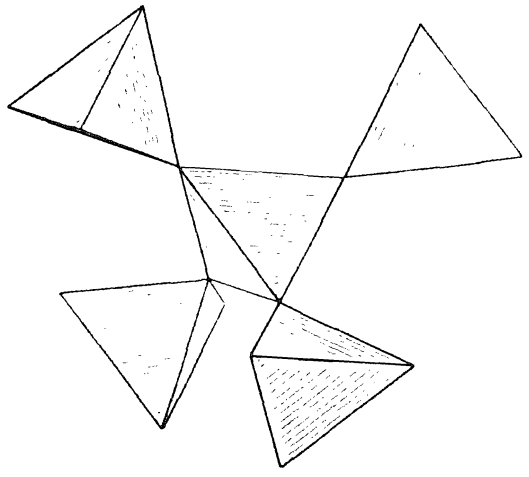

Fig. 1. The Si_5O_{16} group of linked tetrahedra. From Pauling (1933).

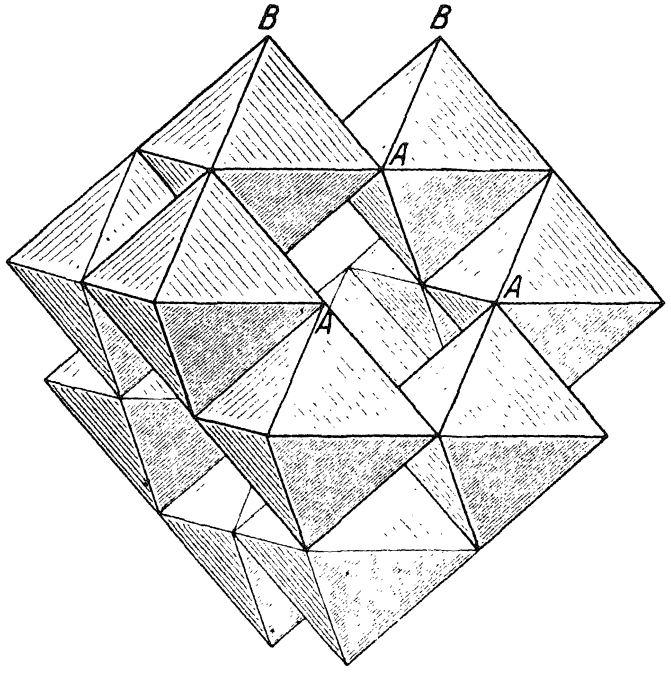

Fig. 2. From Pauling (1933)

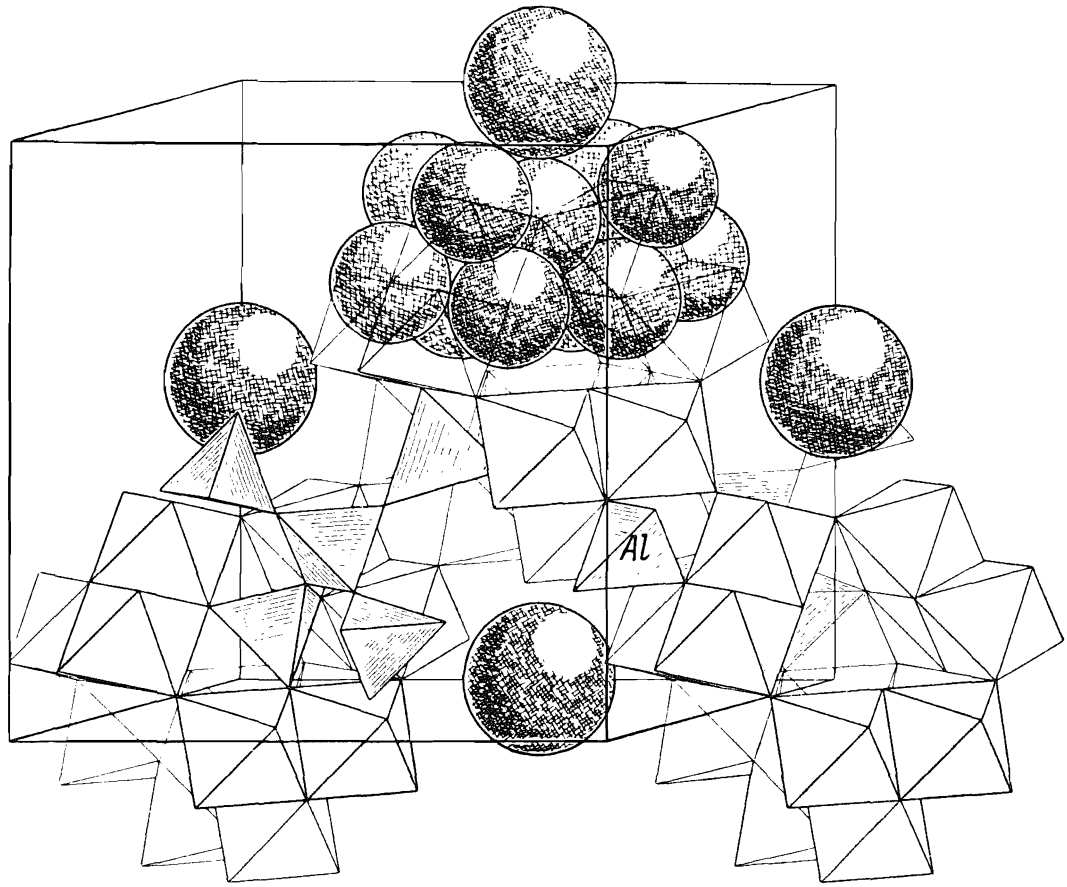

Fig. 3. The zunyite structure. From Pauling (1933).

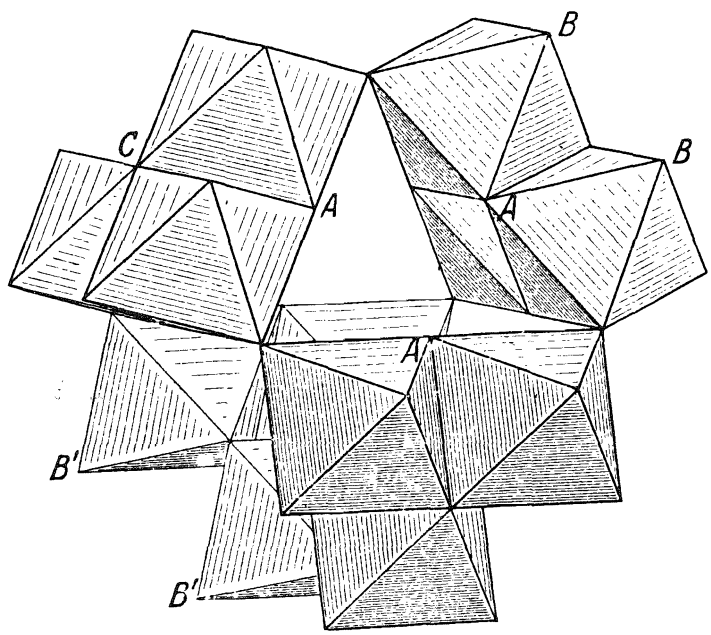

Fig. 4. From Pauling (1933).

> Agreement with the electrostatic valence rule is satisfactory except for the oxygen atoms C (Fig. 4), common to only three octahedra. It is seen, however, that these atoms occur in groups of four, which can be combined to tetrahedra by placing aluminum ions in positions 4e, the total bond strengths then becoming 2 1/4. The four chlorine ions occupy positions 4c, 4b being ruled out by the small Cl^{-}-$O^{=}$ distance it leads to (2.72 Å, sum of radii 3.21 Å). "

The resulting structure is described as follows, using the notation of the International Tables for X-ray Crystallography (1952, p. 325):

4 Cl in b

4 Si_I in c

4 Al_I in d

16 Si_{II} in e, $x_1 = 0.117$

48 Al_{II} in h, $x_7 = 0.089$, $z_7 = -0.228$

16 O_I in e, $x_2 = -0.177$

16 O_{II} in e, $x_3 = 0.184$

24 O_{III} (OH, F) in f, $x_4 = 0.273$

48 O_{IV} (OH, F) in h, $x_5 = 0.181$, $z_5 = 0.545$

48 O_V in h, $x_6 = 0.139$, $z_6 = 0.006$

The main features of the structure may be summarized as follows:

1. The Si_5O_{16} group of linked silicon tetrahedra; no other structure is known to have this group, the only finite groups of linked silica tetrahedra being rings, or else pairs Si_2O_7.

2. The group of coordinated aluminum octahedra: this group is also unique, its closest relative being found in the structure of diaspore.

3. The isolated aluminium tetrahedra: this feature is unique, as is also the linking of the silicon tetrahedra in an aluminosilicate material whose composition would allow all silicon tetrahedra to be isolated and linked with aluminum octahedra or tetrahedra, as in the structures of the polymorphs of Al_2SiO_5.

4. The chlorine atom occupying cavities in the framework of linked octahedra and tetrahedra: this has its counterpart in the structures of sodalite and the ultramarines.

5. The vacancy in the structure at the center of the large group of coordinated aluminum octahedra.

6. Linking of the tetrahedral and octahedral groups: this builds up a sphalerite-type arrangement with the tetrahedral groups at positions corresponding to, say, the zinc atoms and the octahedral groups corresponding to sulfur, and is a typical arrangement in cubic crystals.

IV. THE X-RAY DATA

1. Material.--The zunyite used in the present study is from the Zuñi Mine. The material is the same as used originally by Prof. Pauling, and was obtained by him from R. M. Wilke in Palo Alto, California. It consists of fresh zunyite-guitermanite rock. Samples of this were crushed and the small tetrahedral zunyite crystals were selected by hand under the binocular microscope. Crystals selected varied in size from 0.2 to 0.8 mm, and were clear, well-formed tetrahedra showing a small negative tetrahedral truncation. All crystals from the zunyite-guitermanite rock contain black inclusions, which W. F. Hillebrand (1885, p. 127) identified as rutile. Crystals for the present study were selected as free from these inclusions as possible, and contained at most two or three minute black particles less than .01 mm in size.

Crystals which supplied X-ray data used in the present study are listed in Table I. The octahedral habit of crystal No. 1 resulted from near equal development of the positive and negative tetrahedral faces. This crystal was selected because of its near equant shape, to minimize errors due to absorption.

Each crystal was mounted on the end of a glass fiber attached to a standard goniometer pin. Mounting was by the hot-wire technique using shellac.

Crystals were oriented first by means of a two-circle optical goniometer. Positive tetrahedral faces give strong signals, sometimes sharp and clear, but usually multiple with 3 to 10 signals, forming a pattern extending for several minutes of arc in

latitude and longitude. The angle between face normals was always within 5 minutes of the ideal value, $109^{\circ}\ 28'$, and for sharp signals, within 1 minute of this value.

The orientation was checked and small corrections were made by means of Laue photographs, one of which is reproduced in Fig. 5. It was found, however, that optical orientation was adequate and that only final corrections with the crystals in place in the Weissenberg or oscillation cameras were necessary.

2. X-Ray Photographs.--A list of all X-ray photographs used in this study is given in Table II. The photographs were made on Eastman no-screen X-ray film, and processed by standard procedures. Multiple films (in groups of three) to provide three intensity ranges for a given exposure are lettered a, b, c. With copper radiation the three films were placed directly one behind the other in the camera. With Mo Kα radiation it is necessary to interleave brass foil between the films to get an adequate range of intensities.

3. Oscillation Photographs.--The purpose of these photographs was to check the size of the unit cell, to gather preliminary X-ray intensity data, and to record intensities for reflections occurring at angles too small to observe in the Weissenberg cameras using Mo Kα radiation. The photographs were made on Tube Stand No. 1 in the X-ray laboratory of the Chemistry Department, California Institute of Technology. The X-ray tube of this apparatus is of the self-rectifying "gas tube" type, with aluminium cathode and copper target, operated under continuous evacuation using an air leak to maintain a suitable pressure of

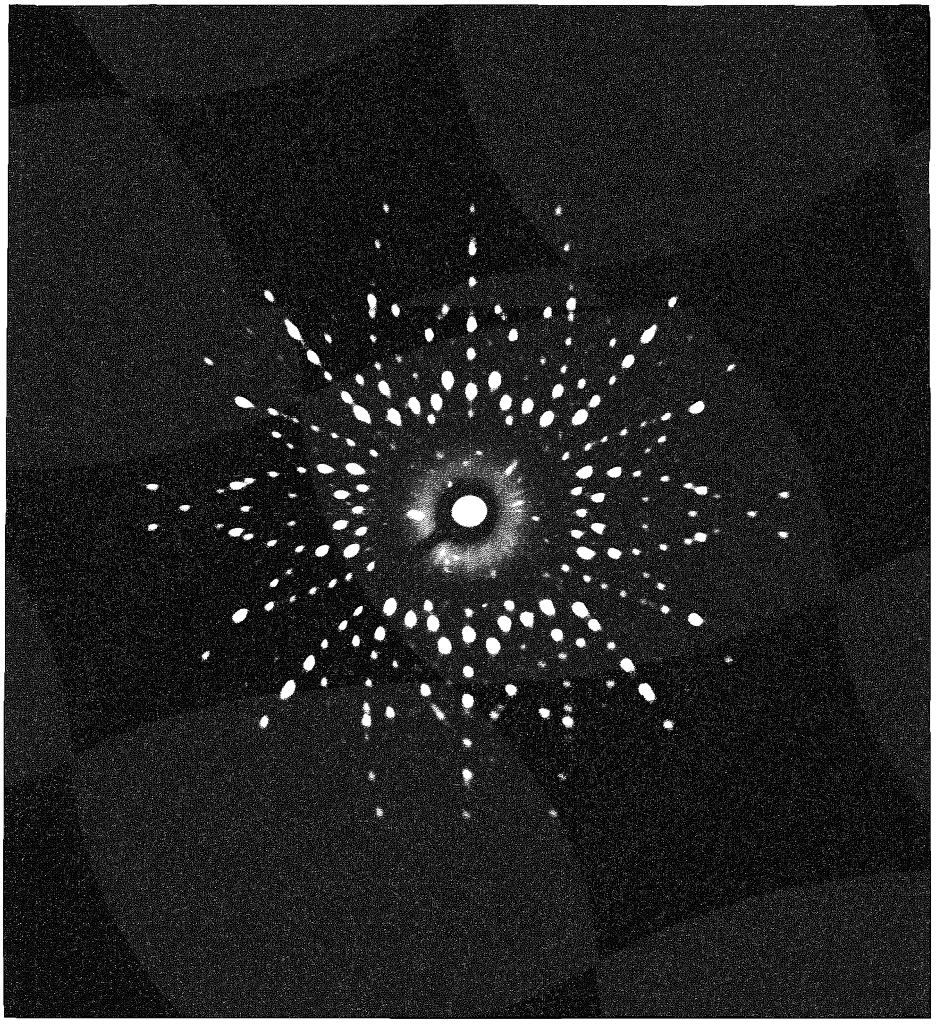

Fig. 5

Beam parallel to [110]

TABLE I

CRYSTALS

Crystal No.	Size	Habit	Rotation Axis	Use
1	0.8 mm	Octahedral	[100]	Weissenberg Ph., Mo Kα
3	0.2	Tetrahedral	[100]	Oscillation, Rotn., Cu Kα
5	0.2	"	[110]	Weissenberg Ph., Mo Kα

TABLE II

X-RAY PHOTOGRAPHS

Film No.	XI.	Purpose	Tube Stand	Camera	Rad.	Filter	Exp. Time	Notes
1	3	Layer line spacing	1	Osc. #1	Cu	none	1.6 hr	Osc. angle 30°
2a-c	"	Intensities	"	"	"	"	3.2	O. a. 15°
3a-c	"	"	"	"	"	"	3.1	"
4a-c	"	"	"	"	"	"	3.1	"
5a-c	"	"	"	"	"	"	3.4	"
7	1	Orient.	6	Weiss. #4544	Mo	"	0.5	O. a. 19°
11a-c	"	Intensities	"	"	"	Zr	14.1	$\ell = 0$
12	3	Cell size	1	C.I.T. Powd.	Cu	none	3.6	Rotation
17a-c	"	Intens. scale	"	Osc. #1	"	"	scaled	Incl. (660)
18a-c	1	"	6	Weiss. #4544	Mo	Zr	"	"
19a-c	"	Intensities	"	"	"	"	14.7	$\ell = 0$
23a-c	"	Intens. scale	"	Weiss. #673	"	"	scaled	Incl. (660)
26a-c	5	Intensities	"	"	"	"	30.5	O. a. 215°
28a-c	"	"	"	"	"	"	47.6	O. a. 125°
29a-c	"	Intens. scale	"	"	"	"	scaled	Incl. (660)

air in the tube. The photographs were made using Camera No. 1, of radius 50.08 $\pm$ 0.02 mm (as measured by J. A. Ibers). One of the photographs is shown in Fig. 6.

The photographs were indexed using a Bernal chart, by the graphical method described by Buerger (1942, p. 196). All equatorial reflections (h k O) were indexed, but only such general reflections (h k l) on higher layer lines as were necessary to complete the set of (h h l) intensities.

Intensities of the reflections were estimated by visual comparison of the spots on the photographs with a set of standard spots. The standard spots were made by taking a series of seven exposures on one set of 3 films, using a given oscillation range, the exposure times for the successive exposures being devised to form a logarithmic scale in logarithmic intervals of 0.1.

Intensities were measured of all equatorial reflections on photographs 2-5 produced by the Cu $K\alpha_1$ and Cu $K\alpha_2$ (when resolved) lines. Intensities were recorded in logarithmic form. The film factor was estimated by averaging the logarithmic differences between intensities of spots due to the same reflection appearing on successive photographs. Insufficient data were available to estimate with confidence the film factors for the pairs (a, b) and (b, c) separately. The film factor determined was 3.7.

Determination of the film factor provides a method of estimating the internal precision of visual estimation, by observing the scatter in the logarithmic differences of (independently estimated) intensities for the same reflection. The standard deviation

TABLE III

COMPARISON OF ESTIMATED INTENSITIES

Reflection	Pauling (1933)	This Investigation
0 2 0	.5	.71
0 4 0	.0	.19
0 6 0	.1	.32
0 8 0	.4	.79
0 10 0	.2	.60
0 12 0	1.0	1.32
2 2 0	.6	.29
2 4 0	.0	.0
2 6 0	.1	.21
2 8 0	1.0	.93
2 10 0	.0	.05
2 12 0	.0	.22
4 4 0	2	1.44
4 6 0	.0	.00
4 8 0	.0	.10
4 10 0	.0	.03
6 6 0	10	10.0
6 8 0	.2	.27
8 8 0	3	3.1

for a single visual measurement was estimated in this way at $\sigma = 0.04$ for moderate and strong reflections, and at $\sigma = 0.08$ for faint reflections. These standard deviations correspond respectively to scatters of about 2°/o and 4°/o in the intensities.

Intensities for resolved $K\alpha_1$ - $K\alpha_2$ doublets were corrected to log $(I_{K\alpha_1} + I_{K\alpha_2})$ by assuming log $I_{K\alpha_1}$ - log $I_{K\alpha_2} = 0.3$. The value estimated for this difference from the X-ray data was 0.38.

The photographs were corrected to the intensity scale of photograph No. 2a by adding constants to the logarithmic intensities of photographs 3-5, the constants being determined by a comparison of the estimated intensities of reflections appearing on more than one photograph. There were four to seven such reflections for each comparison.

The resulting intensities of the 19 equatorial reflections measured by Pauling (1933, p. 450) were reduced to a scale consistent with Pauling's. The comparison is shown in Table III, and indicates the scatter to be expected between the two sets of data.

The logarithmic intensities of the complete set of 37 equatorial reflections (h k O) were then corrected for the Lorentz factor and for the polarization factor (James, 1950, p. 39). This was done by subtracting log $\left(\frac{1 + \cos^2 2\theta}{\sin 2\theta}\right)$ from each reflection, the values of θ being calculated from the Bragg relation

$$\sin\theta = \frac{\lambda\sqrt{h^2 + k^2}}{2a_o}$$

where a_o was taken equal to 13.87 Å.

The resulting logarithmic intensities were used for comparison with intensities derived from Crystal No. 1, as discussed in the next section.

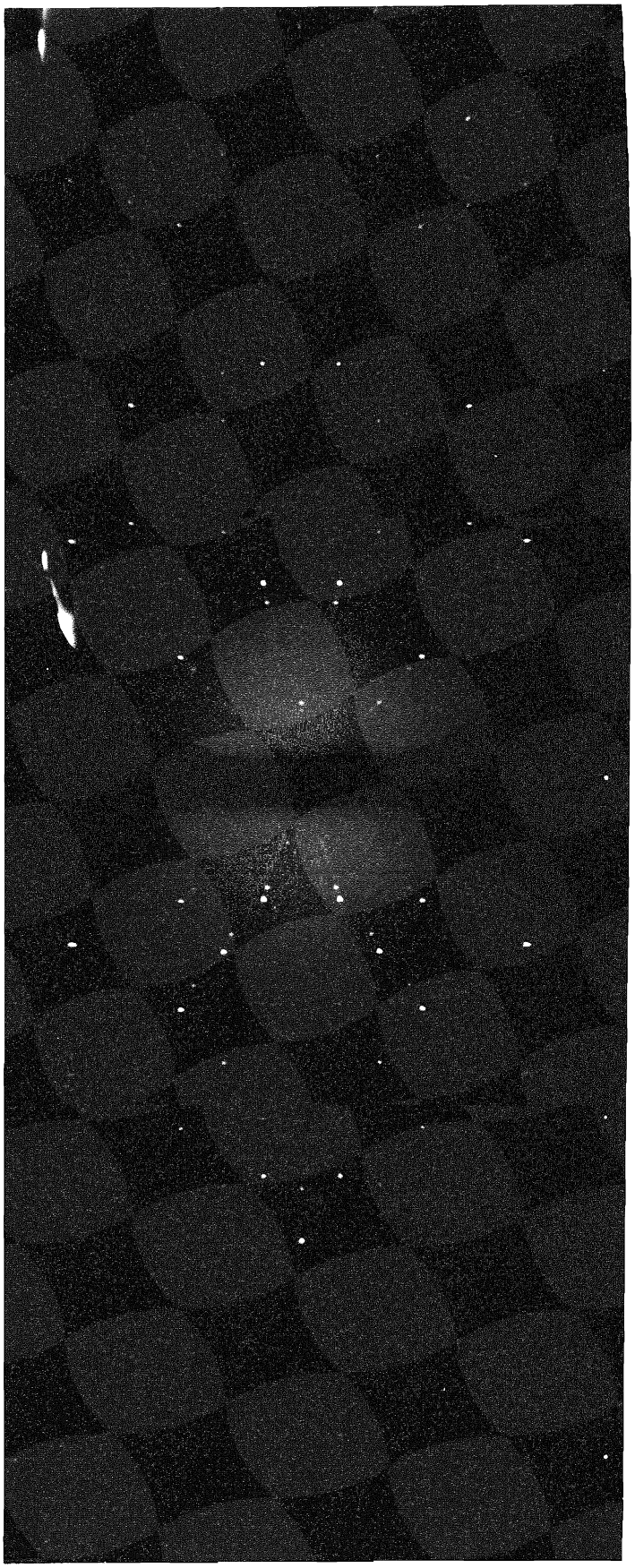

Fig. 6. Photograph 2a.

4. Weissenberg Photographs around [100]. --These photographs, using Crystal No. 1, provided the X-ray intensities for the main refinement of the structure. The photographs were made with standard Buerger-type equi-inclination Weissenberg camera assemblies. The radiation used was from the molybdenum target of a G. E. X_R-4 tube operated at 50,000 volts cathode potential. The radiation was filtered through zirconium.

Owing to the relatively large unit cell size and small wavelength of radiation used, the spacing of the layer lines on photographs made with the Buerger cameras was so small, as shown in Fig. 7, that it was necessary to narrow the layer line screen to a width of about 1 mm, using lead foil, to achieve separation of single layer lines in the Weissenberg arrangement.

A typical equatorial Weissenberg is shown in Fig. 8. Indexing of these photographs is carried out in the usual way with the guidance of lattice-row plats of the kind described by Buerger (1942, p. 274). An unfortunate feature of these photographs is the splitting of the spots, which is particularly prominent on the lower half of the film. This is caused by the presence in the crystal of two separate individuals oriented slightly differently. The prominence of the splitting on one half of the photograph and not on the other is the effect of the translational motion of the Weissenberg camera. The misorientation responsible for the effect consists in a small misorientation $\Delta\phi_1$ about some axis in the equatorial plane, combined with a small azimuthal misorientation $\Delta\phi_2$ about the crystal rotation axis, $\Delta\phi_1$ and $\Delta\phi_2$ being approximately equal. This interpretation is borne out by the fact that

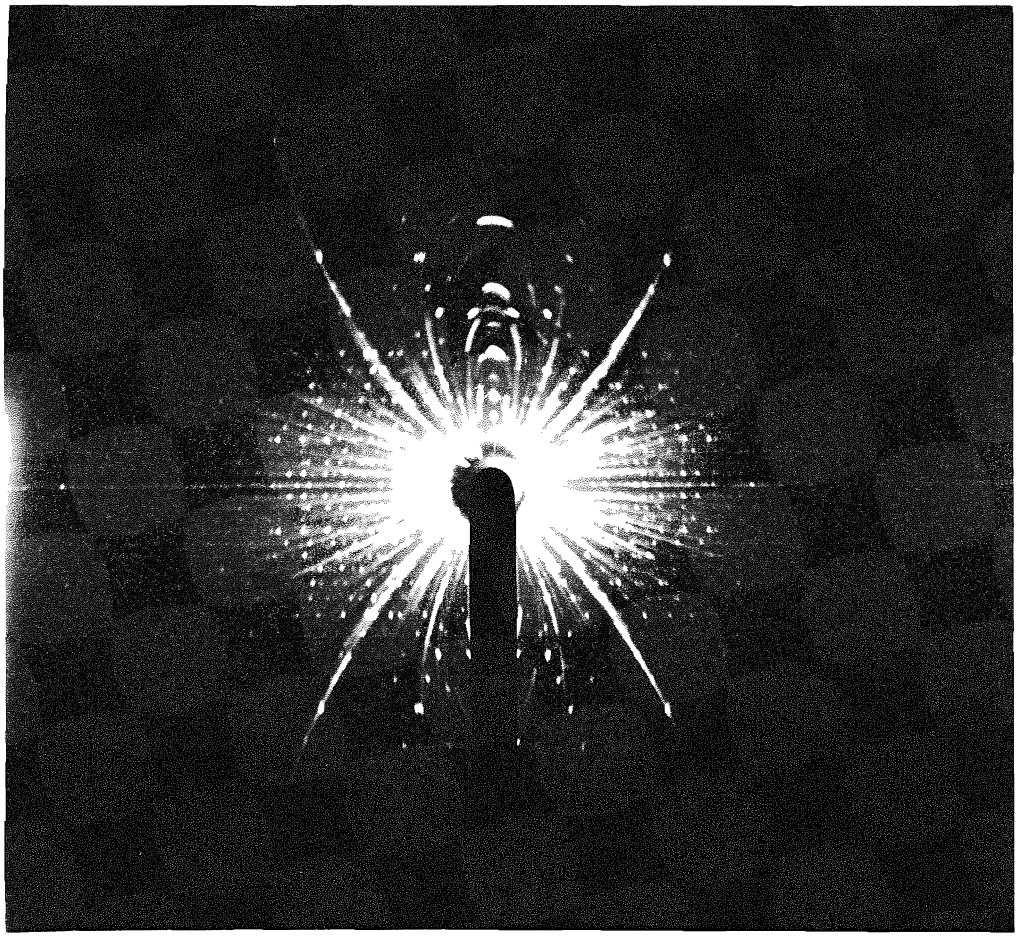

Fig. 7

Note the short layer line spacing.

the splitting is approximately constant for a given central lattice line on a given half of the film.

While this splitting is objectionable, it is not particularly serious, because usual practice (S. Samson, in conversation) is to estimate intensities only on one half of the Weissenberg film, the intensities on opposite sides not being directly comparable owing to the effects of camera translation. Intensities were therefore estimated only on the half of the film showing little to no splitting. Intensity estimation, film factor estimation, and correction for $K\alpha_1$-$K\alpha_2$ doubling and for Lorentz and polarization factors on the Weissenberg films were carried out in the usual way, as described in the previous section. The amount of data (133 reflections) was sufficient to allow separate estimation of the film factors for the front pair and rear pair of films. For the front pair (closer to the crystal) the factor was 4.0 and for the rear pair 5.0, a significant difference. This difference in film factors is presumably due to the greater amount of fluorescent radiation impinging on the middle and back films than on the front film, owing to the fact that the middle and back films are faced with metal on both sides, while the forward side of the front film is free (S. Samson, in conversation).

The number of non-equivalent reflections which could appear on the (h k O) Weissenberg photographs was 163. Of these, 133 were observed. For each of the remaining reflections an estimate was made of the minimum observable intensity, and an intensity was recorded of half this value.

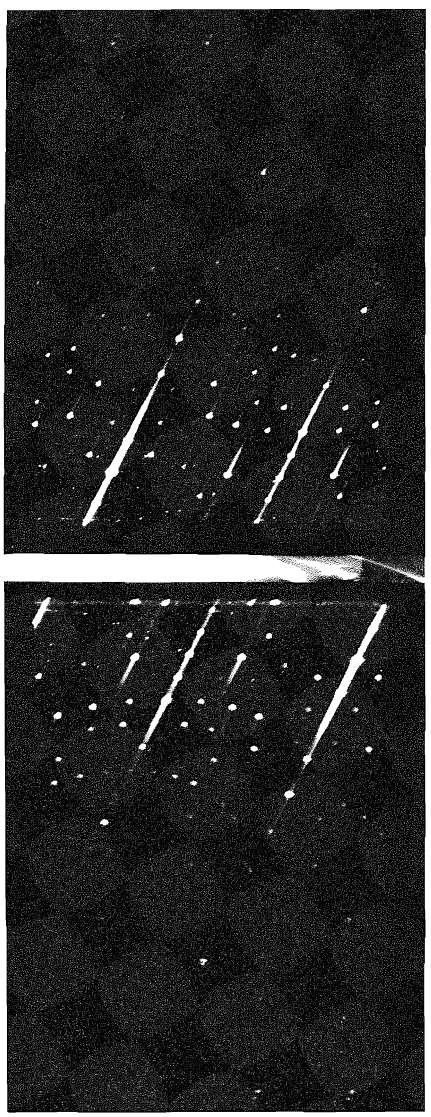

Fig. 8

Intensities of the complete set of (h k O) reflections were estimated both on photographs 11 a-c and photographs 19 a-c. From a comparison of the two sets of data, an estimate of the precision of visual estimation was possible. For intensities greater than 4 times the smallest observable, the standard deviation of the population $\log I_o(19)-\log I_o(11)$ was estimated at 0.07, giving an estimated standard deviation for a single visual estimation of $0.07/\sqrt{2} \approx 0.05$. This corresponds to a scatter of about 12% in the estimated intensities, and is in harmony with variance estimates based on film factor determination. A similar comparison of the Weissenberg data from photographs 11 a-c and the oscillation photograph data (Photos 2-5) gave an estimated standard deviation for the logarithmic difference of 0.09, showing that the oscillation and Weissenberg data were in essential agreement within the limit of estimation error. This latter comparison was made, of course, after correcting the separate sets of data for the Lorentz and polarization effects.

The final set of logarithmic (h k O) intensities was obtained by averaging the data from photographs 2-5, 11 a-c, and 19 a-c.

5. Weissenberg Photographs around [110]. --Because the zunyite structure, having tetrahedral symmetry, has a center of symmetry only in projection on $\{100\}$, the (h k O) data were used for the major refinement, the center of symmetry greatly simplifying the calculations. For the investigation of certain details, however, it was necessary to have non-centrosymmetric data. For this purpose the projection of the structure on $(1\bar{1}0)$

was studied, by using data from equatorial Weissenberg photographs with [110] as rotation axis. These photographs were made using Crystal No. 5. Because of the small size of this crystal, the [110] Weissenbergs have a very different appearance from the [100] Weissenbergs. Photograph 28 is shown in Fig. 9 as an example. The individual spots are elongated into short ovoids, whose axes all have a slope of about 1 on the film, quite distinct from the slope of 2 for central lattice lines, or the horizontal slope of the typical elongated Weissenberg spots produced by rotating a needle-shaped crystal parallel to the needle axis. This slope of one results from the fact that for Crystal No. 5 the angle subtended by the crystal at the film is small compared to the divergence of the X-ray beam.

Reflections on these photographs have indices (h h l). Indexing the spots is complicated slightly by the fact that systematic extinctions cause the row lines parallel to [111] and [11$\bar{1}$] in the reciprocal lattice to be very prominent, while the row lines parallel to [001] and [110] are difficult to follow. Visual estimation and reduction of the intensities were carried out in the same way described in the preceding sections, but Lorentz and polarization corrections were not applied, and intensities were converted directly from the logarithms, after appropriate conversion to a scale approximating $\frac{1}{256} I_c$. Further reduction of the data was accomplished entirely on IBM machines, as described in Chapter VII. The number of possible (h h l) reflections was 410, of which 340 were observed.

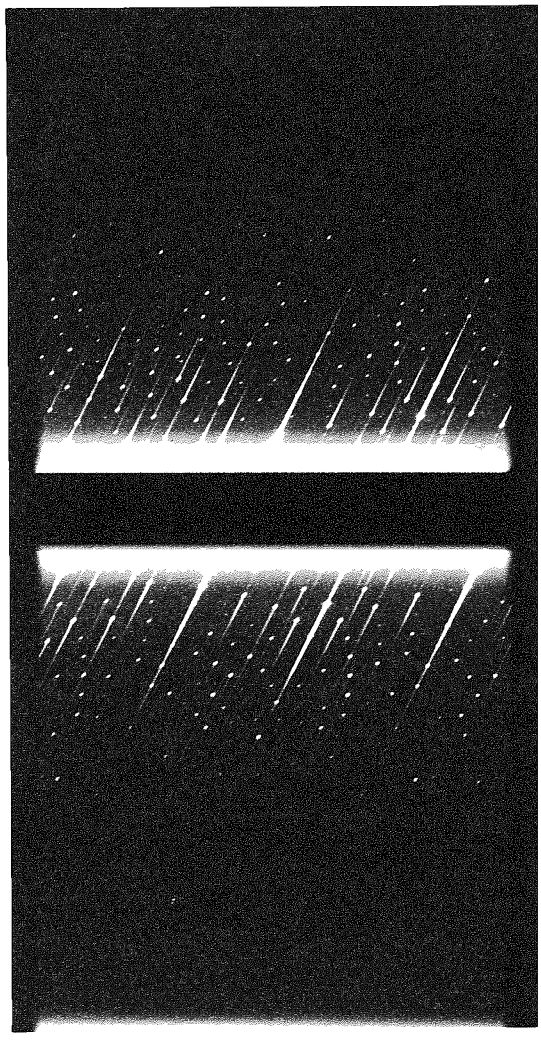

Fig. 9

Intensities for (h O O), (h h O) and (h h h) reflections were measured on both photographs 26 a-c and 28 a-c. The estimated standard deviation for log I_o (28) - log I_o (26) was $\sigma = 0.07$, indicating that the measurement errors for these photographs were essentially the same as for the (h k O) data. Observed and calculated data for (h k O) and (h h l) reflections are given in Appendix II.

6. Densitometric Intensity Measurements.--In the course of refining the structure, it was found that the calculated intensities of the strongest reflections were in every case significantly weaker than the observed intensities, in contrast to the more usual situation where the strong reflections are weaker than expected owing to extinction and multiple reflection (James, 1950, pp. 25 and 49). To investigate this anomalous situation it was necessary to measure accurately the intensities of the strong reflections, which even on the third film are too dense to allow confident visual estimation. Measurements were therefore undertaken with a Capstaff-Purdy densitometer.

The measured H and D curve (density vs. log intensity) of standard intensity films 23 a-c is shown in Fig. 10. The measurements can be reproduced to a precision of one or two hundredths on the (logarithmic) density scale for intensities in the lower part of the curve. For high intensities the measurements become more inaccurate, because of stray light coming into the field of view around the spot. It was found, in fact, that if the ocular of the densitometer is not pressed down

firmly against the film, the H and D curve exhibits a flattening out at the highest densities, as though the upper knee of the curve is reached and the saturation density approached. But there is in fact no such effect, as shown in Fig. 10, which includes measurements up to the highest densities on the standard films.

Using the H and D curve for calibration, intensities were measured for a selected group of reflection on films 11 a-c and 19 a-c. Particular attention was paid to strong spots and to spots lying along central lattice lines, where visual estimation is impaired by the white radiation streak. For each spot a density was measured at the center of the spot, and then a background density of white radiation fog was measured on the low-θ side of the spot (the high-θ side was avoided in most cases because there is frequently a significant contribution to the white radiation streak there by the reflection in question). The spot and background density were converted separately to absolute intensities (not logarithms), subtracted, and the resulting intensity reconverted to logarithmic form for scale factor determination. Comparison of photographs 11 and 19 measured in this way gave an estimated standard deviation of $\sigma = 0.06$ for $\log I_d(11) - \log I_d(19)$, or $\sigma = 0.04$ for a single estimation. This value is significantly higher than the precision of measurement, and shows that intensity measurement is affected by other errors than random errors of measurement.

A comparison of structure factors calculated from the final structure with observed structure factors measured densitometrically and estimated visually is given in Table IV. Although

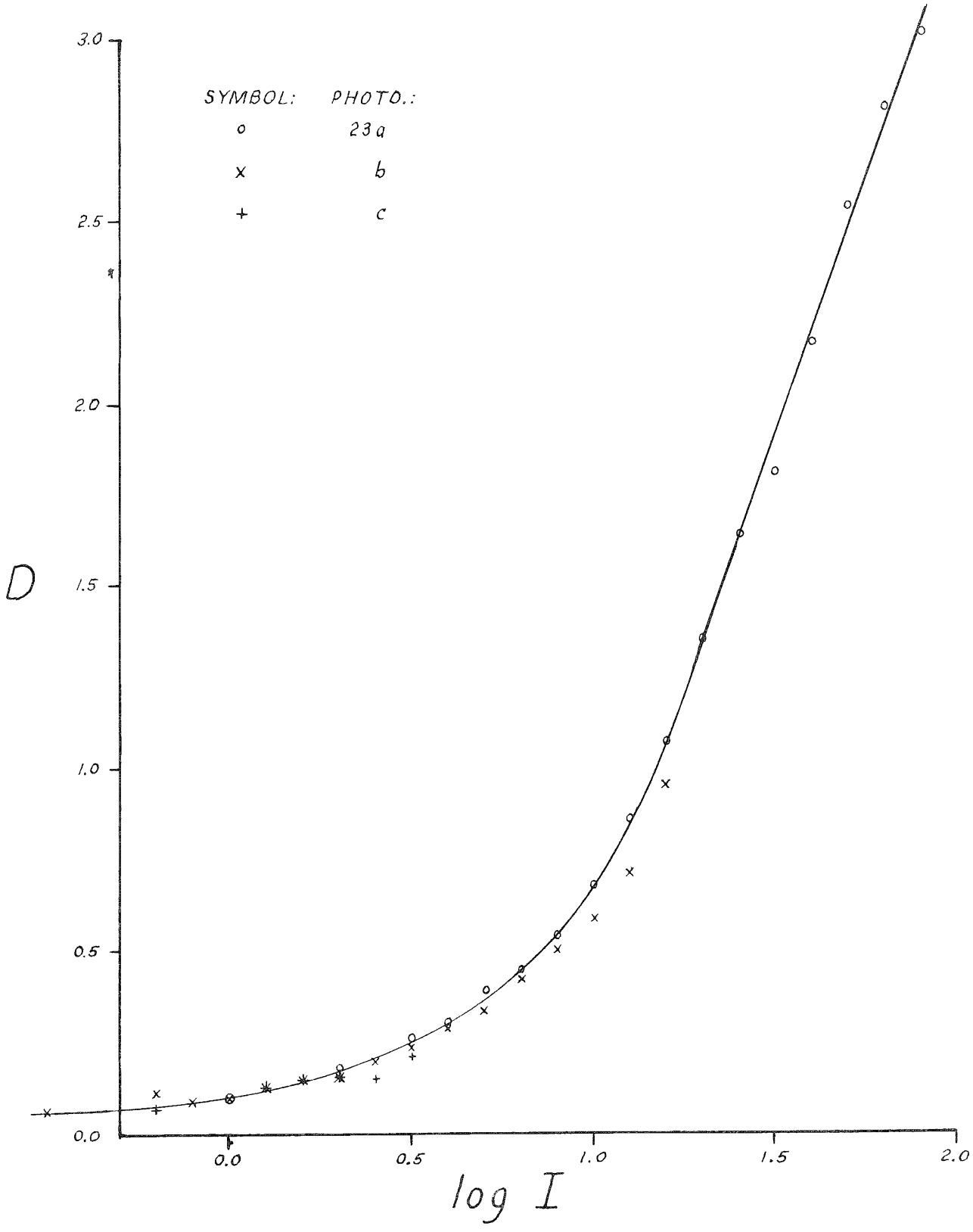

FIG. 10

the residual R_1 for this data is lowered from 0.12 to 0.09 by the densitometric measurements, the improvement does not seem striking. One may justifiably conclude that the improvement does not adequately repay the considerably greater effort required in reducing the measurements. The chief advantage of using the densitometer is that it frees the observor from the plaguing sense of subjectivity attendant on visual estimation.

It is not possible to make densitometric measurements on the (h h l) data, because the spot size produced by Crystal No. 5 was smaller than the field of the densitometer.

7. Comparison of Intensity Estimates.--As has been mentioned, the (h k O) data from photographs 2-5, 11, and 19 showed essential agreement within the error of measurement. Reflections of the type (h h O) and (h O O) occur both among these data and in the (h h l) data derived from photographs 26 and 28. A comparison of these two sets of data showed considerably greater scatter than could be expected from the errors of measurement, the estimated standard deviation of $\Delta = \log I_o(26,28) - \log I_o(11,19)$ being $\sigma = 0.2$. With the idea that this scatter might be due to effects depending on the Bragg angle, such as the Lorentz and polarization corrections, the values of Δ were plotted against $\mathrm{Sin}^2\theta$, as shown in Fig. 11. There is no definite indication of a regression in this plot. When plotted against $\log I_o$, however, a definite linear regression is suggested, as shown in Fig. 12. The scatter about the visually estimated regression line gives a standard deviation estimate of 0.1, much more reasonable in

TABLE IV

RESULTS OF DENSITOMETER MEASUREMENTS

Reflection	F_o Est.	F_o Meas.	F_c
0 4 0	2.5	2.8	2.2
0 6 0	4.5	5.1	3.3
0 8 0	6.3	8.1	8.5
0 10 0	9.0	8.9	9.0
0 12 0	18.0	19.0	18.0
0 14 0	3.6	3.7	3.1
0 16 0	7.0	6.2	6.3
0 18 0	1.2	0.9	0.3
0 20 0	2.2	1.8	2.1
0 22 0	10.0	10.2	10.2
0 24 0	4.0	4.4	4.6
0 26 0	2.2	1.9	2.7
0 28 0	3.2	3.5	3.0
0 30 0	2.5	2.8	3.4
0 32 0	1.8	1.5	2.0
0 34 0	3.2	5.0	4.8
0 36 0	2.8	2.9	3.1
4 4 0	11.0	10.2	10.4
6 6 0	45.0	41.7	36.3
8 8 0	25.0	24.5	22.2
10 10 0	4.0	3.5	4.2
12 12 0	9.0	10.5	9.8
14 14 0	14.0	14.4	14.3
16 16 0	5.0	4.5	5.1
18 18 0	5.0	4.5	5.2
20 20 0	2.2	1.4	2.4
22 22 0	7.0	9.8	9.1
26 26 0	2.0	1.9	2.2

relation to the measurement errors.

The plot of Δ against log I_o shows that there is a distinct tendency for the intensities of strong reflections to be stronger in photographs 26 and 28 than in photographs 11 and 19, and for the reverse for weak reflections, suggesting that there is a difference in contrast γ between the two sets of films, either for the standard intensity films used or for the Weissenberg photographs, or both, but in such a way that the effects are not compensated for in intensity estimation.

This discrepancy between the two sets of intensities we will call the "contrast problem". Although the amount of data available in Fig. 12 can only suggest the effect, the complete study of the (h k O) and (h h l) intensities is able to establish it definitely. The contrast effect has three repercussions: (1) it affects the temperature factors strongly; (2) it causes a problem in the comparison of calculated and observed intensities for strong reflections, giving rise, we believe, to the anomaly mentioned above; and (3) it raises the question as to how great an effect a systematic error of this kind can have on the atomic positions derived.

From an intercomparison of measurements made on the various photographs with the use of different standard intensity films it is possible to argue that the discrepancy between the sets of data is caused by a contrast error in photograph 29. This conclusion should be tested experimentally. The arguments for it are too lengthy to include here, but they are substantiated by a detailed study of the (h h l) intensities, discussed in Chapter IV.

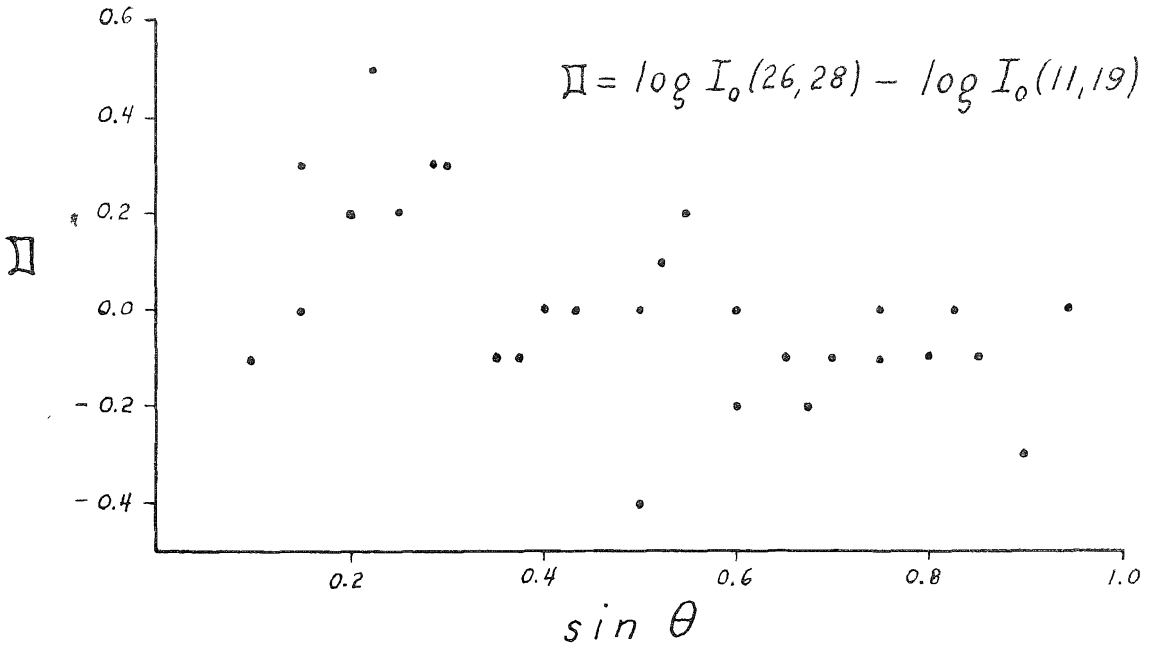
Π = log I₀(26,28) − log I₀(11,19)
Π
0.6
0.4
0.2
0.0
−0.2
−0.4
0.2
0.4
0.6
0.8
1.0
sin θ

FIG. 11

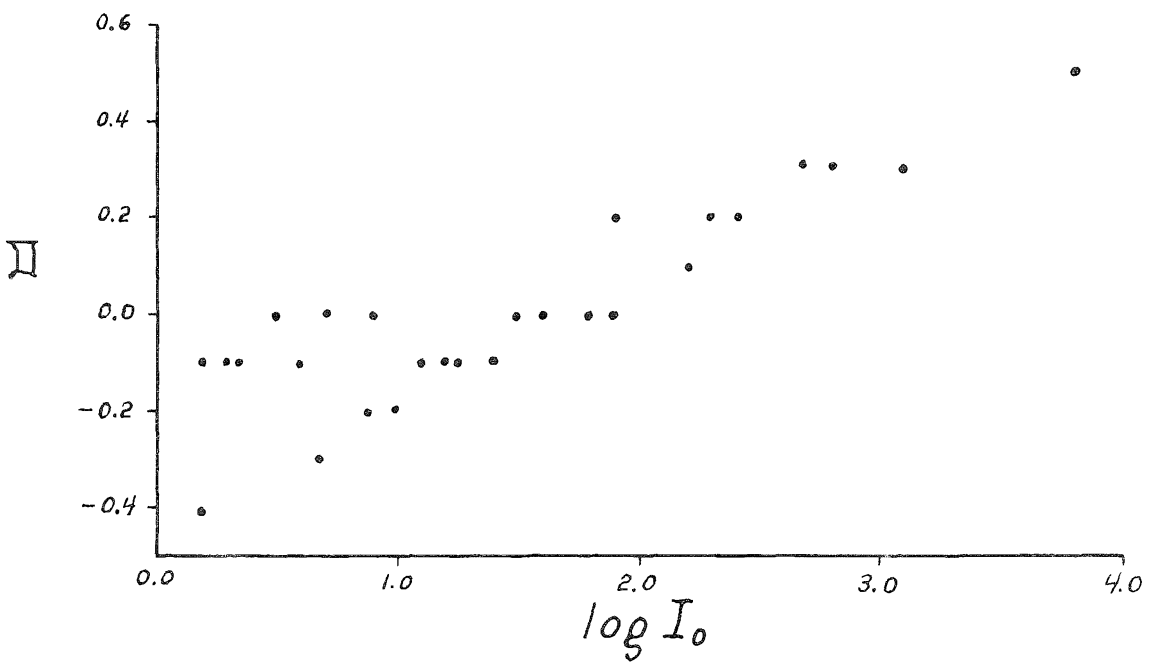
Π
0.6
0.4
0.2
0.0
−0.2
−0.4
0.0
1.0
2.0
3.0
4.0
log I₀

FIG. 12

On the strength of this conclusion, the (h k O) refinement of the structure may be pursued without fear of appreciable systematic errors of the kind introduced by the contrast problem.

8. Absorption Correction. --From data in the Internationale Tabellen (1935, p. 577), the absorption coefficient for Mo Kα is calculated to be $\mu = 10.5\ cm^{-1}$ in a substance of composition $(OH)_{18}\ Al_{13}\ Si_5\ O_{20}\ Cl$ and density $\rho = 2.90$. The optimum crystal size is then 2 mm, almost 3 times as large as the largest crystal used. The absorption corrections for the large crystal (No. 1), which has approximately equant shape, may be judged from Table I, p. 584, of the Internationale Tabellen, which gives absorption corrections to be applied to intensities of reflection from a cylinder of radius r and absorption coefficient μ for various values of the Bragg angle θ. Taking an average equatorial diameter of 0.6 mm for Crystal No. 1, giving $\mu r = 0.3$, the correction factor varies by only 1%, in the range from $\theta = 0^\circ$ to $\theta = 90^\circ$. Although this correction is negligible, the crystal is approaching the upper limit of size for which absorption corrections are small. For $\mu r = 0.5$, the variation is 10%, which is appreciable, though probably not significant, because the probable error of visual intensity estimation is about 10%. These estimates cannot predict the absorption effects due to the departure from cylindrical shape. However, it seems apparent that these effects are negligible for Crystal No. 1, and certainly so for Crystal No. 5.

V. THE SIZE OF THE UNIT CELL

It has been desirable to redetermine the size of the zunyite unit cell to check against previous values and to make certain the conversion from atomic parameters to interatomic distances. Layer-line spacings on oscillation photographs gave a mean value of $\zeta_1 = \lambda_{Cu} / a_o = 0.110$. When this value was used in indexing the oscillation photographs, a systematic difference between expected and observed positions appeared. This difference was proportional to reciprocal radius ξ, and could be eliminated by a revision of ζ_1 to 0.111.

The most accurate determination of ζ_1 was derived from a Straumanis photograph (No. 12, see Fig. 13) made with Crystal No. 3. With the nearly correct value $\zeta_1 = 0.111$ it was possible to attempt indexing of the 3 equatorial spots at highest Bragg angle on the Straumanis photograph. High-angle reflections were used because they give the most accurate determination of a_o, the accuracy being proportional to

$$\left[\frac{d}{d\theta} a_o\right]^{-1} \propto \tan\theta$$

which increases as $\theta \longrightarrow 90^\circ$. Bragg angles were measured by the usual Straumanis technique, using three reflections at small angle to fix the $2\theta = 0^\circ$ position. The reflections were found to be (12. 12. 0), (16. 6. 0) and (16. 8. 0) and gave values $\zeta_1 = 0.1111$, 0.1110, and 0.11104, the last value being for (16. 8. 0), at a Bragg angle $\theta = 83.^\circ 3$.

These measurements were regarded as preliminary, and were made on a North American-Phillips powder film-measuring viewer. The amount of data available on the Straumanis photograph (about

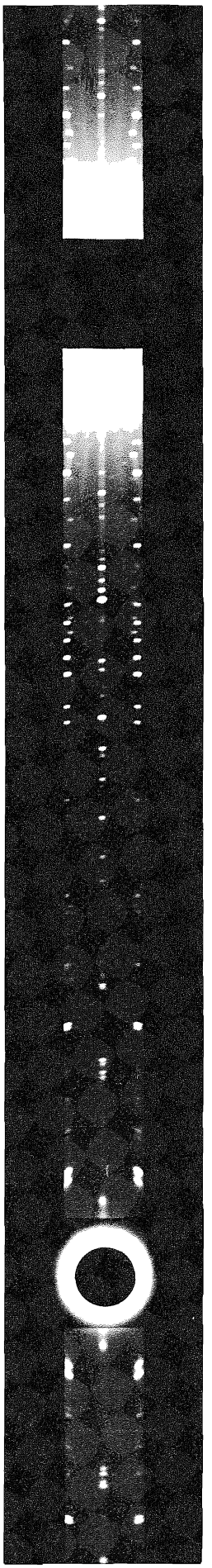

Fig. 13

50 equatorial reflections) would make possible an accurate statistical determination of the cell size. Although this has not been carried out, the results of the preliminary measurements show that we can adopt with some confidence the value $\zeta_1 = 0.11104 \pm .00005$.

Using the most recent value (Clark, 1956) $\lambda_{Cu\ K\alpha} = 1.5405$ Å, we derive $a_o = 13.87_4 \pm .007$ Å. This value is to be compared with Pauling's (1933, p. 442) value of $a_o = 13.82$ Å. The ratio 13.874/13.82 = 1.0039 is in part accounted for by the difference between the "Ångstrom" units employed in 1933, now called k X.U., and present-day Angstrom units, there being 1.0020 Å in one k X.U.

VI. THE PROCEDURE OF TESTING AND REFINING THE STRUCTURE

1. General. -- The present study of the zunyite structure can be divided into three phases: (1) testing and preliminary refinement using a limited part of the (h k O) data; (2) systematic refinement by least squares and difference synthesis methods using all (h k O) data; (3) final study of (h h l) data for comparison with results of the (h k O) refinement and for answering certain questions which could not be tested with (h k O) data.

The testing and preliminary refinement was carried out by hand calculation of structure factors and of Fourier line and plane projections. Systematic refinement began with the use of the least squares method, but difficulties in applying this method to the refinement of temperature parameters made it desirable to use difference maps so that the effects of parameter changes could be directly seen. After refinement of temperature parameters using this method, the final refinement of the structure was completed by the least squares method. The calculations required for handling (h h l) data are so extensive that only a limited study of these data could be made. However, projections on the $(1\bar{1}0)$ plane verified all of the essential results of the (h k O) refinement.

In this chapter we describe this refinement process from the standpoint of the results obtained and of the motivation for the procedure. Our aim is to present a relatively coherent picture of the refinement and to point out the special problems which arose, problems which seem to be of general interest in connection with modern structural refinement methods. To do this we postpone discussion or

derivation of the details of these methods until later chapters.

2. Testing and Preliminary Refinement. -- The zunyite space group has tetrahedral symmetry and therefore has no centers of symmetry. The projection of T_d^2 on the $\{100\}$ plane has the plane group symmetry p4m (International Tables, 1952, p. 66). Because this plane group contains 2-fold axes, it is centrosymmetric, corresponding to the fact that the octahedron and tetrahedron cannot be distinguished when projected onto $\{100\}$. Because all crystallographic calculations are simplified for centrosymmetry, because refinement may be expected to be faster for centrosymmetric than for non-centrosymmetric data, and because the variances of atomic positions derived from a given amount of data are expected to be twice as great for non-centrosymmetric structures as for centrosymmetric ones (Cruickshank, 1950, p. 72), the $\{100\}$ projection was chosen for the main refinement of the structure. This projection is described by the (h k O) data.

Preliminary testing of the structure was carried out using (h k O) data out to $\sin^2\theta/\lambda^2 = 0.5\,\text{Å}^{-2}$, slightly beyond the copper limit at $0.42\,\text{Å}^{-2}$. There were 43 reflections in this group. Structure factors were calculated by hand for these reflections, and converted to logarithmic intensities without application of a Debye temperature factor correction. The differences $\log I'_o - \log I'_c$ (the primes indicating that the intensities are corrected for the Lorentz and polarization effects) were plotted against $(\sin^2\theta/\lambda^2)$. Although there was considerable scatter in the points, it was possible to estimate a linear regression line, and thus to determine provisional scale and temperature factors for the data. The calculated logarithmic intensities were then corrected for

thermal vibration using the provisional temperature factor parameter $B = 0.61$. Observed and calculated logarithmic intensities so corrected were reduced to the same scale and then converted to structure factor values and compared. The resulting residual R_1 was 0.33. This value is not entirely representative, because it is based only on data but $\sin^2\theta/\lambda^2 = 0.5$, but it serves to show the general initial agreement between calculated and observed structure factors for (h k O) data. It is surprisingly higher than the value $R'_1 = 0.29$ derived from the intensities calculated and observed by Pauling (see p. 9). The reason for this was not definitely determined, though it may be due to the fact that Pauling's (h k O), (h k 1), and (h k 2) data went out only to $\sin^2\theta/\lambda^2 = 0.20$, with (h h h) data out to 0.32. Thus the resolution of Pauling's data was lower than for our preliminary (h k O) data, so that small errors in atomic positions would have relatively smaller effects on the calculated structure factors. Another reason for the better agreement in Pauling's calculations may be the lower dispersion of the distribution function for intensities from acentric structures, as mentioned by Wilson (1950, p. 398): only 30% of Pauling's data came from the centrosymmetric projection on $\{100\}$. While our value $R_1 = 0.33$ was higher than Pauling's, it still was well below the value 0.5 suggested by Lipson and Cochran (1953, p. 147) as the upper limit for acceptable centrosymmetric trial structures.

The success of line projections, on [100] and [110], encouraged the preparation of a two-dimensional Fourier synthesis, which we will designate F_o I (the line projections will not be discussed). This synthesis, a projection of the structure on the (100) plane, made use of

all (h k O) data for which structure factors had been calculated, that is, but to the limit $(\sin\theta/\lambda)^2 = 0.5$. In addition (h O O) and (h h O) refections out to $(\sin\theta/\lambda)^2 = 0.8$ were included. Of the 49 (h k O) reflections in this group, three were omitted because their signs were in doubt at this stage. Calculation of the synthesis was carried out by hand, using Beevers-Lipson strips.

The resulting electron density map is given in Fig. 14, which shows only the asymmetric unit of the projected structure, comprising 1/32 of the projected area of the unit cell (see Fig. 25 c). The atomic positions assumed in the trial structure are plotted, using small crosses. The general representation of the assumed structure is good. The electron density is high at all positions where atoms were assumed to be located. In addition, there are several unexpected peaks. None of these peaks reach the height of the lowest well-defined atomic peak, the single oxygen peak at O'_{IV}, though they approach the height of the somewhat diffuse single oxygen peak at O''_{III}. It was originally thought that these low peaks, or some of them, might represent electron density localized near protons in the structure, but all of them proved later to be false.

The resolving power of F_o I is about 0.5 Å. The Al'_{II} and Si_{II} peaks, at about this distance, are separated but not strongly resolved. The Al''_{II} peak is not resolved from its mirror image in the adjacent asymmetric unit. The O'_V atom is lost entirely, although it doubtless contributes to displacing the Si_{II} peak away from its assumed position.

F_o I suggests that several atoms are displaced from their assumed positions in the structure. The biggest displacement is

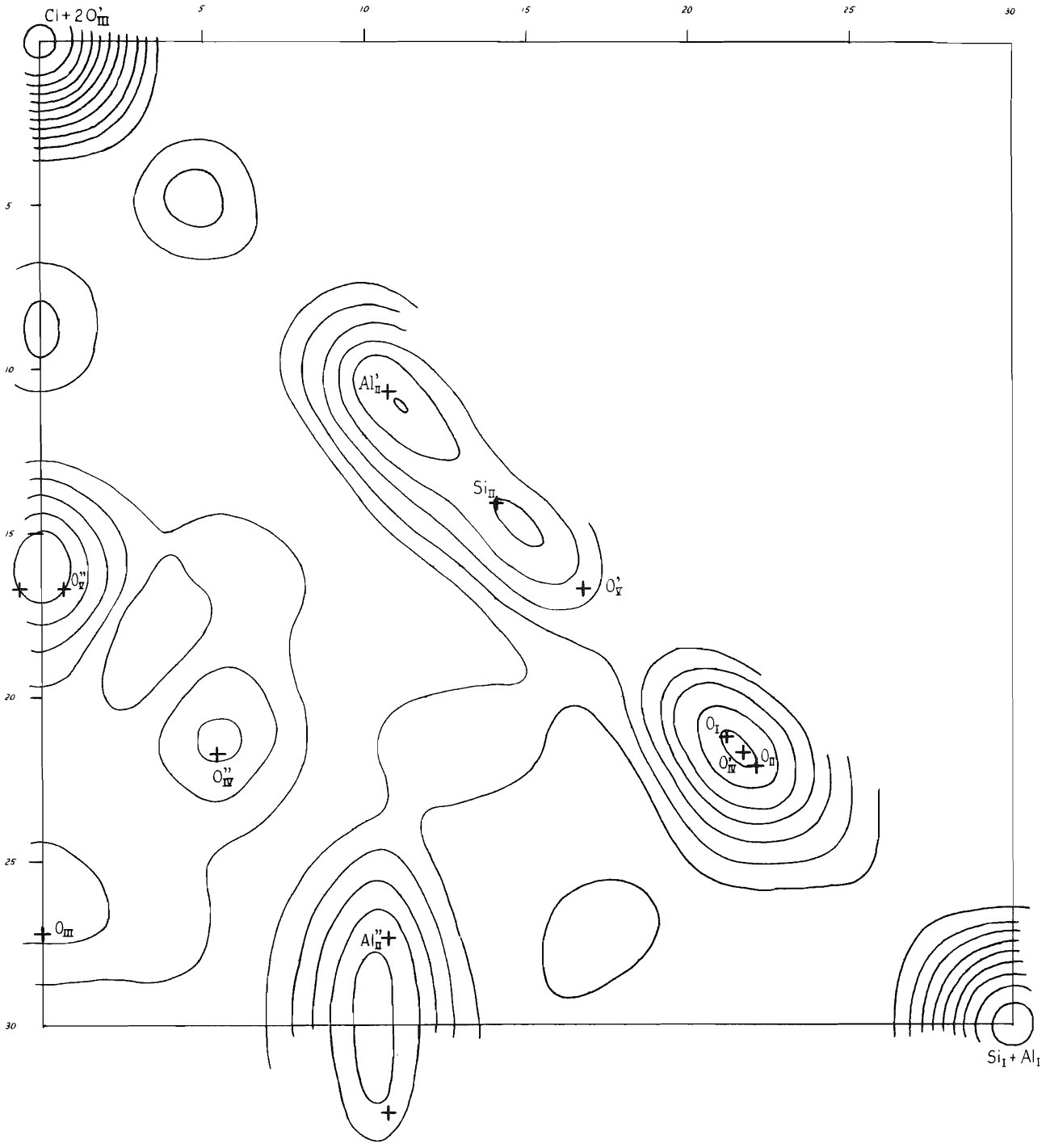
Cl + 2O'III
5
10
15
20
25
30
Al'II
SiII
O'V
O"V
O"IV
OI
O'IV
OII
OIII
Al"II
SiI + AlI

Fig. 14

indicated for O_{III}. The lack of resolution of the Al''_{II} peaks suggests that these atoms are actually closer together (as seen in the projection) than assumed. The same is indicated for O_V by the shape of the double O''_V peak. A displacement of this double peak is also suggested.

Parameter changes corresponding to the indicated atomic displacements for Al_{II}, O_{III}, and O_V were estimated from F_o I. The new positions for O_{III} and O_V were chosen at the centers of the corresponding peaks. The z coordinate of O_V, which is the displacement of O''_V away from the mirror line located along the [100] axis, was taken to be zero because of the shape of the double O''_V peak, which is elongated along [100] rather than transverse to it. The z parameter of Al_{II}, which determines the separation of Al''_{II} from its mirror image, was changed. The new value of $z_{Al_{II}}$ was derived by a method suggested by Professor Pauling, in which the distance between two appropriately shaped one-atom peaks was adjusted to give an unresolved double peak of the observed shape. The new parameters chosen in this way are contained in Table V, which summarizes the parameter values obtained at successive stages of the refinement.

With the use of the three new parameters, structure factors for 12 reflections showing particularly large discrepancies were recalculated to see if the parameter changes tended to improve the agreement between calculated and observed values. No improvement in the general agreement was evident. Structure factors for (h O O) reflections out to (24. 0. 0) were then systematically recalculated, and it was found that the residual R_1 for these 12 reflections, originally at 0. 25, remained at this value as a result of the parameter changes. The meaning of this

TABLE V

PARAMETER REFINEMENT
VALUES OF THE PARAMETERS AT STAGES IN THE REFINEMENT

SF	0	I	II	III	VI	VIII	XI	XIII	Final
Result of:	Trial	LSO	LSI	LSII	ΔFIII	ΔFIV LSV	SFVIII	LSVIII	
R_1	0.33	0.27	0.17	0.175	0.123	0.117	R_1 --- R'_1 0.27	R_1 0.18 R'_1 0.27	
Data	43(hkO)	(hkO)	(hkO)	(hkO)	(hkO)	(hkO)	(hhl)	(hhl)	
Si_{II} x_1	.117	.117	.114	.1145	.1139	.1141	.1141	.1141	.1141
O_I x_2	-.177	-.177	-.173	-.1742	-.1737	-.1747	-.1747	-.1733	-.174
O_{II} x_3	.184	.184	.184	.1828	.1823	.1818	.1818	.1818	.1818
O_{III} x_4	.273	.282	.279	.2791	.2799	.2796	.2796	.2776	.279
O_{IV} x_5	.181	.181	.179	.1793	.1793	.1793	.1793	.1793	.1793
O_{IV} z_5	.545	.545	.547	.5471	.5471	.5466	.5466	.5479	.547
O_V x_6	.139	.139	.139	.1389	.1382	.1385	.1385	.1385	.1385
O_V z_6	.006	.006	.002	.0010	.0010	.0000	.0000	.0000	.0000
Al_{II} x_7	.089	.089	.085	.0853	.0853	.0853	.0853	.0853	.0853
Al_{II} z_7	-.228	-.232	-.233	-.2330	-.2330	-.2333	-.2333	-.2333	-.2333
$\mathcal{M}$	1.00	1.00	.93	.92	.92	.92	.92	.92	
B_{Si}					.28	.24	.24	.24	
B_{Al}					.26	.24	.24	.24	
B_{Cl}	0.6	0.5	0.5	0.5	.77	.90	.90	.90	
B_{OH}					.57	.62	.62	.62	
B_O						.52	.52	.52	

peculiar result was investigated by carrying out a simplified least squares adjustment of the (h O O) data, in which the three contributions to the structure factor from the three atoms O_{III}, O_V, and Al_{II} were treated as the independent variables. This calculation showed that the O_V atom should not have been moved at all, and that the O_{III} and Al_{II} atoms should be moved by the full amount indicated by F_o I. Upon moving O_V back to its original position and recalculating structure factors for the (h O O) reflections, R_1 for these reflections dropped to 0.20.

Later work showed that the position of the double O_V'' peak was displaced in F_o I, due, probably, to series termination effects. The shape of the peak was, however, correct, and the suggested choice of $z_{O_V} = .000$ was in fact later established.

The studies described above served to establish that the trial structure was essentially correct, at least as seen in projection on {100}, and they suggested that it would refine. A program of systematic refinement was therefore undertaken. This program consisted of, first, a series of least squares refinements, followed by several refinements using the methods of difference synthesis, and finally a last least squares refinement. The change from least squares to difference synthesis refinement was not planned in advance, but was dictated by difficulties which arose in the course of the refinement.

3. Systematic Refinement. -- The lengthy calculations required for the systematic refinement procedures were carried out by punched-card methods on the IBM machines of the C.I.T. Digital Computing Laboratory, 206 Throop Hall. Using the scale factor derived in the

the preliminary calculations, the (h k O) structure factors were reduced to the absolute scale of the calculated structure factors. These structure factors, together with the appropriate atomic scattering factors for each reflection, and other information, were punched onto IBM cards and thereafter all major calculations were carried out by machine.

The first step in systematic structural refinement was calculation of structure factors for all (h k O) reflections, and comparison with observed values. The first of these calculations using all the (h k O) data was designated S.F.I. The parameters used in S.F.I. were those given by the trial structure for all atoms except O_{III} and Al_{II}, for which the parameters derived from F_o I. were used. The temperature factor parameter B was arbitrarily taken to be 0.5. The results of S.F.I. gave a residual $R_1 = 0.27$. Considering that the original value $R_1 = 0.33$ was derived from data only out as far as the copper limit, it is seen that the preliminary parameter change derived from F_o I. caused a marked improvement in the agreement.

A least squares adjustment of the calculated structure factors was then made for variation of all positional parameters, and for temperature parameter B and for scale factor $\mathcal{A}$ (which was taken equal to 1.00 in S.F.I.). This calculation was designated L.S.I. It was carried out in the fullest detail of the least squares method, with the use of all terms of the normal equation matrix. Two sets of normal equations were derived. In L.S.I.A., all the (h k O) data were used except for a group of about 15 reflections rejected because of uncertainty in the sign of F_o. In L.S.I C , only reflections for which $\sin^2\theta/\lambda^2 \leq 0.6$ were included. Almost all the parameter shifts

derived from L.S.I C were larger than those from L.S.I A, suggesting that at this stage in the refinement the structure factor derivatives were not sufficiently reliable for high order reflections to give a satisfactory indication of the required parameter changes. For the sake of more rapid convergence of the refinement, therefore, the positional parameter shifts given by L.S.I C were adopted.

The parameter changes derived from L.S.I are given in Table VI, along with all parameter changes calculated in this study.

With use of the new parameters from L.S.I C , including the new scale factor but not a new temperature factor, structure factors for all (h k O) reflections were recalculated (S.F.II). The residual R_1 dropped to 0.17, a distinct improvement.

A second least squares refinement was then made (L.S.II), with variation for positional parameters only, and with use of (h k O) reflections for which $\sin^2\theta/\lambda^2 \leq 1.1$ (about 90 reflections). The parameter shifts obtained were all small (Table X), only 3 shifts being as large as .001.

Surprisingly, the residual derived from the new parameters went up slightly, to 0.175. There are three possible reasons for this: (1) the least squares adjustment was for only part of the (h k O) data, whereas R_1 is calculated for all the (h k O) data; (2) the least squares adjustment is for minimization of the weighted sum of squares of differences between calculated and observed structure factors, whereas R_1 is calculated from the unweighted sum of absolute values (not squared) of the differences; (3) there were errors in the calculations. Although we did not investigate the question closely, the general

TABLE VI

PARAMETER CHANGES DERIVED IN THE REFINEMENT

Refinement:		F_o I	LS O	LS I. A	LS I. C	LS II	LS III
Used data from:		Trial	Trial	LS O	LS O	LS I	LS II
Results calc. in:		-	SF I	-	SF II	SF III	SF IV
Resulting R_1:		-	0.27	-	0.17	0.175	0.134[5]
SI_{II}	Δx_1	-	-	-.002	-.003	.005	-
O_I	Δx_2	-	-	.005	.004	-.0012	-
O_{II}	Δx_3	-	-	.001	.000	-.0012	-
O_{III}	Δx_4	.009	.009	-.002	-.003	.0001	-
O_{IV}	Δx_5	-	-	.000	-.002	.0003	-
	Δz_5	-	-	.000	.002	.0001	-
O_V	Δx_6	-.005	.000	.000	.000	-.0001	-
	Δz_6	-.006	.000	-.003	-.004	-.0019[4]	-
Al_{II}	Δx_7	-	-	-.003	-.004	.0003	-
	Δz_7	-.004	-.004	.000	-.001	.0000	-
	$\Delta \mathcal{U}$	-	-	-.09	-.07	-	-.015
	ΔB_{Si}						-.22
	ΔB_{Al}						-.16
	ΔB_{Cl}	-	-	-.07	-.13[1]	-	-.06[2](+.10)
	$\Delta B_{OH, F}$						.05
	ΔB_O						
Range: $\frac{\sin^2\theta}{2} \leqslant$		0.5	0.5 (h00) only	1.9	0.6	1.1	1.9

TABLE VI (Continued)

PARAMETER CHANGES DERIVED IN THE REFINEMENT

Refinement:		ΔF I	ΔF III	ΔF IV	LS V	LS V + ΔF III	LS VIII
Used data from:		LS II	LS III*	F III	F IV	-	SF XI
Results calc. in:		-	SF VI	SF VII[3]	SF VIII	-	SF XIII
Resulting R_1:		-	0.123	0.121	0.117	-	0.18
Si_{II}	Δx_1	-	-.0006	.0002	.0002	-.0004	.0000
O_I	Δx_2	-	.0005	.0000	-.0010	-.0005	.0014
O_{II}	Δx_3	-	-.0005	.0000	-.0005	-.0010	.0000
O_{III}	Δx_4	-	.0008	.0000	-.0003	.0005	.0000
O_{IV}	Δx_5	-	.0000	.0000	.0000	.0000	.0000
	Δz_5	-	.0000	.0000	-.0005	-.0005	-.0020
O_V	Δx_6	-	-.0007	.0000	.0003	.0004	.0013
	Δz_6	-	.0000	.0000	-.0010	-.0010	.0000
Al_{II}	Δx_7	-	.0000	.0002	.0000	.0000	.0000
	Δz_7		.0000	.0000	-.0003	.0003	.0000
	Δ *vl*	-	-	-	-		
	ΔB_{Si}	-.18	.00	-.02	-		
	ΔB_{Al}	-.18	-.08	.00	-		
	ΔB_{Cl}	.24	+.17	+.09	-		
	$\Delta B_{OH, F}$	.0	.02	+.05	-		
	ΔB_O	.0		-.05	-		
Range: $\frac{\sin^2\theta}{2} \leq$		1.9	1.9	1.9	1.9	1.9	1.9

NOTES TO TABLE VI

1. This parameter change not applied in S. F. II.

2. The value given in parenthesis is obtained by disregarding off-diagonal coefficients in the normal equation matrix. See p.57.

3. Calculated only for change in temperature parameters.

4. Change actually applied in S. F. III: =. 0010.

5. Half of the improvement of this value over the S. F. III value was due to a revision of the (660) and (880) intensities as a result of remeasurement. Though this revision cannot be completely justified, it is retained in Table VI, because it entered into all later calculations.

statistical validity of the least squares method leads us to think that (2) is probably the correct explanation.

But whatever the explanation, it seemed apparent at this point that the positional parameters had pretty well converged to final values, and that further least squares calculations of the same kind would not be worthwhile. Consequently a complete Fourier synthesis and a difference synthesis were prepared using the results of S. F. III for assigning signs to the observed structure factors and for deriving $F_o - F_c$ values.

The electron density map, called F_o II, is shown in Fig. 15. The comparison of F_o II with F_o I is striking. In F_o II the atomic peaks have become rounded and symmetrical and there are no significant false peaks and no areas of negative electron density. Most striking is the improvement in resolution. Al''_{II} is now well resolved from its mirror image, and O'_V is distinctly separated from the Si_{II} peak.

The contrast between F_o II and F_o I shows decisively that copper radiation does not provide adequate resolution for satisfactory description of ionic crystals. This contention conflicts with the commonly quoted statement (for example, J. H. Sturdivant, in lectures on crystal structure methods) that molybdenum radiation is not worthwhile unless necessary to avoid absorption effects, because of the longer exposure times required. Dr. Sturdivant (in lecture) defines the "resolution" of a given X-ray reflection somewhat arbitrarily as $\mu r = \pi$ where $\mu = 4\pi \sin\theta/\lambda$ and r is the minimum separation of two electrons that can be detected as separate particles using a reflection at Bragg angle θ. The maximum "resolution" is then $r = \lambda/4$. This

corresponds to the half-wavelength for the highest frequency terms in the observable Fourier analysis of the electron density, and would seem to be a reasonable measure of the smallest detail in the electron density that can be portrayed. For Cu Kα this limit is 0.4 Å, and 0.2 Å for Mo Kα. Since the atomic peaks (except Cl) on F_o II are 0.4 - 0.5 Å in width, clearly copper radiation is inadequate for describing their shape in any but the crudest way, whereas molybdenum radiation may be expected to give at least a second order description of the atomic shapes. The reason for the usual discrediting of molybdenum radiation seems to be that in organic structures the large thermal motions of the atoms make the atomic shapes much broader and more diffuse, so that on photographs with molybdenum radiation the high order reflections do not appear because temperature factors are so small (large values of B).

The atomic positions plotted on F_o II are the positions used in S. F. III, which differ but little from the final positions. The only conspicuous difference is for the O''_V positions, which coincide ($z = 0$) in the final structure. With the exception of the O'_V peak, all assumed atomic positions lie close to the electron density maxima of the corresponding peaks. The O'_V peak is doubtless displaced on account of the overlap with the outer part of the Si_{II} atom (as seen in this projection).

All atomic positions are therefore well defined except the positions of O_I, O_{II}, and O'_{IV} in the large multiple oxygen peak. Because of the complete overlapping of these three atoms,

without any chance of resolution, it might be thought that good atomic positions for them could not be derived from refinement of (h k 0) data. Actually, good positions can be obtained. O_{IV} occurs in a separate peak (O''_{IV}) where its x and z parameters can both be determined. The resolution of the X-ray data is so great that when all (h k 0) reflections are included in a least squares calculation, the size of the off-diagonal coefficient (in the normal equation matrix) representing the interaction of the O_I parameter change with the O_{II} parameter change is only 20% of the diagonal coefficients, so that the two parameter changes, while not independent, are nevertheless well distinguished.

It is therefore possible to derive accurate positions for O_I, O_{II}, and O_{IV} from (h k 0) data. Statistical study (Chapter XII) shows that probable errors for the corresponding parameters are about twice as great as for parameters derived from isolated peaks. For values of the greatest reliability, therefore, it would be necessary to work either with 3-dimensional data or with a projection in which O_I, O_{II}, and O_{IV} are resolved.

But although O_I and O_{II} positions can be derived from the (h k 0) data, it is not possible to establish which position corresponds to which atom, for the tetrahedral positions around (1/4, 1/4, 1/4) and around (3/4, 3/4, 3/4) are indistinguishable in the $\{100\}$ projection. There are, of course, strong chemical arguments which indicate the proper assignment. But verification by means of X-rays is not possible with the (h k 0) data.

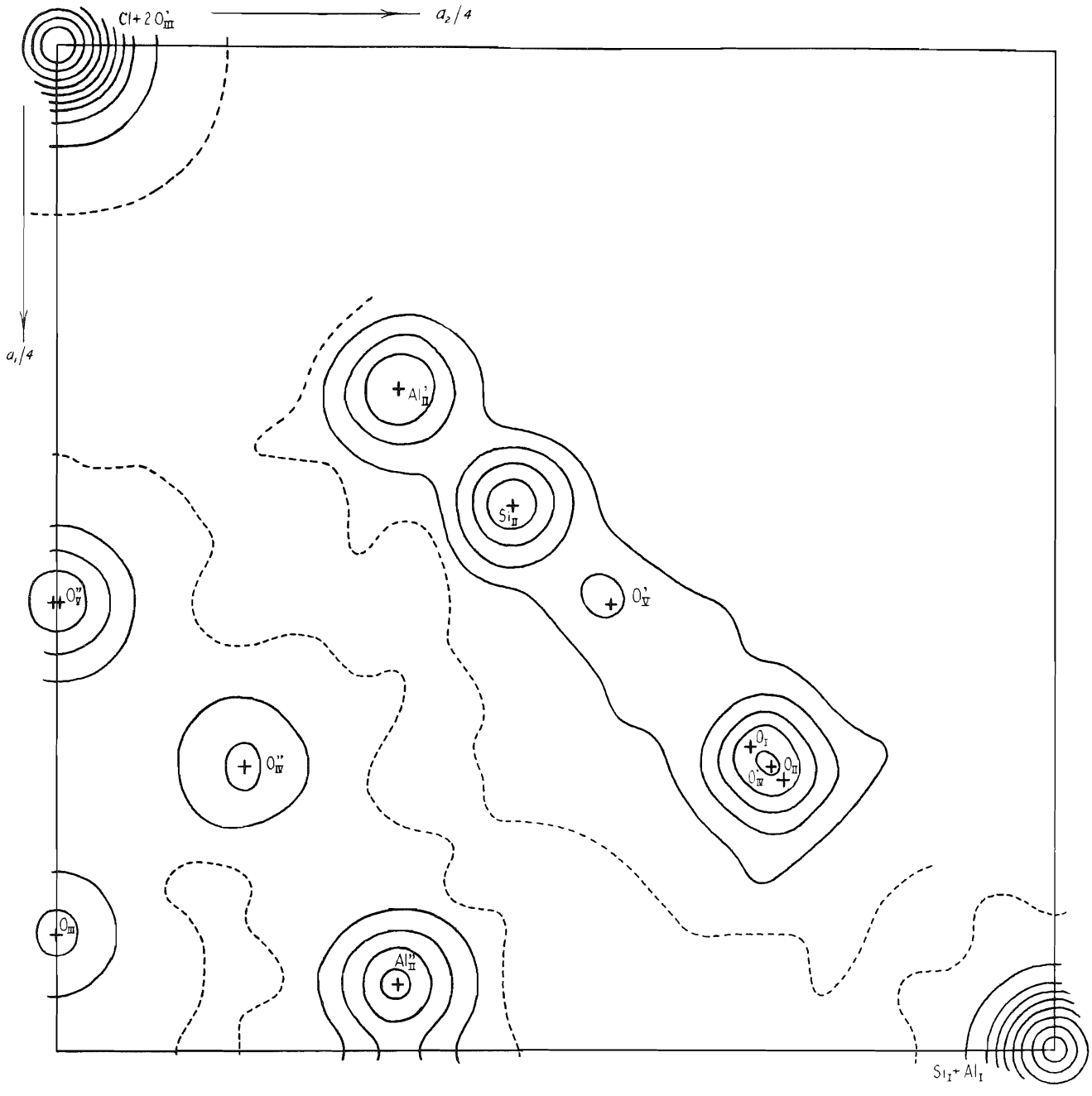

Fig. 15

Contour interval approximately 15 e A^{-2}.

Contour at 7 e A^{-2} shown dotted.

The difference synthesis prepared with the results of S. F. III is designated ΔFI and is shown in Fig. 16. The principal features exhibited by this map are the large "hole" (negative area) at the origin and the large peak, surrounded by a trough, at 1/4, 1/4. Each aluminium and silicon atom on the projection, in fact, lies at a peak. There is thus clear indication that the amplitude of thermal vibration, assumed to be the same for all atoms, is distinctly different for different atoms in the structure. The effects of the temperature factor errors so swamp any indications of positional parameter error as to make determinations of the latter quite unreliable. Hence it is necessary to evaluate the correct temperature parameters B for the individual atoms and thereby smooth out the difference map before further positional parameter refinement is undertaken.

To determine the correct temperature parameters, least squares adjustment of the (h k 0) data was carried out for variation of B_{Si}, B_{Al}, $B_{OH,O}$, and B_{Cl}. The results of this calculation, called L. S. III, were surprising. B_{Si} and B_{Al} decreased, as expected, and B_{OH} increased slightly (Table VI). But B_{Cl}, instead of increasing strongly, decreased slightly. This decrease was caused by the interaction through off-diagonal terms of ΔB_{Cl} with ΔB_{Si} and ΔB_{Al}. Such interaction did not seem reasonable physically, in spite of the results of the mathematics, and so a value of ΔB_{Cl} was calculated ignoring off-diagonal terms. The result, $\Delta B_{Cl} = +0.12$, when compared to $\Delta B_{Si} = -0.22$ and $B_{Al} = -0.16$, was simply out of all proportion to the relative

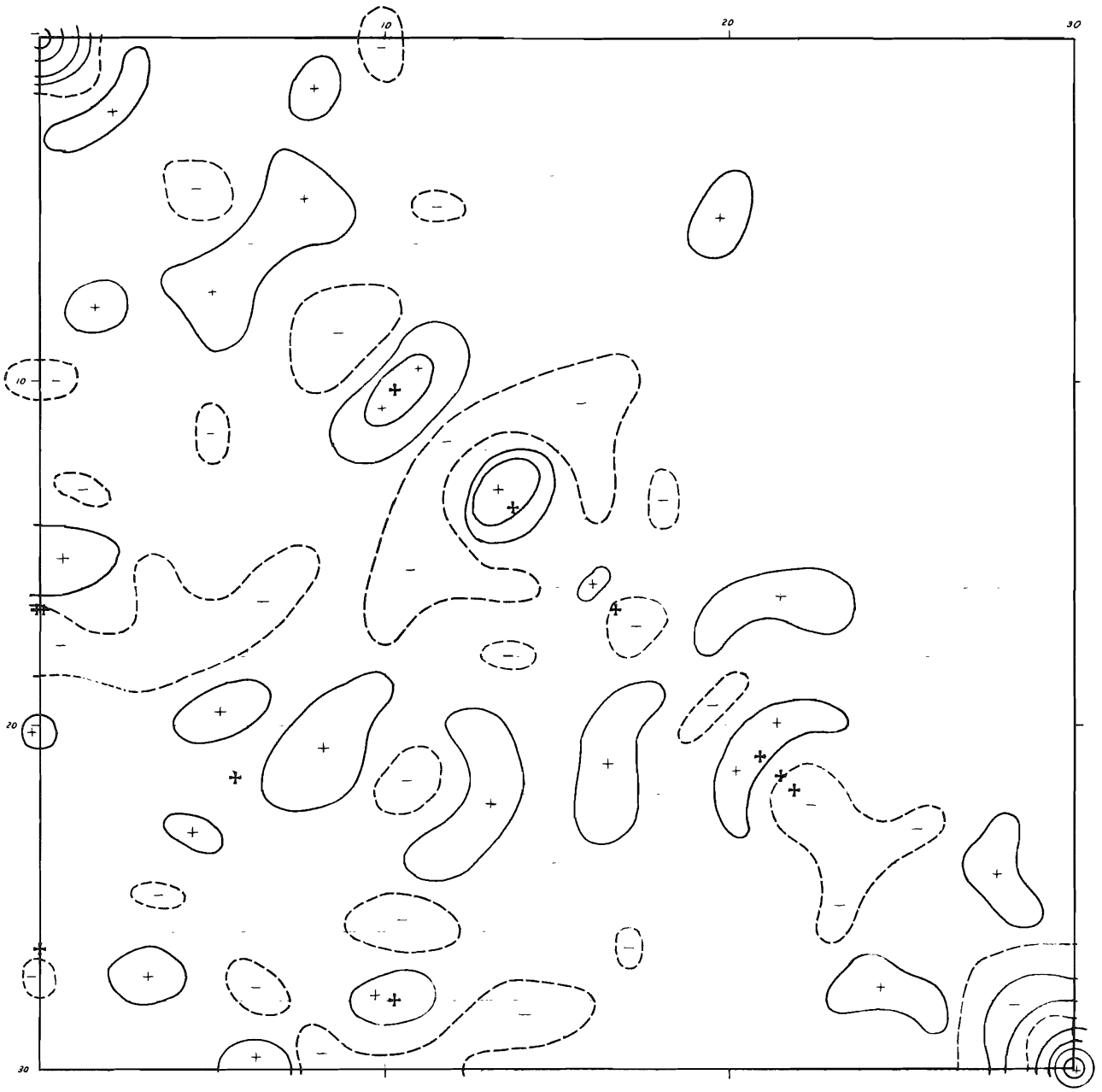

Fig. 16 -- Difference Synthesis ΔF I.

Contour interval approximately 3 e A^{-2}

trough depth and peak heights for the single Cl trough and the single Al^{t}_{II} and Si_{II} peaks. Without any question the largest temperature parameter change was expected for chlorine.

These unsatisfactory results raised the possibility that the electron deficiency at the origin might be due to a statistical deficiency of chlorine atoms in the structure. Such an interpretation was favored by the weak shoulder around the Cl trough, when compared to the deep trough surrounding the Al_I-Si_I peak at 1/4, 1/4. The reported analyses of zunyite showed no strong suggestion of a deficiency of chlorine, however. Nevertheless, a least squares adjustment for variation of a compositional parameter a for chlorine was carried out to test this possibility. When the previously calculated values of the ΔB's were introduced into the additional normal equation involving Δa, the value $\Delta a = +0.011$ was calculated. This allowed no change of the chlorine parameter, because $a = 1.00$ represented 100% occupation of the chlorine sites in the structure. When the normal equations were solved simultaneously with inclusion of terms due to Δa but ignoring interactions of ΔB_{Cl} with ΔB_{Si} and ΔB_{Al}, the result obtained was $\Delta a = -0.08$, $\Delta B_{Cl} = -0.015$, $\Delta B_{OH} = +0.031$. This value for Δa was not in agreement with what could be estimated from the depth of the trough at the origin.

These contradictions and discrepancies caused us to lose confidence in the least squares method when applied to this problem. The fact that the method gives reasonable values for ΔB_{Si},

ΔB_{Al}, and ΔB_{OH} is evidence that the calculations were carried out correctly. There was abundant opportunity for checking the calculations, too, because of the repetition involved in setting up to calculate the normal equations for compositional parameter variation. We are unable to explain these difficulties. Perhaps they are related to the greater probable error of electron density at special positions (Cruickshank and Rollett, 1953).

Because of these difficulties we turned to methods of deriving temperature factors directly from difference maps. A method for this has been given by Cochran (1951 b). For reasons given in Chapter X, however, we found it desirable to develop our own methods independently. The resulting formulae were applied to ΔF I. In succeeding difference maps, temperature parameter correction was carried out synchronously with positional parameter correction also derived from the difference maps. By these procedures R_1 was lowered from 0.154 to 0.121.

The last difference map that was calculated is shown in Fig. 18. Irregularities attributable to parameter errors have been largely removed. The final temperature parameter corrections were calculated from the remaining irregularities around atomic positions. There are several regions showing irregularities not associated with atomic positions. These irregularities can presumably be due only to errors in the X-ray data. The shapes of some of the irregularities around atoms along the diagonal (x, x) suggest possible applicability of anisotropic temperature factors. The most pronounced indication is the negative region on the [110] diagonal, adjacent to the Si_I-Al_I peak. This

feature suggests a need for tetrahedral temperature factors for these atoms. Application of such factors was studied, but theoretical considerations (Chapter XI) indicated that the observed electron density discrepancies could not be accounted for by any reasonable atomic motions of the required symmetry.

The Cl + $2O_{III}$ position still presents a problem. At the stage of refinement of ΔF IV, the increased B_{Cl} has wiped out all vestiges of the positive shoulder around the trough at the center of the atom. The final trough is probably the effect of an error in the Fourier scale, as discussed in Chapter X.

Because the effective weighting system in difference synthesis refinement differs from the weighting system used in least squares refinement (Cochran, 1948, p. 139), it is to be expected that coordinates obtained by the two methods may differ slightly. The structure had for practical purposes reached complete refinement using the difference synthesis method (see Table VI under the heading ΔF IV, where all positional parameter shifts are very small). Because least squares refinement is more satisfactory statistically, however, we returned to this method to see (1) what effect temperature factor refinement had on positional parameters given by the least squares method, and (2) how greatly coordinates determined by least squares and difference synthesis methods differ in a practical case. The results of the final least squares refinement performed on (h k 0) data (L.S. V.) are shown in Table VI. Although all parameter changes are small, there is a general small readjustment from the values given by the difference syntheses.

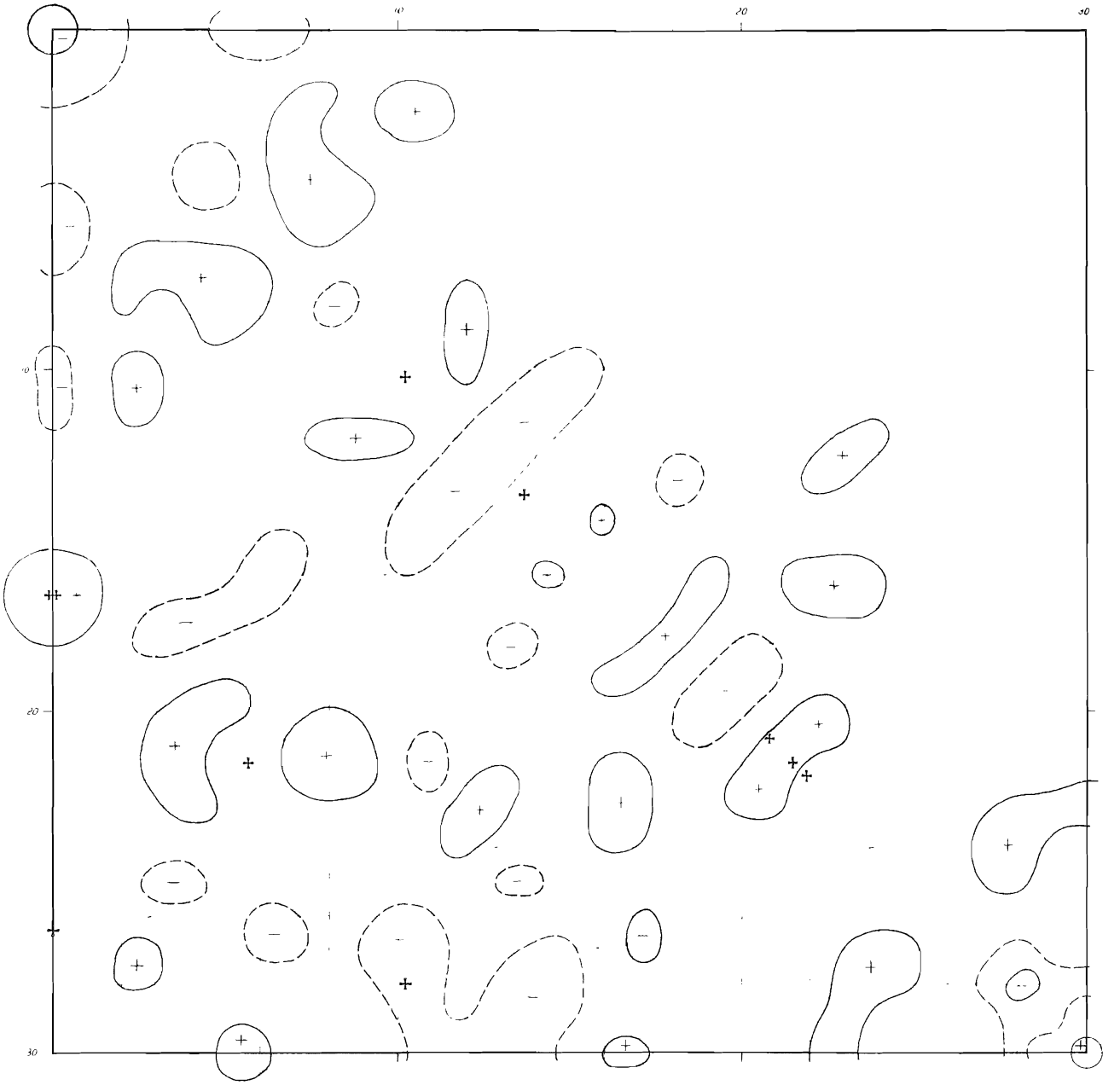

Fig. 17 -- Difference Synthesis ΔF IV.

Contour interval approximately 3 e A^{-2}

These readjustments are of the same order of magnitude as the parameter variances derived in Chapter XII, a fact which seems to be in contradiction with the statement by Lipson and Cochran (1953, p. 283) that "all reasonable systems of weighting lead to coordinates which differ by amounts small compared with the random errors of the final coordinates."

It is necessary to consider the question, whether the results of L.S. VII show the (h k 0) refinement to be converged or not, in the least-squares sense. Strictly speaking, they do not, because convergence requires that the coordinate changes calculated from the normal equations should be zero. Strictly speaking, therefore, at least one additional least squares refinement of the (h k 0) data would be required to test the convergence. In discontinuing the refinement at this stage, we were prompted by two considerations: (1) The refinement may be regarded as converged when coordinate changes are small compared to coordinate variances; and (2) in a rapidly converging refinement, if the coordinate changes resulting from a least squares calculation are of the size of the coordinate variances, it may be expected that the changes given by the next least squares adjustment will be small compared to coordinate variances. In the present case we have removed the effects of the difference synthesis coordinate refinement by combining the results of ΔFIII plus L.S. VII in a separate column in Table VI. The sequence of significant least squares refinements is then L.S.0 (except 0_V), L.S.I, L.S.II, and (ΔFIII + L.S. VII). (The 0_V coordinate changes in L.S.0 are not to be considered, because x_6 and z_6

were not treated as independent in L.S.0). It is seen from a comparison of L.S.0 , L.S.I , and L.S.II that the convergence was rapid. Most coordinate changes in L.S.II are only a tenth as large as those in L.S.I. The main exceptions are Δx_2 and Δx_3, the parameter shifts for O_I and O_{II}, which, because of the overlap, cannot be expected to converge rapidly without inclusion of all the (h k 0) data. Δz_6 is a special exception, discussed below.

Comparison of the parameter changes in L.S.II with those in (ΔFIII + L.S. VIII) shows, however, that the latter are generally as large or somewhat larger than the former, and that both are about the size of the parameter variances, all of which are less than 0.001, (see Chapter XIII). This demonstrates the effects on positional parameters of correction of temperature parameters. It is expected that these effects should be of the order of magnitude of the parameter variances, or larger. Because no further temperature parameter correction would be required in further refinement of the structure, it seems reasonable, in view of the rapid coordinate convergence in the sequence L.S.I - L.S.II, that coordinate changes derived by refinement of the coordinates obtained in L.S. VII would be small compared to the coordinate variances. These considerations, although reasonable, should be tested by computation while the punched cards are still available. That such calculations have not been carried out is due principally to the fact that more serious problems were found in calculations carried out with the (h h l) intensities.

The z coordinate of O_V, z_6, presented a peculiar problem

in the refinement. The shapes of the double $0''_V$ peaks in F_o I and F_o II indicated quite unequivocally that we should take $z_6=0$. L.S.I forced z_6 down to 0.002. The Δz_6 of L.S.II would have given $z_6 = 0.0001$, but, because $\partial F_c/\partial z_6 = 0$ strictly for $z_6 = 0$, we chose $z_6 = 0.0010$ to observe the next refinement. Difference maps are unable to predict a parameter shift in such a case, but L.S.VII gave $\Delta z_6 = -0.0010$. Hence z_6 is certainly less than 0.0010 and may well be strictly zero.

4. Study of (h h l) Data. --The chief reasons for the desirability of studying the structure in other than {100} projection are as follows: (1) inability to distinguish between 0_I and 0_{II} in the {100} projection, and relatively large uncertainty in the parameter values derived; (2) relatively large variance for the z_6 parameter (0_V) owing to overlap with 0_I and 0_{II}; (3) inability to choose an accurate value for z_6 when it is so near zero, without carrying out a series of least squares refinements for this parameter; (4) inability to make a reasonable statistical estimate of the variance of z_6, without going to a second order theory; (5) inability to distinguish the positions (0, 0, 0) where a vacancy is assumed in the trial structure, and $(\frac{1}{2}, \frac{1}{2}, \frac{1}{2})$, where the chlorine atom has been placed; (6) desirability of a refinement using independent data.

The last point has been emphasized by Sten Samson (in conversation). The practical investigator, while he makes use of the statistical methods developed by Cruickshank and others to assess the reliability of the coordinates he has derived, would

very much like to see the theoretical results put to a practical test by independent refinement of the same structure using independent data, either from different layer lines or from a different projection.

It was originally thought that final refinement of the O_I and O_{II} positions could be carried out with the use of (h h h) data, but exploratory calculations did not bear this out. We will not discuss the (h h h) calculations in detail, but simply present the results of the projection of the structure on [111] using this data. Projections of ρ_o, ρ_c, and $\rho_o - \rho_c$ on [111] are shown in Fig. 18, and it can be seen that the observed intensities, when used with phases determined from the calculated intensities, account for all the major features of the assumed structure.

One study using the (h h h) data should be mentioned: a study of the position of the chlorine atom. Although structural reasons require placing the chlorine atom at $(\frac{1}{2}, \frac{1}{2}, \frac{1}{2})$ rather than at (0 0 0), it seemed desirable to test the possibility that the vacancy in the structure at (0, 0, 0) might be occupied by chlorine to some extent. A series of structure factor calculations for the (h h h) data were made, with successively 0%, 5%, 10%, 15% and 20% of the chlorine removed from the $(\frac{1}{2}, \frac{1}{2}, \frac{1}{2})$ position and placed at (0, 0, 0). The respective residuals $R_1' = \sum |I_o - I_c| \Big/ \sum I_o$ which resulted were 0.252, 0.256, 0.259, 0.263, and 0.267. From these calculations there is therefore no suggestion of chlorine at (0, 0, 0). Although not the best calculations for the purpose,

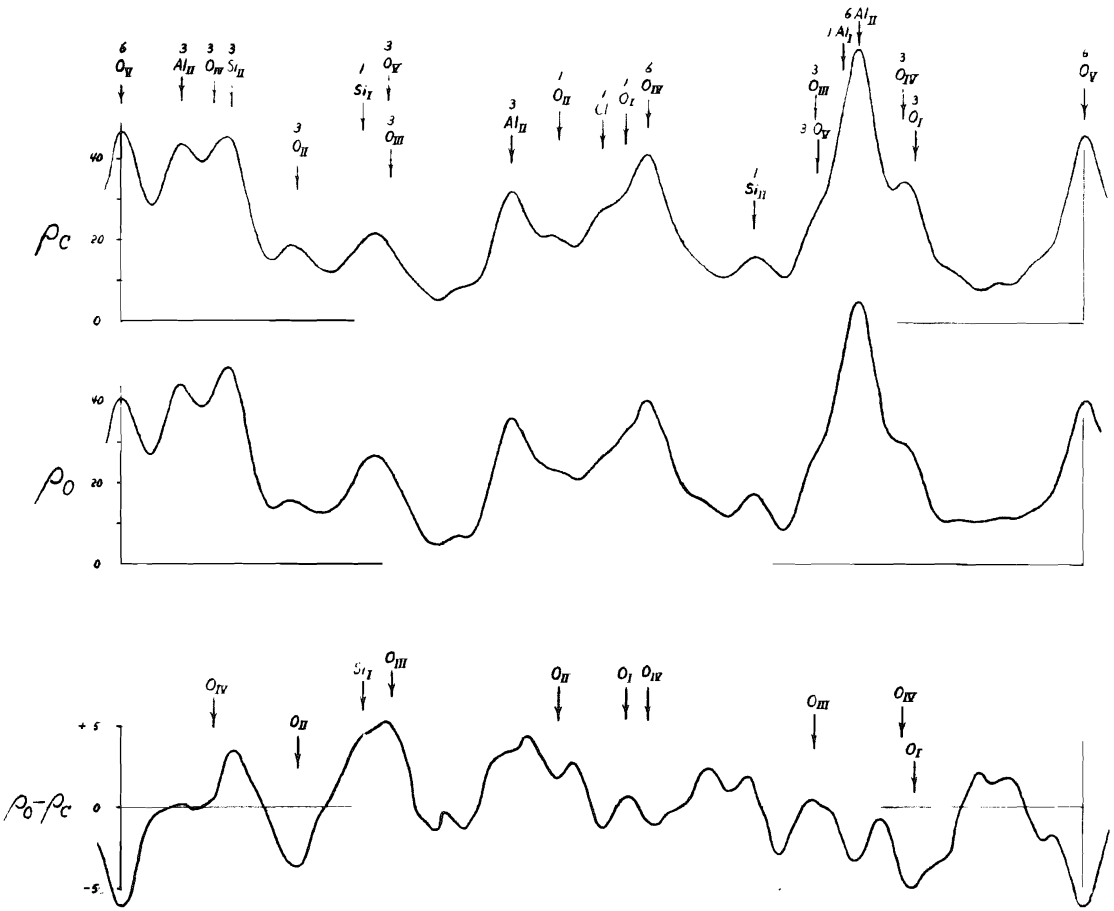

Fig. 18 -- Projection on [111]

Projection interval: 1/3 the body diagonal of the unit cell.

these results can probably also be interpreted to mean that the vacancy at (0, 0, 0) is not occupied to any extent by F^- or OH^- either.

The (h h h) calculations showed that more extensive non-centrosymmetric data would have to be used if detailed information about the structure was sought. Although X-ray photographs of upper layer lines (h k l) (l > 0) were available for Crystal No. 1, the (h h l) data from Crystal No. 5 were chosen, first, because this data was completely independent of the data obtained with Crystal No. 1, and second, because by construction of the $(1\bar{1}0)$ projection using the (h h l) data it should be possible to verify the identification of 0_I and 0_{II} directly.

The treatment of the (h h l) data was satisfying in that it was carried out with the maximum efficiency of IBM techniques. It was possible to handle two and a half times as much data as used in the (h k 0) refinement, and to carry out calculations of considerably greater complexity, in a time much shorter than was required for the development and use of procedures for the (h k 0)refinement. Nevertheless, the length and complexity of the calculations, caused by the non-centrosymmetry of the $(1\bar{1}0)$ projection, would have made systematic refinement quite tedious. Because of these limitations, the treatment of the (h h l) data was restricted to the following calculations: (1) a first structure factor calculation (S. F. XI), using the parameters derived in L. S. V; (2) a least-squares adjustment for positional parameters only (L. S. VIII); (3) a structure factor recalculation based on

the new positions (S.F. XIII); (4) a Fourier synthesis and a difference synthesis, projecting the structure onto the $(1\bar{1}0)$ plane.

S.F. XI gave a residual $R_1' = 0.27$ (actually 0.268). This corresponds to a value $R_1 = 0.18$, as determined by a direct calculation in which the square roots of I_o and I_c were extracted. The least squares adjustment (L.S. VIII) gave parameter changes listed in Table XI and discussed in Chapter VIII. The sizes of these changes is about the same as those obtained in L.S. V except for three shifts of more than 0.001. Although one of these shifts was for O_I, inspection of the Fourier synthesis F_o III (Fig. 19) showed that O_I and O_{II} had been correctly identified in the $\{100\}$ projection. The three parameter changes mentioned were the only changes considered significant, and were the only ones actually applied, as listed in Table VI. Upon recalculating structure factors with these changes, R_1' went up very slightly, to 0.270. We believe this effect is analogous to the slight increase in R_1 observed as a result of L.S. II. The parameter changes of L.S. II were applied to data more in need of temperature-parameter than of positional-parameter correction. The same is discovered to be the case in L.S. VIII.

Appendix II shows that there is a marked tendency for reflections with intensities greater than about 80.0 to be observed stronger than they are calculated, and the reverse for reflections less intense than this. Such an effect is immediately suggestive of temperature parameter error. This is brought out in striking fashion in the $(1\bar{1}0)$ difference synthesis (ΔF V), shown in Fig. 20. At the position of almost every atom there is a crater-like

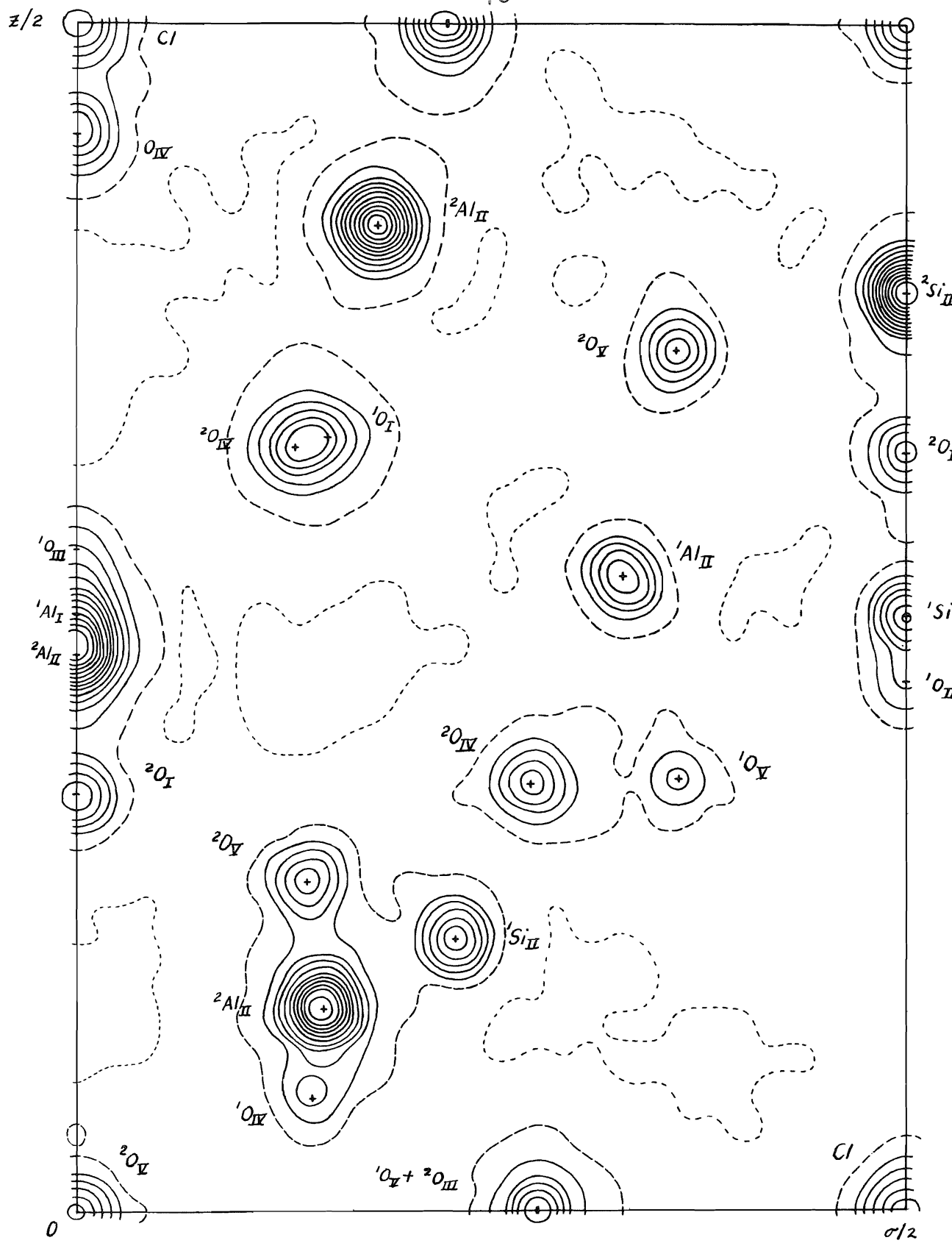

Fig. 19

Contour interval 20 e A^{-2}. Superscripts designate multiplicity (Table XII).

peak, a ring of positive density with a deep depression at the center. By applying the methods used for correcting temperature parameters for the (h k 0) data, it is estimated that an increase of 0.2-0.3 A^{-2} is required for B_{Si} and B_{Al}. This amounts to approximately doubling the B_{Si} and B_{Al}, which corresponds to a doubling of the absolute temperature. Although it is possible that the X-ray photographs of Crystals No. 1 and 5 were prepared at different ambient temperature, the absolute temperature doubling represents no possible temperature effect, but instead a systematic error in the X-ray intensity data. The recognition of this fact establishes beyond doubt the "contrast effect" which we have discussed previously, but which could only be imperfectly substantiated in direct comparisons of the (h k 0) and (h h l) data.

In a further attempt to determine which set of data contains the systematic error (supposing that only one does!), we have made a study of the first 223 $\overset{(hhl)}{\wedge}$ reflections from Appendix II. Values of $\delta = \log I_o' - \log I_c$ for these reflections are plotted against $(\sin\theta/\lambda)^2$ in Fig. 21, and against $\log I_o$ (not $\log I_o'$) in Fig. 22. It is seen that both plots exhibit regression, though we have not drawn in regression lines so as not to prejudice the reader's judgment. In Fig. 25 the regression line drops off linearly with increasing $(\sin\theta/\lambda)^2$, as would be expected for a general temperature parameter error. This slope continues out to about $(\sin\theta/\lambda)^2 = 1.0$, and the slope of the line out to this point corresponds to a temperature parameter error of $\Delta B = 0.22$, essentially what is observed on ΔF V. But beyond $(\sin\theta/\lambda)^2 = 1.0$,

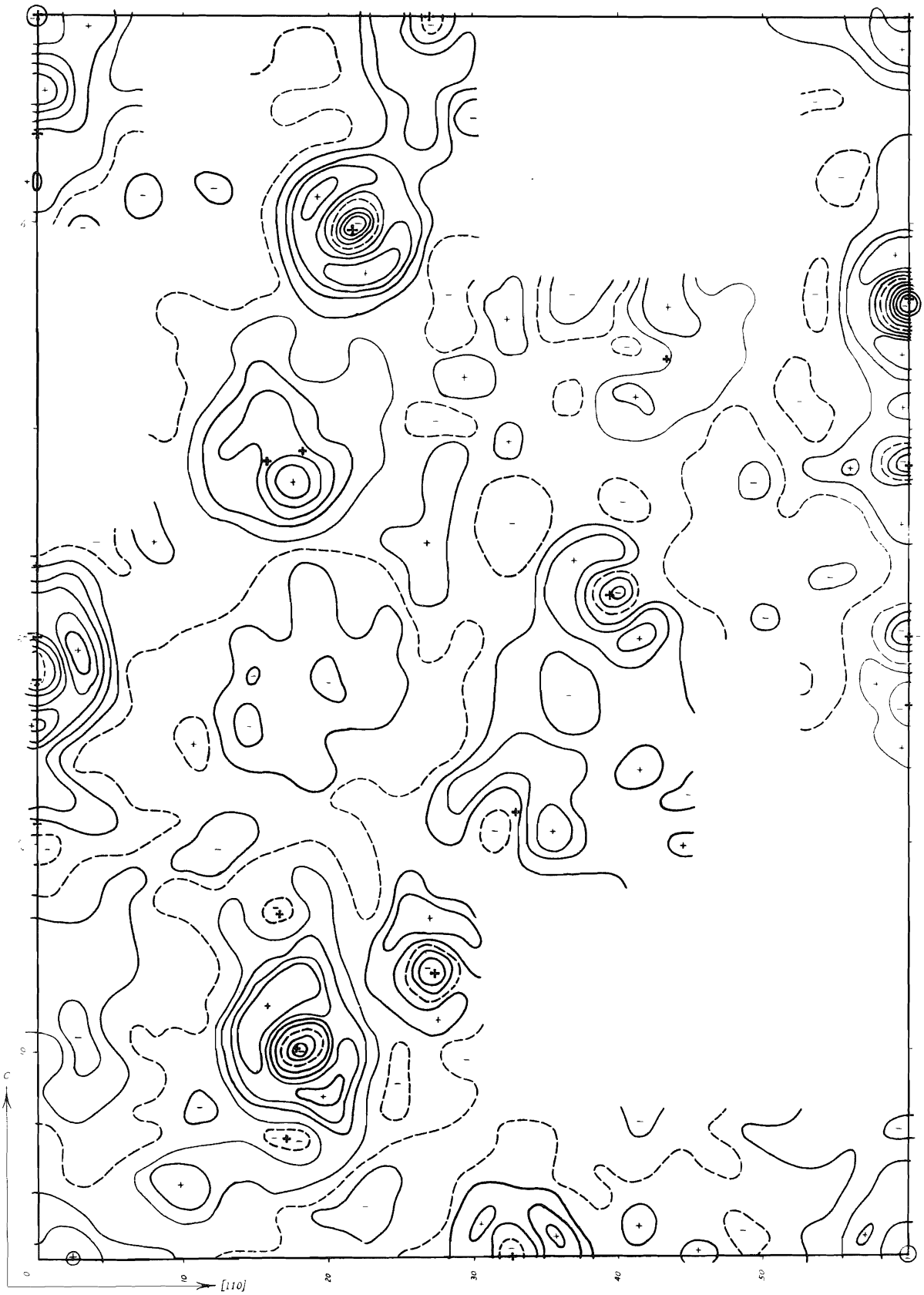

Fig. 20 -- Difference Synthesis ΔF V.

Contour interval 4 e A^{-2}.
Atomic positions as in Fig. 19

the regression no longer continues downward, but instead stabilizes at approximately a constant value of δ. There is a great enough number of points at large angles to show that this effect is real.

In Fig. 26, on the other hand, there is seen to be a distinct linear regression of δ against $\log I_0$ which persists over the entire range of $\log I_0$ except for a discrepancy at the lower end of the curve, below $\log I_0 \approx 0.4$. The few points in this lowest region are unreliable at best, because their intensities are estimated from the faintest suggestion of evidence of a spot on the photographs. The three highest intensities drop below the regression line, an effect which could be ascribed to extinction, although in view of the previous discussion of the strong reflection problem we hesitate to do this. The slope of the regression line would be about 0.17, which is in tolerable agreement with slopes encountered in the previous discussion of the contrast effect.

On the basis of Figs. 21 and 22, we submit that a regression curve can more reasonably be fitted to Fig. 22 than to Fig. 21, and that the regression curve in Fig. 22 represents the true physical effect--a contrast error--and that the regression in Fig. 21 is to be regarded simply as a consequence of the regression in Fig. 22. While these considerations locate the contrast error in the (h h l) data, it should be pointed out that the case is far from watertight, and that the type of argument presented here cannot really be relied upon without further investigation. For example, it is possible that by small positional parameter changes the calculated intensities of the high order reflections

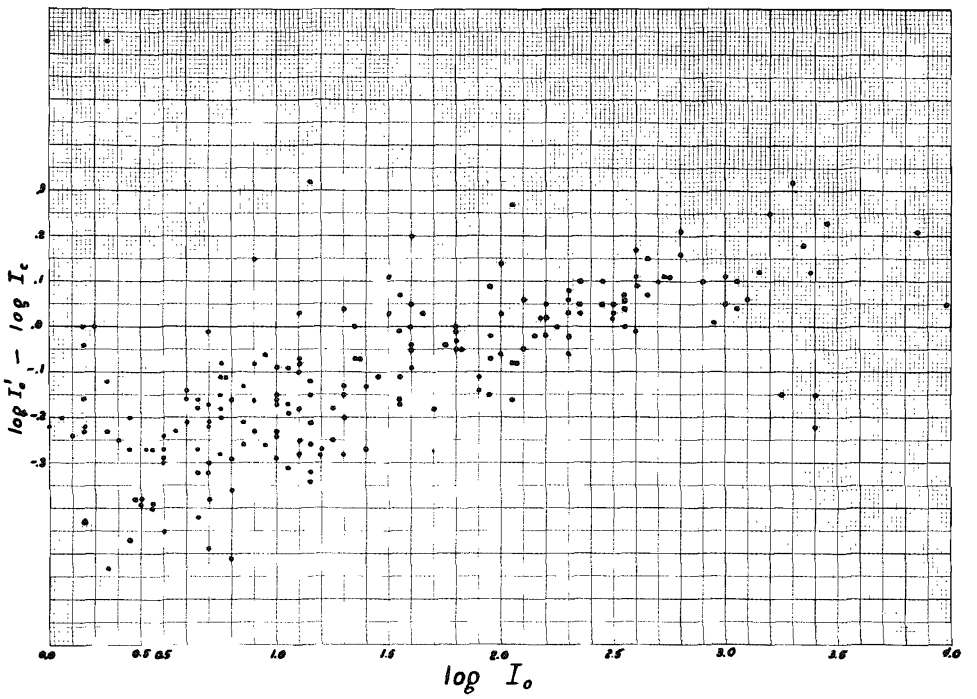

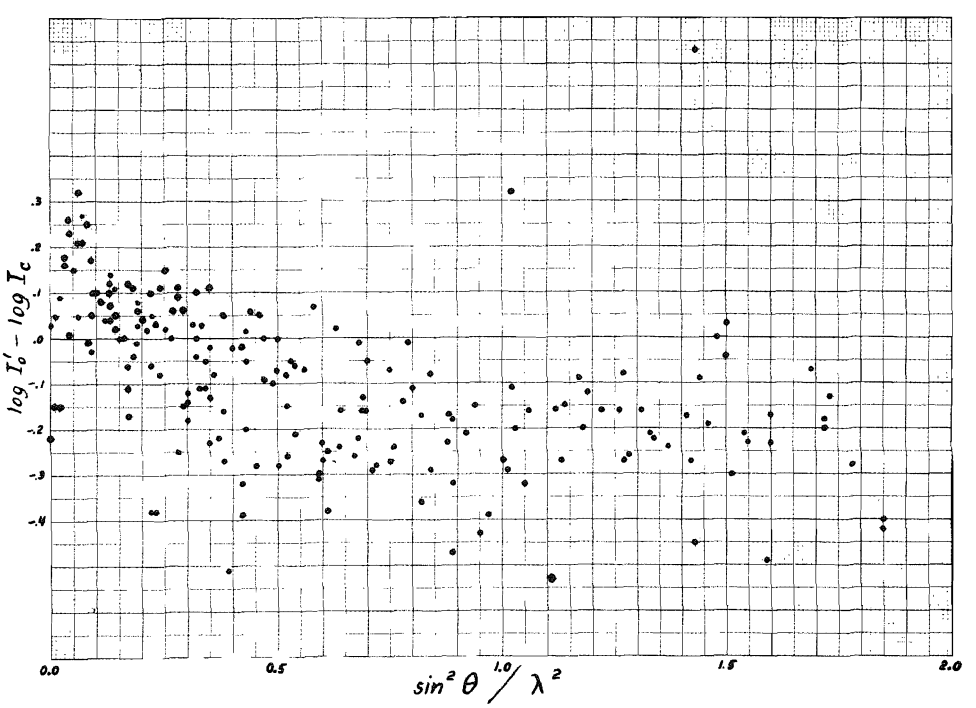

Fig. 21 (below) and Fig. 22 (above)

in Fig. 21 could be increased enough to produce a linear regression over the entire range of $(\sin \theta/\lambda)^2$. The increase required is by more than a factor of 2 for the highest angles, which seems unlikely, though perhaps possible.

Some features of the ΔF V map point toward conclusions similar to those reached in the last paragraph. While in general there is a crater-shaped peak at each atomic position, and while in general the height of the crater walls and the depth of the central depressions are roughly proportional to the heights of the atomic peaks in the Fourier synthesis F_oIII (Fig. 19), there are some conspicuous exceptions: the double peak $^1O_I + {}^2O_{IV}$, the Cl peak, the ^2O_V peak at (43.4, 43.4), the $^2O_{IV}$ peak at (0, 54.4), and the oxygen peaks in the vicinity of Al_I. Except for the latter group of oxygen peaks, overlap with other atoms is inadequate to account for most of the irregularities observed. For our purposes here a detailed study of these peaks would be unnecessarily lengthy, but we believe that the failure of the temperature parameter effect to appear as expected for some peaks is another indication that the effect is not truly one of temperature factor error, but one which only simulates it. The deviations would be produced by the high order reflections which do not follow the required regression trend of δ vs. $(\sin \theta/\lambda)^2$. It does not appear that small motions of the atoms corresponding to the deviating peaks could in all cases effect new peak shapes that would be in harmony with the general temperature parameter error implied by ΔF V.

This somewhat protracted discussion of the meaning of the discrepancies in the (h h l) data has been prompted by the necessity

to choose between the results of the (h k 0) and (h h l) refinements in adopting final positional parameters to describe the structure. The parameter shifts given by L.S. VIII are of sizes similar to those of the positional parameter variances derived from the (h k 0) data, and actually up to several times larger for the parameter shifts given in Table XI. These shifts are analogous to the parameter shifts given by L.S. II, i.e., before temperature parameter correction. It may be that the shifts given by L.S. VIII are mainly in response to the systematic errors, and that correction of these errors would reduce the shifts to small values. Because we are unable to make such a correction with confidence on the basis of present evidence, we can test the significance of the parameter shifts only by comparing them with the estimated parameter variances. In Fig. 23 the magnitudes of all 20 parameter changes given under L.S. VIII are plotted in histogram form as a frequency diagram (for a detailed discussion of these parameter changes, see Chapter VIII).

Also plotted is the normal distribution for the same number of observations and with variance $\sigma^2 = (0.001)^2$, which is the value which we have adopted as the limiting variance for all parameters, as a result of the statistical considerations of Chapter XII. The actual estimated variances (Table XVI) all lie below this limiting value, the average value being $(0.0005)^2$. The value $(0.0004)^2$ is predicted by Booth's (1946) method from a consideration of the random errors of measurement. We conclude, therefore, that the systematic and random differences between the

(h k 0) and (h h l) sets of data result in differences between parameter values which are significantly larger than differences to be expected from Cruickshank's statistical theory, and in fact about twice as large on the average; but that adoption of a limiting parameter variance of $(0.001)^2$ for all positional parameters, as we have done independently and without consideration of the contrast problem, leads to agreement between the results of (h k 0) and (h h l) refinement to within the accuracy claimed.

The upshot of these considerations is the choice of final parameters for the zunyite structure: we have adopted the values given by the (h k 0) refinement, except where they are in conflict with the (h h l) refinement to the extent of a parameter difference of greater than 0.001, as given under L.S. VIII in Table VI. In this case we have rounded off the (h k 0) results in the direction of the (h h l) prediction, to the nearest whole multiple of 0.001. The procedure is somewhat arbitrary, but we regard the result as being good to 0.001 (estimated as variance). The final parameters are given in the last column in Table IX.

Parenthetically we may add that the study of the (h h l) data, although apparently raising more problems than it solves, gives a valuable insight into the difficulties of accurate X-ray structural analysis. The problems raised have made our discussion of the refinement of the zunyite structure more lengthy and involved than we should have wished. This entire chapter, in fact, is a great deal more cumbersome than should have been required by a straightforward application of the modern structural methods that we have used. To some extent the various complications

we have discussed may perhaps be criticized as imaginary. But we believe that these complications express in some essential way the nature of a refinement process required to get parameters of the highest accuracy and to assess intelligently that accuracy. It is often said that structural refinement is a matter of pure routine. Our experience leads us to the belief that pure routine is a difficult thing to apply to X-ray data in practice.

VII. THE CALCULATION OF STRUCTURE FACTORS

1. Atomic Scattering Factors. -- f-values for atoms in the zunyite structure were obtained from the recently calculated values given by Berghnis et al. (1955). We will refer to these as the McGillavry values. The values given in the paper were plotted against $\sin\theta/\lambda$, smooth curves were drawn through the points, and f-values for the (h k 0) reflections were read from these curves. In the (h h l) calculations all f-values were derived from punched cards. The punched cards were prepared using the IBM 604 computer. For selected values of $\sin^2\theta/\lambda^2$, the computer interpolated linearly between the MacGillavry values. Linear interpolation between the values was considered accurate enough for our calculations. The f-values for (h k 0) calculations were taken to one decimal place, and for the (h h l) calculations to two places.

Scattering factors for Si^{+4}, Al^{+3}, Cl^{-}, and F^{-} were available from the MacGillavry data, but no recent scattering factors have been published for $O^{=}$. In view of the fact that atomic shapes are not critical in structural refinement, we used semiempirical methods of obtaining f-values for $O^{=}$ from published values of O and F^{-}, rather than contemplating the extensive calculations required to derive scattering factors from electronic wave functions.

First consider the comparison of scattering factors for isoelectronic atoms. Suppose that the difference in nuclear charge produces a simple scaling of the atomic shape: $U_2(\kappa) = kU_1(\varkappa\kappa)$ where $U_1(\kappa)$ is the radial charge density in atom 1, and $\varkappa$ is the size-scaling factor. k is a factor to be determined from

$$\int_0^\infty U_1(r)\,dr = \int_0^\infty U_2(r)\,dr$$

so that $k = \varkappa$. From the fact that the most probable radial distance (from the nucleus) for an electron in a hydrogen-like wave function is the radius of the corresponding Bohr orbit,

$$a = \frac{n^2 \hbar^2}{me^2(Z-s)}$$

(Pauling and Wilson, 1935, p. 140), where s is the screening constant appropriate to the orbit, the scaling factor may be taken in the form

$$\varkappa = \frac{Z_1 - s}{Z_2 - s}$$

where s is supposed not to differ greatly for ions whose nuclear charges differ by one electron unit. The scattering factors (James, 1950, p. 97) are then related by

$$f_2(\mu) = \int_0^\infty U_2(r)\,\frac{\sin \mu r}{\mu r}\,dr = f_1\left(\frac{\mu}{\varkappa}\right)$$

where $\mu = 4\pi \sin\theta/\lambda$. Thus for values μ_1, μ_2 such that $f_1(\mu_1) = f_2(\mu_2)$, we should expect $\mu_1/\mu_2 = \varkappa$.

If scattering factors for F^-, obtained from the MacGillavry data quoted above, are compared with scattering factors for Ne (Brown, 1933, p. 214), it is found that the ratio μ_{Ne} / μ_F - is a function of μ_F-, varying from 1.42 for low angles to 1.13 for $\sin\theta_F$-$/\lambda = 1.1$. This is a demonstration of the fact that the simple model of a scaled atom is

inadequate. The effective screening constant s depends on the distance from the nucleus. The $\varkappa$ for low μ is appropriate to an "average" screening constant for the whole atom, while the $\varkappa$ for high μ corresponds to scattering only from the innermost electrons and should therefore approach the unscreened value $\varkappa = 10/9 = 1.11$.

For a rough calculation, we may suppose that $\bar{s}(\mu)$ is the same for $O^=$, F^-, and Ne, where $\bar{s}(\mu)$ is the appropriate "average" screening constant for scattering at an angle defined by μ. Then we have

$$\bar{s}(\mu_{F^-}) = \frac{9\varkappa(\mu_{F^-}) - 10}{\varkappa(\mu_{F^-}) - 1}$$

so that

$$\varkappa'(\mu_{F^-}) = \frac{\mu_{F^-}}{\mu_{O^=}} = \frac{9 - \bar{s}}{8 - \bar{s}} = \frac{1}{2 - \varkappa(\mu_{F^-})} .$$

This relation has been used to calculate scattering factors for $O^=$ from scattering factors for F^-, and the results are given in column 1 of Table VII.

A second set of values was obtained by correcting the MacGillavry values for atomic oxygen with the difference between the values for $O^=$ and O given in the compilation of the Internationale Tabellen (1935, p. 571).

There is general agreement between the values obtained in these two ways, except for $\mu < 0.3$, where values obtained in the second way are higher by up to 0.4 electrons. In our (h k 0) calculations we used the second set of values.

A third set of $O^=$ f-values was obtained through the kindess of E. L. Eichhorn of the Gates and Crellin Laboratories. These are

TABLE VII

ATOMIC SCATTERING FACTORS FOR $O^{=}$

$\frac{\sin\theta}{\lambda}$	1	2	3
0.00	10.0	10.0	10.00
0.05	9.1	---	9.54
0.10	7.8	8.2	8.33
0.15	6.5	---	6.82
0.20	5.4	5.8	5.42
0.25	4.5	---	4.33
0.30	3.8	4.0	3.60
0.35	3.3	---	3.13
0.40	2.9	2.8	2.80
0.50	2.2	2.2	2.28
0.60	1.9	1.9	1.94
0.70	1.7	1.7	1.71
0.80	1.5	1.5	1.57
0.90	1.4	1.4	1.46
1.00	1.4	1.4	1.37
1.10	1.3	1.3	1.30
1.20	1.2	1.2	1.22
1.30	1.2	1.2	1.14

1. By method of Chapter VI, Section 1.

2. MacGillavry values for atomic oxygen, corrected by the difference between values for $O^{=}$ and 0 from the Internationale Tabellen.

3. Values courtesy of E. L. Eichhorn, extrapolated using MacGillavry values (atomic oxygen) for $\frac{\sin\theta}{\lambda} > 0.60$.

semi-empirical values derived by Frank Eiland. Though they cover the $\sin\theta/\lambda$ range only out to the copper limit, it is found that they can be matched nicely to atomic O values for higher values of $\sin\theta/\lambda$. These values were used in the (h h l) calculations. The slight difference in scattering factors between the (h k 0) and (h h l) calculations could cause a change in effective temperature factors for the oxygen atoms, but this change would be small compared to the differences actually observed between the two sets of data.

Scattering factors for O_I, O_{II}, and O_V were taken to be the $f_{O^=}$ values. For O_{III} and O_{IV} the values used were $f = 0.8 f_{O^=} + 0.2 f_{F^-}$, corresponding approximately to the fluorine content of the mineral.

2. Structure Factor for T_d^2. -- Although given in the International Tables (1952, p. 508), we derive the structure factor briefly here, so as to show the forms it takes for various point positions. The coordinates of the general position are x, y, z; $\bar{x},\bar{y},z$; $\bar{x}$, y, $\bar{z}$; x, $\bar{y}$, $\bar{z}$; and all coordinates obtained by cyclic and acyclic permutation of indices and by adding the four face-centering translations. The structure factor, which gives the amplitude and phase of the X-ray waves scattered by the contents of one unit cell through an angle defined by the reciprocal vector $\bar{h}$, relative to the wave which would be so scattered by a single Thomson electron at the origin of the unit cell, is

$$F = \sum f_i \, e^{2\pi i \, \bar{h} \cdot \bar{r}_i}$$

where $\bar{r}_i$ is the position of the center of the i'th atom. Consider, first, part of the contribution from the general position:

$$\phi_{xyz} = e^{2\pi i (hx + ky + lz)} + e^{2\pi i (hx - ky - lz)} + e^{2\pi i (-hx + ky - lz)} + e^{2\pi i (-hx - ky + lz)}$$

$$= (a_1 + i a_2)(b_1 + i b_2)(c_1 + i c_2) + (\ + \ )(\ - \ )(\ - \ ) + (\ - \ )(\ + \ )(\ - \ ) + (\ - \ )(\ - \ )(\ + \ )$$

$$= 4 a_1 b_1 c_1 + 4 i^3 a_2 b_2 c_2$$

where $a_1 = \cos 2\pi hx$,

$a_2 = \sin 2\pi hx$, etc. All cross product terms vanish because each of them occurs four times, half with a plus sign and half with minus. The contribution to the structure factor for a given point position p is

$$F_p = 4 f_i \sum_{P(x,y,z)} \phi_{xyz}$$

where the sum is over the permutations of x, y, and z, and the factor 4 is introduced by the face centering translation for allowed reflections. Hence for point position 48h = (x, x , z), the number of permutations is 3 and we have $F_h = A_h + i B_h$,

$$\tfrac{1}{16} A_h = (\cos 2\pi hx \cos 2\pi kx \cos 2\pi lz + \cos 2\pi hz \cos 2\pi kx \cos 2\pi lx + \cos 2\pi hx \cos 2\pi kz \cos 2\pi lx) f_i = A' f_i \qquad (1)$$

$$\tfrac{1}{16} B_h = \text{replace cos by sin} = B' f_i \qquad (2)$$

Let us now write for any point position p that is a special case of 48h = (x , x, z),

$$A_p = \gamma_p A_h \quad , \quad B_p = \gamma_p B_h \ .$$

If we expand by the same procedure used above, we obtain the following set of γ values:

Point position (Wyckoff)	48 h	24 f	16 e	4
γ	1	1/2	1/3	1/12

The structure factor is then calculated as

$$F = \sum_{p_i} \left(\gamma_{p_i} A_h(p_i) + i \gamma_{p_i} B_h(p_i) \right) ,$$

where the sum is over atoms by point positions, and we simply put in for (x, x, z) the appropriate coordinates for the atom in question. This is the form must suitable for calculation, because we can write

$$F = 16 \sum_{p_i} f_i \gamma_{p_i} (A' - i B') \tag{3}$$

and treat all atoms alike, with scattering factors $f_i \gamma_{p_i}$ where

$$f_i = f_i^0 \, e^{-B_i \vartheta} \tag{4}$$

and

$$\vartheta = \sin^2\theta / \lambda^2 \quad . \tag{5}$$

3. Calculation of Structure Factors for (h k 0) data. -- When $l = 0$, Equation 3 can be written out specifically as

$$\tfrac{1}{16} F_c = \Big\{ \sum_j \beta_j f_j \cos 2\pi h x_j \cos 2\pi k z_j \qquad \text{(Part a)} \tag{6}$$
$$+ \tfrac{1}{4} f_{Cl} + \tfrac{1}{4} (f_{Si} + f_{Al})(-1)^{\frac{h+k}{2}} + \tfrac{1}{2} f_{OH} \Big\} \mathcal{U} \, e^{-B\vartheta}$$

where we have assumed a common temperature factor for all atoms, and have introduced the scale factor $\mathcal{U}$. It is seen that the structure factor is real for $l = 0$.

The form (6) is the one used in all hand calculations and in IBM calculations carried out before introduction of separate temperature parameters for the separate atoms. Part a is the only part depending on the positional parameters, and consists of 14 terms coded by the number j as shown in Table VIII.

Equation 6 and Table VIII have been written to show the form that is suitable for machine computation, which we discuss in section 4.

TABLE VIII

CODING TABLE FOR (hkO)

STRUCTURE FACTOR CALCULATIONS

Atom	No.	Code (j)	β_j	f_j	x_j	z_j
Si_{II}	1	01	1	f_{Si}	x_1	x_1
O_I	2	02	1	f_O	x_2	x_2
O_{II}	3	03	1	f_O	x_3	x_3
O_{III}	4	04	1/2	f_{OH}	x_4	0
		05	1/2	f_{OH}	0	x_4
O_{IV}	5	06	1	f_{OH}	x_5	z_5
		07	1	f_{OH}	x_5	z_5
		08	1	f_{OH}	z_5	x_5
O_V	6	09	1	f_O	x_6	x_6
		10	1	f_O	x_6	z_6
		11	1	f_O	z_6	x_6
Al_{II}	7	12	1	f_{Al}	x_7	x_7
		13	1	f_{Al}	x_7	z_7
		14	1	f_{Al}	z_7	x_7

In hand calculation the terms given in the table are simply written out in full, and the trigonometric parts obtained from tables (Buerger, 1941).

4. Evaluation of Scale and Temperature Factors. -- Let us write equation 6 in the form

$$F_c = F_c' \mathcal{U} e^{-B\mathcal{S}}$$

In a preliminary calculation which gives values of F_c', we wish to choose a scale for F_o such that $F_o \approx F_c$. If the original observed values are F_o' on an arbitrary scale, and we wish to have $\mathcal{U} = 1.0$, then we need to choose a scale factor A so as to make

$$A F_o' \approx F_c' e^{-B\mathcal{S}}$$

One can plot $\log(F_o'/F_c')$ against $\mathcal{S}$ and fit a regression line to the resulting array of points. Because we require

$$\log \frac{F_o'}{F_c'} \approx -\log A - B \log e \cdot \mathcal{S} = a - B^* \mathcal{S} ,$$

we call -log A the intercept of the regression line and -B log e the slope.

It is customary to perform some averaging process for reflections in suitable intervals of $\mathcal{S}$, so as to reduce the scatter of points around the regression line. In our work we have instead fitted the regression line directly, and have asked the question, what is the best way to do this on statistical grounds?

For centrosymmetric structures Wilson (1949) has shown that the structure factors corresponding to a given Bragg angle are, for sufficiently large angles, distributed according to

$$P(F)\,dF = \frac{1}{\sqrt{2\pi\Sigma}}\, e^{-\frac{F^2}{2\Sigma}}\, dF$$

where $\Sigma = \sum_i f_i^2$ summed over the atoms in the structure, the f_i being atomic scattering factors appropriate for the Bragg angle concerned. We have disregarded cell centering as it does not affect the result. We may assume (Wilson, 1950, p. 397) that the calculated values F_c and the observed values F_o are both distributed in this way. Then letting $\Delta = \ln \frac{F_o}{F_c}$ we find that

$$P(\Delta)\,d\Delta = \frac{1}{2\pi}\,\operatorname{sech}\Delta\; d\Delta$$

Because of the interesting fact that Σ drops out, the distribution of Δ is the same for any value of θ or $\mathcal{R}$, which makes possible a simple procedure of estimating the scale and temperature factors. Introducing $F_o = AF_o'$, $F_c = F_c' e^{-B\mathcal{R}}$, and $\Gamma = \ln \frac{F_o'}{F_c'}$ we find

$$P(\Gamma)\,d\Gamma = \frac{1}{2\pi}\,\operatorname{sech}\,(\Gamma + \varkappa - B\mathcal{R})$$

where $\varkappa = -\log A$.

If we now have a series of observations $(\Gamma_i, \mathcal{R}_i)$, the best choice of $\varkappa$ and B will be that which maximizes the likelihood function (Mood, 1950, p. 153):

$$L = \left(\frac{1}{2\pi}\right)^N \prod_{i=1}^{N} \operatorname{sech}\,(\Gamma_i + \varkappa - B\mathcal{R}_i)$$

In other words, we require

$$\frac{\partial L}{\partial \varkappa} = 0$$

or simply

$$\sum_i \tanh\left(\Gamma_i + \varkappa - \mathcal{B}\mathcal{R}_i\right) = 0 \ .$$

Similarly, from $\partial L/\partial \mathcal{B} = 0$ we have

$$\sum_i \mathcal{R}_i \tanh\left(\Gamma_i + \varkappa - \mathcal{B}\mathcal{R}_i\right) = 0$$

Because of the shape of the tanh x function, we may write these relations approximately

$$\sum_{i=1}^{r}\left(\Gamma_i + \varkappa - \mathcal{B}\mathcal{R}_i\right) + \sum_{i=r+1}^{N}(\pm 1) = 0$$

$$\sum_{i=1}^{r}\mathcal{R}_i\left(\Gamma_i + \varkappa - \mathcal{B}\mathcal{R}_i\right) + \sum_{i=r+1}^{N}(\pm 1)\,\mathcal{R}_i = 0 \ ,$$

where the summation from 1 to r is over values of the argument for which tank x $\approx$ x, and the remaining terms are for large $|x|$, where $|\tanh x| \approx 1$. The maximum likelihood estimate of the scale and temperature factors is thus seen to be in the form of a simple least squares fit to a linear regression line, with the additional feature of a "cut off" which prevents large discrepancies from making large contributions to the solution. For the scatter encountered in our data, the "cut off" feature was unimportant. Hence we simply used the least squares fitting procedure.

The above considerations apply to the case where the scatter in Γ is due to errors in the trial structure. This may well be true in the early part of a structural investigation, and our treatment actually applies rigorously only to the case of a randomly chosen trial structure. At a later stage, the scatter will be due in part to random errors of measurement, and in part to systematic errors which we can not evaluate, and therefore must disregard in this discussion. Because of the logarithmic nature of the intensity measuring process, the observations Γ_i will be normally distributed around the regression line, with a dispersion independent of $\mathcal{R}$. Hence a least squares fit is appropriate for measurement errors, and therefore, in view of the above results, for errors of either kind.

4. Calculation of (h k 0) Structure Factors With The Use of IBM Machines. -- The machines used in the calculations described here are: (1) electronic digital computer, type 604, with punch unit, type 521; (2) reproducing and summary punch, type 514; (3) collator, type 77; (4) accounting machine (tabulator), type 402; and (5) card sorter. These machines are described in manuals published by the International Business Machines Corporation (for example, 1954).

Crystallographic calculations for cubic space groups are more cumbersome than calculations for space groups of lower symmetry. The high symmetry produces a large number of positions equivalent to a given atom, and this gives rise to complicated structure factor expressions when the contributions of equivalent atoms are combined so that the structure factor can be written in terms of contributions of non-equivalent atoms only. The high symmetry also makes possible a

variety of special positions of different multiplicity, for each of which the structure factor contribution takes on a different form. For hand calculation these features present no difficulty and in fact are a distinct advantage, because the greater the number of contributions that can be combined into a single term due to space group equivalence, the shorter is the required computation. For machine calculation, however, it is desirable to be able to treat every atom by one routine procedure, or at least by one of a limited number of procedures, depending, say, on parity of (h + k), etc. This could be done for cubic space groups by ignoring the space group equivalence of atoms, treating each atom as independent, and using structure factor expressions for a space group of lower symmetry (say, orthorhombic). Such a procedure would have two disadvantages: (1) the number of equivalent atoms is so large (e.g. up to 24 for the structural unit in T_d^2, neglecting the face-centering repetition) that machine calculating time would be lengthened far beyond the additional time required for the preparation of more complicated calculation programs, especially if the calculation is to be repeated several times and with a large amount of data; and (2) the procedure would run into great difficulty in least squares calculations, where it is necessary to vary the parameters for all equivalent atoms synchronously--unless, of course, the equivalent atoms are treated as non-equivalent in the least squares refinement, in which case the power of the refinement procedure is greatly reduced.

An alternative approach is to take the structure factor expressions as given in terms of non-equivalent atoms, and to code the calculations in such a way that the proper procedure is followed for each

point position. This method requires complicated program for the computer, which is a disadvantage because testing and perfecting a complicated program can use considerable computer time. More fundamental is the fact that storage space in the computer is limited, so that for the more complicated calculations it is impossible to read enough information into the computer and still have room for the answer to appear, if the structure factor contribution from a given point position is to be computed in full in one operation – that is, from the information contained on one IBM card.

We have followed an intermediate method. The structure factor expression, in terms of the contributions of non-equivalent atoms, is rewritten in such a way that each term has the same form. For (h k 0) calculation, the form is as shown in equation 6, where j is a code number designating a particular term in the structure factor expression, and β_j is a constant factor by which the f_j must be multiplied so as to give the correct contributions from the different point positions. When written in this way, and when coded as shown in Table VIII, atoms in point position 16e require one term, in 24f two terms, and in 48h three terms. The resulting calculation for Part a of the structure factor expression can be carried out easily with the machines, and the complications introduced into least squares calculations are not excessive.

In our calculation of structure factors on the IBM machines, we have used the conventional system in which trigonometric terms are calculated on "detail cards" and the calculated structure factors are punched out on "reflection cards". In our first calculations, Part a of equation 6 was calculated from the detail cards, there being 14 detail

cards (one for each value of j) for each reflection. Part b (the parameter-insensitive contribution) was calculated as the reflection cards passed through the machine, and in the same operation Parts a and b were added, multiplied by $\mathcal{W}$ and by $e^{-B\mathfrak{R}}$ and the result punched, as well as $F_o - F_c$. The need to vary temperature parameters separately for each atom required the system to be changed to the simple form

$$\frac{1}{16}F_c = \left\{ \sum \beta_j f_j e^{-B_j \mathfrak{R}} \cos 2\pi h x_j \cos 2\pi k z_j \right\} \mathcal{W} . \qquad (7)$$

The number of detail cards per reflection was thus increased to 18, but the calculating program was simplified.

Values of $e^{-B\mathfrak{R}}$ were originally obtained by gang punching from a permanent master deck of e^{-x} values. This method is cumbersome, as it requires first calculating $B\mathfrak{R}$ values for each card, and becomes particularly unwieldy when the e^{-x} values must be gang punched onto all 3,000 detail cards. We therefore computed the e^{-x} values on the 604 computer, using the permanent e^{-x} control panels designed by E. L. Eichhorn. In this setup the B and $\mathfrak{R}$ values were given to the machine separately and the multiplication carried out internally.

5. Calculation of (h h l) Structure Factors.--The structure factor for (h h l) reflections is in general complex, and it is necessary to calculate both real and imaginary parts. For (h h l), equations 1 and 2 become

(8)

$$A' = \cos^2 2\pi hx \cos 2\pi lz + 2 \cos 2\pi hz \cos 2\pi hx \cos 2\pi lx$$

$$B' = \text{replace cos by sin} \qquad (9)$$

Because of the form of A_h, it is no longer advantageous to separate the structure factor contribution for a given atom into several terms. The reason for this is that the general term would have to contain three different trigonometric factors. It is possible to calculate only two cosine values and two sine values in one operation on the 604, and so all cards must be run through the machine twice in any case. It is therefore more economical to calculate the four cosines and four sines required in equations 8 and 9, which can also be done in two passages of all cards through the machine. The storage capacity of the 604 is such that one can then calculate and punch $\sum_i f_i \gamma_i A'_i$ in one operation, and then, in an operation identical except for interchanging sines for the corresponding cosines, $\sum_i f_i \gamma_i B'_i$. This procedure requires only one detail card per atom for each reflection. The final step of the (h h l) calculations, which is carried out after separation of the reflection cards from detail cards, is to form $A^2 + B^2 = I$, and $I_0 - I_c$.

Pages 96,97 are missing.

VIII. ADJUSTMENT OF PARAMETERS BY THE LEAST SQUARES METHOD

1. Principles.--The least squares method of parameter adjustment was introduced into crystallography by E. W. Hughes (1941). It consists of minimizing a weighted sum of the squares of the discrepancies between observed and calculated structure factors: $\sum_h w_h \left[F_o(h) - F_c(h)\right]^2 = \min.$ This is accomplished in successive steps, by making parameter changes Δx_i, which, to first order, change the discrepancies to

$$F_o - F_c' = F_o - F_c - \sum_i \frac{\partial F_c}{\partial x_i} \Delta x_i$$

The best parameter changes are those which minimize the weighted sum:

$$\frac{\partial}{\partial \Delta x_i} \sum_h w_h \left(F_o - F_c'\right)^2 = 0$$

The resulting equations,

$$\sum_i \Delta x_i \sum_h \frac{\partial F_c}{\partial x_i} \frac{\partial F_c}{\partial x_j} w_h = \sum_h w_h \left(F_o - F_c\right) \frac{\partial F_c}{\partial x_j} \qquad (10)$$

are known as the normal equations. The number of normal equations is equal to the number of parameter changes, so that the latter are completely determined.

2. Procedure for (h k 0) Data: Positional Parameters.--Our method of carrying out (h k 0) structure factor calculations has the result that a given parameter may enter into the contributions of from one to three detail cards for any one reflection. This introduces a complication into the least squares calculation, because only a part of $\partial F_c / \partial x_j$ can be calculated from one detail card if x_j also occurs in the trigonometric arguments

of other cards. The cards were therefore divided into three classes on the basis of their contributions to the structure factor derivatives, as shown in Table IX.

A further complication is caused by the fact that for some atoms $\partial F_c/\partial x$ is to be obtained from one detail card, for some from two, and for some from three cards. In the usual application of least-squares theory, off-diagonal coefficients of the normal equations are neglected, and only the coefficient $\sum_h w_h (\partial F_c/\partial x_j)^2$ is calculated. The derivatives are calculated and squared and the sum carried out in one operation, the information being read from the detail cards, which are sorted by atoms, and the results punched on summary cards which follow each pack corresponding to a given atom. Such a procedure would be more difficult with multiple card groups for each reflection, as in our calculations, though it would still be possible with proper control punching. But for off-diagonal coefficients, which it was necessary for us to calculate, the merging and separating operations that would have to be carried out, in addition to the control complications, make this procedure unmanageable.

We therefore resorted to a procedure suggested by L. L. Merritt (in conversation), in which a set of "observational equation cards" is prepared from the detail cards, and the observational equation cards are then used to calculate the normal equations. The detail cards are sorted by atom number (not by code number), and the sequence in h and k is preserved so that for a given atom all detail cards corresponding to a given reflection remain

TABLE IX

CALCULATION OF STRUCTURE FACTOR DERIVATIVES

Class	Contribution to $\frac{\partial F}{\partial x_i}$	Contribution to $\frac{\partial F}{\partial z_i}$	Codes
I	$2\pi h \sin 2\pi hx_j \cos 2\pi kz_j + 2\pi k \cos 2\pi hx_j \sin 2\pi kz_j$	0	1, 2, 3, 4, 6, 9, 12
II	$2\pi h \sin 2\pi hx_j \cos 2\pi kz_j$	$2\pi k \cos 2\pi hx_j \sin 2\pi kz_j$	7, 10, 13
III	$2\pi k \cos 2\pi hx_j \sin 2\pi kz_j$	$2\pi h \sin 2\pi hx_j \cos 2\pi kz_j$	8, 11, 14

together. The observational equation cards, one for each reflection, are merged with the detail cards so that each observational equations card follows the group of detail cards for the corresponding reflection. The merged cards are passed through the computer, and the derivatives are calculated on the detail cards and punched on the observational equation cards. The derivatives are of course obtained by adding the contributions from the several cards if the detail card group is multiple. Calculation of the contributions is controlled by pilot selectors actuated by control punches corresponding to classes I, II, and III of the detail cards. This procedure enables all atoms to be treated alike, and minimizes the amount of merging and separating required.

Summation to form the coefficients and constant terms in the normal equations is then carried out with the small pack of observational equation cards, the derivatives being read from the various fields as required. While cumbersome, this method is much more flexible than the standard technique, and enables all coefficients in the normal equations to be calculated.

3. Weighting Systems. -- The weighting factors in equation 10 are introduced to take into account the fact that the differences $(F_o - F_c)$ are of different reliability for different reflections, the expected scatter being proportional to $|F_o|$ because of the logarithmic nature of the intensity measurement process. In considering what weighting factors would be most appropriate, the maximum likelihood principle may be applied. If the discrepancies $F_o(h) - F_c(h)$, where h labels the reflections, are normally distributed with zero means and variances σ_h^2, then this principle

leads to the least squares criterion with weighting factors $w_h = \frac{\sigma_o^2}{\sigma_h^2}$ where σ_o^2 is arbitrary. This was the weighting system used originally by Hughes (1941), the standard deviations being taken proportional to $|F_o|$ for the stronger reflections.

If we consider the normal equations, however, this weighting system seems anomalous. The constant term in each normal equation may be regarded as a measure of the correlation between the structure factor discrepancies and the changes in those discrepancies which would result on altering a given parameter. In constructing this correlation, we would want to require that the discrepancies for all reflections contribute on an equal basis, so that the contributions to the correlation from all reflections, large and small, are on the average equal. Because the magnitudes of the derivatives $\partial F/\partial x$ are essentially independent of the magnitudes of the F_c's except for a broad correlation depending on the magnitudes of the f-values, it is seen from equation 10 that the reflections are taken on an equal basis in the above sense by choosing $w_h = \sigma_o / \sigma_h$. If we choose $w_h = \sigma_o^2 / \sigma_h^2$, as suggested by the maximum likelihood principle, then the stronger a given reflection, the less it contributes to the correlation which determines the parameter shifts.

The anomalous contradiction of these points of view has led us to investigate the weighting question more fully. We have found that the maximum likelihood weighting can be justified on more general grounds, and we have been able to make somewhat plausible the basis for the failure of our intuition in the argument of the last paragraph.

It is possible to avoid the maximum likelihood and least squares criteria altogether by considering the question, what is the best way to choose the Δx_i regardless of what criterion is used? There are two properties that reasonable estimators should have: They must be unbiased, so that the estimated value of Δx_i is on the average equal to the true parameter error, and they should have the lowest variances possible, so that on refining the structure with independent sets of data the random errors of measurement will have the smallest possible effect on the estimated parameters. If in addition we ask that for mathematical simplicity and to be consistent with our first-order theory, the Δx_i be given as linear functions of the $(F_o(h) - F_c(h))$ values, then we have specified the three conditions for "best linear unbiasedness" of the estimators. Kempthorne (1952, pp. 54-46, and p. 64) has shown that these three conditions alone give estimators which are identical with those derived from the maximum likelihood criterion, and in particular they specify that the weights should be $w_h = \sigma_o^2 / \sigma_h^2$.

The significance of the "best linear unbiasedness" property can be seen in terms of the normal equations, in which, for simplicity, we keep only the diagonal coefficients, so that the equations may be written

$$\sum_h w_h \alpha_{hj}^2 \Delta x_j = \sum_h w_h \alpha_{hj} y_h$$

Here the y_h are the discrepancies and are taken to have variances σ_h^2 . Since the Δx_j are given as a linear combination of the y_h , the Central Limit Theorem (Cramer, 1937, pp. 56-60) shows that, regardless of the distributions of the y_h , the variance of

the estimator Δx_j approaches (for a large number of reflections) the value

$$\sigma^2_{\Delta x_j} = \frac{\sum (w_h \alpha_{hj})^2 \sigma_h^2}{\left(\sum w_h \alpha_{hj}^2\right)^2} .$$

If we now ask for weights which minimize the $\sigma^2_{\Delta x_j}$, we require

$$\frac{\partial \sigma^2_{\Delta x_j}}{\partial w_k} = 0$$

from which

$$w_k = \frac{c}{\sigma_k^2}$$

where c is a constant, independent of k. This is the weighting system given by the maximum likelihood criterion.

Our intuition in this matter may be bolstered by considering a limiting case. Suppose that for some reason (that we need not specify) the F_o for one reflection, say k, were very accurately known. This would mean that σ_k was very small. If the structure were nearly correct, $F_o(k) - F_c(k) \sim \sigma_k$. Now the fact that $F_o(k)$ is so accurately known means that no parameter change can be carried out which allows $F_o(k) - F_c(k)$ to become larger than $\sim \sigma_k$. In other words, for parameter changes Δx_i we must have

$$\sum_i \frac{\partial F_c(k)}{\partial x_i} \Delta x_i \sim \sigma_k \sim 0 .$$

Now compare the results of least-squares calculations using the two weighting systems in question. If $w_h = \sigma_o / \sigma_h$, then the contribution

$$\sigma_o \frac{F_o(k) - F_c(k)}{\sigma_k} \frac{\partial F_c}{\partial x_j}$$

to the correlation term in the least squares calculation is of the same order of magnitude as the contributions from other reflections,

so that k plays no special role and a more or less "usual" set of normal equations results (usual except for the domination of the coefficient matrix by the k terms). But if $w_h = \sigma_0^2 / \sigma_h^2$, the contributions of reflection k dominate both on the right and on the left of equation 10, and all normal equations reduce simply to

$$\sum \frac{\partial F_c(k)}{\partial x_i} \Delta x_i = F_o(k) - F_c(k) \sim 0$$

since we suppose the structure is already good enough that $F_o(k) - F_c(k) \sim \sigma_k$.

Thus the maximum-likelihood weighting takes care of this special case in a reasonable way, whereas the weighting $w_h = \sigma_0 / \sigma_h$ does not. Parenthetically we may add that the solution for the parameter shifts in this case would be completed by use of the method of Lagrange multipliers, using as the function for minimization

$$\sum_h w_h \left(F_o - F_c' \right)^2 + \lambda \sum_i \frac{\partial F_c(k)}{\partial x_i} \Delta x_i$$

and imposing the condition $\sum_i \frac{\partial F_c(k)}{\partial x_i} \Delta x_i = F_o(k) - F_c(k)$, which would remove the dominating k terms from the resulting summations.

This discussion, while it may seem far-fetched, is pertinent to our refinement of the zunyite structure. On the basis of the normal equation argument above, we originally adopted weights for the (h k 0) refinement according to the system $w_h = K / |F_o(h)|$. The incorrectness of these weights was not realized until the calculations were completed. We might fear on this account that the parameter values derived are subject to some error. While it is likely that the values would change somewhat upon application of

the correct weighting system, the statistical theory shows that the values would not be likely to change by amounts larger than the calculated standard deviations. This follows from the fact that the least squares refinement gives an unbiased estimate of the parameters whether or not it is optimally weighted (cf. Kempthorne, 1952, p. 55, eqn. 12). The main effect of the weighting system used by us is therefore to give estimated parameter variances somewhat larger than could have been secured with optimal weighting. These considerations are not very worrisome, because we have seen that the limiting standard deviation, which best describes the probable accuracy of our parameters, is larger than any of the standard deviations we have estimated statistically.

In practice, of course, the relation $\sigma_h = K_1 |F_o(h)|$ cannot be applied over the entire range of intensities, because of the increasing uncertainty of the intensity estimates for very faint reflections. We have used a weighting system similar to the one employed by Hughes (1941). It is shown in Fig. 28, as applied to the (h h l) data, for which we used the correct weighting system $w_h = \sigma_o^2 / \sigma_h^2$. The shape of the weighting curve for the (h k 0) data was similar to Fig. 28.

Fig. 28 shows that in handling the (h h l) data we tried two different weighting systems, called W_1 and W_2, with low and high "cut off" respectively. A comparison of the results of W_1 and W_2 will be given in section 6.

4. Results of the (h k 0) Least Squares Calculations. -- The procedure followed in solving the normal equations was to reduce them to a standard form by dividing each equation by the

TABLE X

COEFFICIENTS IN THE NORMAL EQUATION MATRIX

FOR L. S. I.

A. Data out to $\sin^2\theta/\lambda^2 \leq 1.9$

	x_1	x_2	x_3	x_4	x_5	z_5	x_6	z_6	x_7	z_7
x_1	1.00	0.01	0.01	0.00	0.01	0.00	-0.08	-0.06	-0.16	0.08
x_2	0.03	1.00	-0.36	0.03	-0.78	-0.07	-0.01	0.03	0.12	0.01
x_3	0.06	-0.46	1.00	-0.04	1.00	0.10	-0.29	0.15	-0.30	0.08
x_4	-0.05	0.06	-0.08	1.00	-0.22	-0.05	0.11	-0.08	0.09	0.32
x_5	0.03	-0.42	0.41	-0.05	1.00	0.08	-0.11	0.06	-0.20	0.12
z_5	-0.01	-0.08	0.09	-0.03	0.17	1.00	-0.18	0.15	-0.17	-0.02
x_6	-0.18	0.00	-0.09	0.02	-0.09	-0.06	1.00	0.03	-0.16	0.10
z_6	-0.44	0.04	0.16	-0.05	0.14	0.18	0.10	1.00	0.12	0.03
x_7	-0.10	0.02	-0.03	0.01	-0.05	-0.02	-0.05	0.01	1.00	-0.04
z_7	0.10	0.00	0.02	0.04	0.06	0.00	0.06	0.00	-0.08	1.00

B. Data out to $\sin^2\theta/\lambda^2 \leq 0.6$

x_1	1.00	0.04	0.02	-0.02	0.01	-0.04	-0.03	-0.02	-0.36	0.08
x_2	0.24	1.00	-0.61	0.02	-0.90	-0.10	0.07	-0.02	0.20	0.23
x_3	0.15	-0.74	1.00	-0.08	0.99	0.19	-0.21	0.03	-0.45	-0.03
x_4	-0.30	0.04	-0.16	1.00	-0.14	0.06	0.36	-0.11	0.15	0.82
x_5	0.03	-0.47	0.43	-0.03	1.00	0.14	-0.15	0.03	-0.39	0.00
z_5	-0.24	-0.09	0.14	0.03	0.25	1.00	-0.17	0.04	-0.43	-0.09
x_6	-0.08	0.02	-0.06	0.06	-0.11	-0.07	1.00	0.02	-0.05	0.19
z_6	-0.45	-0.05	0.08	-0.14	0.15	0.13	0.16	1.00	0.24	0.07
x_7	-0.19	0.02	-0.03	0.01	-0.06	-0.04	-0.01	0.01	1.00	-0.11
z_7	0.08	0.03	0.00	0.05	0.00	-0.01	0.07	0.00	-0.19	1.00

coefficient of its diagonal term, to produce such an array as shown in Table X. The Table shows for comparison two sets of normal equations obtained by taking the same set of data, in A using all reflections, and in C using reflections only out to $(\sin\theta/\lambda)^2 = 0.6$. It is seen that even with all the data, some of the off-diagonal coefficients are non-negligible. The most noticeable are the coefficients corresponding to the $O_I - O_{II} - O'_{IV}$ overlap. The resolution obtained in L.S. V was greater than in L. S. I A, because in the latter about 30 reflections were eliminated due to indeterminate sign of F_o. In L.S V, the $x_2 x_3$ coefficient was -0.19 and the $x_3 x_2$ was -0.20. Note that the coefficients $x_2 x_5$ and $x_3 x_5$ remain surprisingly high, in spite of the presence of the resolved O''_{IV} atom.

Solution of the normal equations was accomplished by neglecting all off-diagonal terms less than 0.1 (at first, higher values), and solving the resulting equations, by iteration where small off-diagonal coefficients were involved, and simultaneously for the three equations for Δx_2, Δx_3 and Δx_5.

5. Least Squares Calculations for Variation of Scale and Temperature Factors. -- We list here the equations used for variation of scale factor and of temperature parameters for separate atoms:

$$\sum_h w_h F_c^2 \Delta a - \sum_i \Delta B_i \sum_h w_h F_c \hat{F}_i \mathcal{S}_h = \sum_h w_h F_c (F_o - F_c)$$

$$\sum_h w_h F_c \hat{F}_j \mathcal{S}_h \Delta a - \sum_i \Delta B_i \sum_h w_h \hat{F}_i \hat{F}_j \mathcal{S}_h^2 = \sum_h w_h \mathcal{S}_h \hat{F}_j (F_o - F_c)$$

where $\Delta a = \Delta \mathcal{U} / \mathcal{U}$

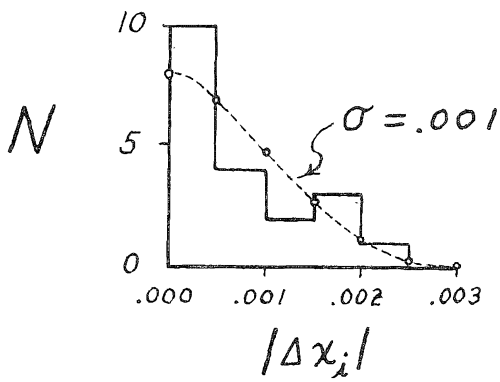

FIG. 23

PARAMETER CHANGES IN L.S. VIII

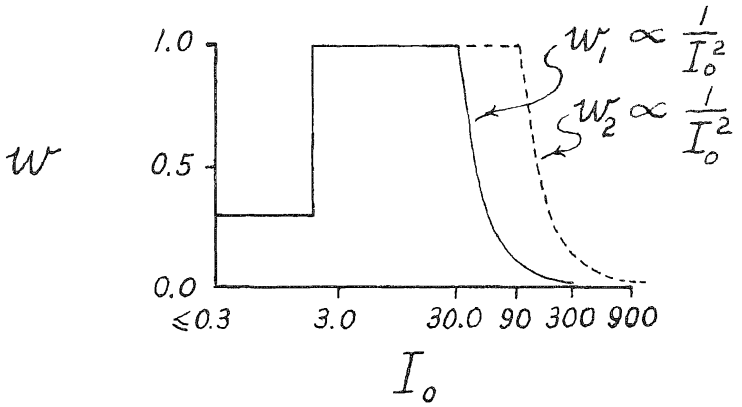

FIG. 24

WEIGHTING SYSTEMS FOR (hhl)

and

$$\hat{F}_i = \ell\ell\, e^{-B_i \vartheta_h} \sum_{j \in i} \beta_j f_j \cos 2\pi h x_j \cos 2\pi k z_j$$

where the summation $j \in i$ is over the code numbers corresponding to a given atom.

Variation of compositional parameter for chlorine, by putting f_{Cl} (actual) $= \alpha\, f_{Cl}$ (100%), adds the equation

$$\sum_h w_h \hat{F}_{Cl}^2 \Delta\alpha + \sum_h w_h F_c \hat{F}_{Cl} \Delta a - \sum_i \Delta B_i \sum_h w_h \hat{F}_i \hat{F}_{Cl} \vartheta_h = \sum_h w_h (F_o - F_c) \hat{F}_{Cl}$$

plus appropriate off-diagonal terms in the previous equations.

6. Least Squares Refinement of (h h l) Data. --This is by far the most complicated calculation carried out in the present study. We describe it here completely but compactly, with apologies for laconism.

Variation is for minimization of

$$\sum_h w_h (I_o - I_c)^2$$

where $I_c = A^2 + B^2$.

This leads to normal equations

$$4\pi \sum_h w_h \left(A \frac{\partial A}{\partial \xi_i} + B \frac{\partial B}{\partial \xi_i} \right)^2 \Delta x_i = \sum_h w_h \Delta I \left(A \frac{\partial A}{\partial \xi_i} + B \frac{\partial B}{\partial \xi_i} \right)$$

where $\xi_i = 2\pi x_i$. Off-diagonal terms were omitted, as justified by the large amount of data.

$$-\frac{\partial A}{\partial \xi} = [\underset{(1)}{2h \cos h\xi} \underset{(4)}{\cos l\xi \sin h\xi} + \underset{(3)}{2h \cos h\xi} \underset{(2)}{\cos l\xi \sin h\xi} + 2l \cos h\xi \cos h\xi \sin l\xi\,]\, f e^{-B\vartheta}$$

$$-\frac{\partial B}{\partial \xi} = \textit{interchange sin and cos}$$

$$-\frac{\partial A}{\partial \xi} = [\,l \cos^2 h\xi \sin l\xi + 2h \cos h\xi \cos l\xi \sin h\xi\,]\, f e^{-B\vartheta}$$

$$-\frac{\partial B}{\partial \xi} = \textit{interchange sin and cos}$$

TABLE XI

RESULTS OF (hhl) LEAST SQUARES CALCULATIONS

	L. S. VII		L. S. VIII		Accept for S. F. XIII
	w_1	w_2	w_1	w_2	
x_1	.0005	.0018	.0002	.0005	.000
x_2	.0031	.0057	.0012	.0016	+.0014
x_3	.0041	.0108	.0003	.0004	.000
x_4	-.0060	-.0093	-.0019	-.0020	-.0020
x_5	.0000	.0000	-.0004	+.0005	.000
z_5	.0039	.0082	.0015	.0012	+.0013
x_6	.0021	.0046	.0000	-.0007	.000
z_6	.0001	.0020	-.0002	.0000	.000
x_7	.0002	.0004	.0000	-.0002	.000
z_7	.0000	.0000	.0005	-.0003	.000

Procedure:

1. From detail cards, separate atoms Al_I, Si_I, Cl.

2. Calculate and punch on detail cards:

$$D_x^1 A \equiv [(\cos 1 \cos 4 + \cos 2 \cos 3) \sin 1 \cdot 2h + \cos 1 \cos 3 \sin 2 \cdot 2l] T_i$$

$$D_x^2 A \equiv [(\cos 1 \cos 2 + \quad 0 \quad) \sin 3 \cdot 2h + \cos 1 \cos 1 \sin 4 \cdot 1] T_i$$

$D_x^1 B \equiv$ } interchange sin and cos
$D_x^2 B \equiv$ }

$$T_i = e^{-B_i \mathfrak{R}}$$

This requires 4 trips for all cards through the machine. Simultaneously punch Y in col. 5 for atoms 1 - 3.

3. Detail cards are filled, so reproduce, retaining basic data plus the D's. Merge new detail cards, which remain sorted on h, l, with reflection cards, and gang punch A, $\bar{B}$, and ΔI onto detail cards. Remove reflection cards. ($\bar{B} = -B$).

4. Calculate and punch on detail cards:

	$\mathfrak{A}_x =$	$\mathfrak{A}_z =$
Y Col. 5	$A(D_x^1 A + D_x^2 A) - \bar{B}(D_x^1 B + D_x^2 B)$	0
NY Col. 5	$A D_x^1 A - \bar{B} D_x^1 B$	$A D_x^2 A - \bar{B} D_x^2 B$

5. Sort detail cards by atom, with a normal equation summary card to follow each atom.

6. Calculate on detail cards, and punch on summary cards:

$$\sum_h w_h (\mathfrak{A}_x \gamma_i f_i)^2 \quad \text{and} \quad \sum_h w_h (\mathfrak{A}_x \gamma_i f_i) \Delta I$$

and, as appropriate, the corresponding terms with $\mathfrak{A}_z$ replacing $\mathfrak{A}_x$. These are the numerical constants in the normal equations, less a factor (-4π) on the left-hand side.

The final summations were carried out twice, using weighting systems W_1 and W_2. The parameter changes calculated from the results are given under L.S. VII in Table XI. It is seen that the changes using W_2 (high "cut off") are about twice as great as those using W_1. An investigation revealed two serious errors in the least squares data. The errors were in the observed intensities I_o of (115) and (333), and were caused by mistakes in conversion of logarithmic intensities to absolute intensities for punching onto cards. These errors caused: (1) erroneous values of ΔI; (2) abnormally high weights for these reflections, both of which are strong, and for both of which the I_o values in error had been too low. The errors were corrected by hand, and it was found that these reflections made large contributions to the least squares correlation constants. The corrected results are given under L.S. VIII. For the larger shifts, W_1 and W_2 give about the same results. This is an interesting example of the use of two weighting systems to indicate errors and to distinguish between probably significant and probably non-significant parameter changes.

IX. CALCULATION OF FOURIER SYNTHESES AND DIFFERENCE SYNTHESES

1. Projection on {100}. -- The electron density in a crystal is given in terms of the structure factors for X-ray diffraction, assuming no anomalous scattering, by (Lipson and Cochran, 1953, p. 12)

$$\rho(x,y,z) = \frac{1}{V} \sum_{h}^{+\infty} \sum_{k}^{+\infty} \sum_{l}^{+\infty} F(hkl)\, e^{-2\pi i (hx + ky + lz)} \qquad (11)$$

where V is the volume of the unit cell. Although x, y, z are given in fractions of the cell edges, the density in equation 11 is given in electrons per unit volume, and the number of electrons in a volume dx dy dz is $a_o^3 \rho\, dx\, dy\, dz$. From the list of coordinates of the general position in T_d^2 (Chapter VII) it can be shown that

$$F(hkl) = F(h\bar{k}\bar{l}) = F(\bar{h}\bar{k}l) = F(\bar{h}k\bar{l})$$
$$= F^*(\bar{h}\bar{k}\bar{l}) = F^*(\bar{h}kl) = F^*(hk\bar{l}) = F^*(h\bar{k}l) \qquad (12)$$

With these conditions, and with F = A + iB, equation 11 reduces to the result given in the International Tables (1952, p. 489):

$$\rho = \frac{8}{V} \sum_{0}^{\infty} \sum_{0}^{\infty} \sum_{0}^{\infty} (A \cos 2\pi hx \cos 2\pi ky \cos 2\pi lz - B \sin 2\pi hx \sin 2\pi ky \sin 2\pi lz)$$

This result is not very useful, however, as it fails to show the proper treatment for special structure factors with low multiplicity (Lipson and Cochran, 1953, pp. 76-78). Starting with equation 11, we project the density onto (001):

$$\rho(x,y) = \int_0^{a_o} \rho a_o dz = \frac{1}{A} \sum_{-\infty}^{\infty} \sum F(hk0)\, e^{-2\pi i (hx + ky)}$$

where $V = a_o^3$ and $A = a_o^2$. Introducing conditions 12, and remembering that F (h k 0) is real, we obtain

$$\rho(x,y) = \frac{1}{A} \sum_{-\infty}^{\infty}\sum F(hk0) \cos 2\pi hx \cos 2\pi ky \qquad (13)$$

where multiplicity is now explicitly taken into account. Now define

$$\begin{aligned} C(000) &= \tfrac{1}{2}\mathcal{U} F(000) = \mathcal{U}\ (1156) \\ C(h00) &= C(0h0) = F_o'(h00)\ ,\quad h \neq 0 \\ C(hk0) &= C(kh0) = 2F_o'(hk0)\ ,\quad h,k \neq 0\ , \end{aligned} \qquad (14)$$

and write, in consideration of equation 7,

$$F(hk0) = \frac{16}{\mathcal{U}} F_o'(hk0)\ ,$$

where F_o' is the observed structure factor on the scale of Appendix II. Then

$$\rho(x,y) = \frac{32}{A\mathcal{U}} \sum_{k=0}^{\infty} \cos 2\pi ky \sum_{h=0}^{\infty} C(hk0) \cos 2\pi hx\ .$$

This is the form of the actual computations, and is suitable for calculation with Beevers-Lipson strips or by IBM methods. In the actual computations, of course, only the summations are carried out, using amplitudes C as defined above. The constant $32/A\mathcal{U}$ is to be used in converting the results to electron units.

Hand calculation of $\rho(x, y)$ using Beevers-Lipson strips is a straightforward but tedious procedure. Strips in intervals of 60ths of the cell were used to calculate projections in 120ths by halving the frequencies and separating odd and even half-frequencies. The chief difficulty in hand calculation is the

possibility for error. One error in the first summation produces 31 errors in the final summation, for a projection 1/4 x 1/4 of the cell in size. Fortunately the presence of the diagonal mirror plane makes it possible, by calculating the full 1/4 x 1/4 projection, to have a direct check on the internal consistency of the calculations. By this device an error in the first summation can be quickly located before much computational effort is lost.

Except for F_o I, all syntheses were calculated by IBM methods, using the system devised by Professor Verner Schomaker and described by R. A. Pasternak (1954). Coding of first detail cards and transfer of the proper amplitudes to these cards, according to equations 14, was performed in one operation on the 604 computer, using the reflection cards from (h k 0) structure factor calculations.

Difference syntheses are carried out by the same method as equation 15, but with $F'_o - F'_c$ substituted for F'_o in equations 14, and with the term C(000) dropped.

2. Projections on $(1\bar{1}0)$.--Because the correct formulation of procedure for this projection requires some care, we give it here in detail. Starting with the density, equation 11, we make a change of variable $\sigma = x+y$, $\tau = x-y$, so that

$$\rho(\sigma,\tau,z) = \frac{1}{2V}\sum\sum\sum F\, e^{-2\pi i\left(\frac{h+k}{2}\sigma + \frac{-h+k}{2}\tau + lz\right)}.$$

Now project on $(1\bar{1}0)$. As shown in Fig. 25a,

$$\rho(\sigma,z) = \int_0^2 \rho\, a_o\, d\tau = \frac{1}{a_o^2}\sum\sum F(hhl)\, e^{-2\pi i(h\sigma+lz)}.$$

Per unit area in the 110 plane, the density becomes

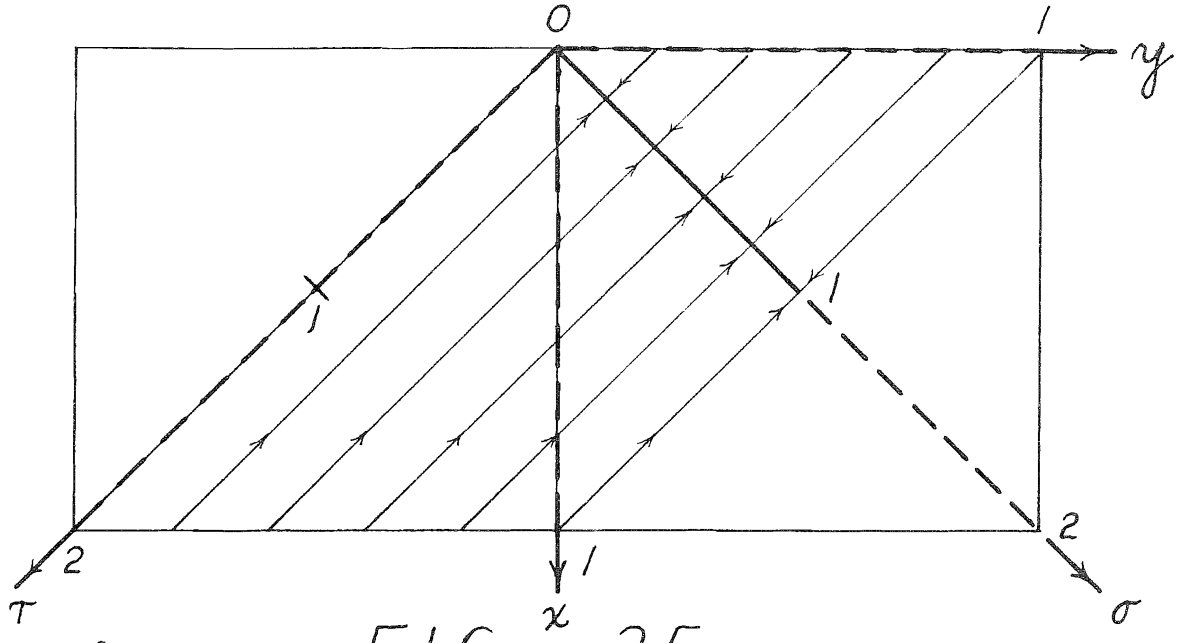

FIG. 25a
METHOD OF PROJECTING ONTO (1$\bar{1}$0)

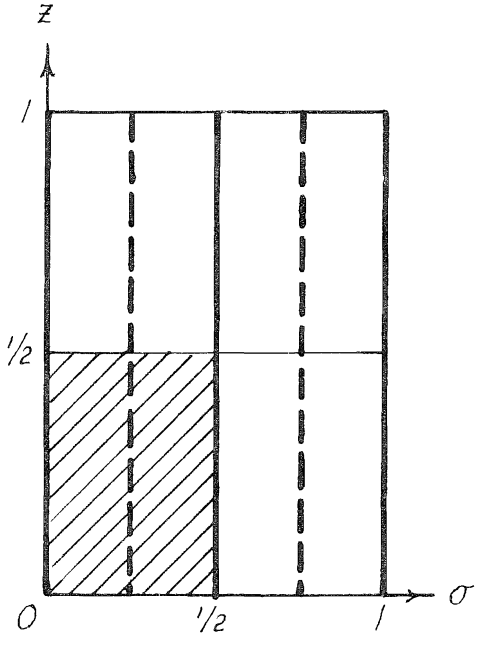

25b

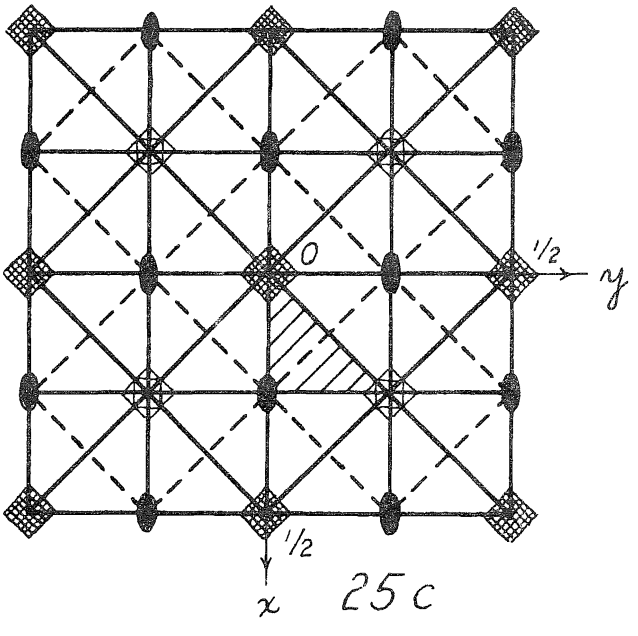

25c

SYMMETRY OF THE PROJECTIONS

25b: (1$\bar{1}$0) 25c: {100}
ASYMMETRIC UNITS SHADED

$$\rho(\sigma,z) = \frac{\sqrt{2}}{a_o^2} \sum\sum F\, e^{-2\pi i (h\sigma + lz)}$$

since an interval $d\sigma$ corresponds to a distance $a_o\, d\sigma/\sqrt{2}$. Now using conditions 12, and expanding, we find that

$$\rho(\sigma,z) = \frac{2\sqrt{2}}{a_o^2} \sum_0^\infty \sum_0^\infty \cos 2\pi h\sigma \left[A^\dagger(hhl)\cos 2\pi lz + B^\dagger(hhl)\sin 2\pi lz \right]$$

where

$$\begin{aligned} A^\dagger(000) &= \tfrac{1}{2} F(000) \\ A^\dagger(001) &= A(001), \quad l \neq 0 \\ B^\dagger(001) &= 0 \\ A^\dagger(hh0) &= A(hh0), \quad h \neq 0 \\ A^\dagger(hhl) &= 2A(hhl), \quad h,l \neq 0 \\ B^\dagger(hhl) &= 2B(hhl) \end{aligned} \tag{16}$$

If in accordance with our calculations we now define

$$\hat{A}_o = \frac{1}{16} A^\dagger, \quad \hat{B}_o = \frac{1}{16} B^\dagger$$

then we obtain the result used in practice:

$$\rho(\sigma,z) = \frac{32\sqrt{2}}{a_o^2} \sum_0^\infty \cos 2\pi h\sigma \sum_0^\infty \left(\hat{A}_o \cos 2\pi lz + \hat{B}_o \sin 2\pi lz \right). \tag{17}$$

The resulting projection has plane group symmetry cm, as shown in Fig. 29b. The unique unit, shaded in the figure, has dimensions 1/2 x 1/2. The mirror planes are represented in equation 17 by the fact that $\rho(\sigma, z) = \rho(-\sigma, z)$ and the centering translation by $\rho(\sigma, z) = \rho(\sigma + 1/2, z + 1/2)$ which follows from the fact that

h and l are always of the same parity for a given term in the series.

The amplitudes A and B are derived by taking the magnitude $|F_o|$ to be $\sqrt{I_o}$ and taking the phase of F_o to be the phase of F_c. The amplitudes are therefore calculated from

$$\hat{A}_o = \sqrt{I_o}\,\frac{A_c}{\sqrt{I_c}} \quad , \quad \hat{B}_o = \sqrt{I_o}\,\frac{B_c}{\sqrt{I_c}} \quad .$$

The difference synthesis amplitudes are simply $\hat{A}_o - \hat{A}_c$ and $\hat{B}_o - \hat{B}_c$ (where $\hat{B}_c = \frac{1}{16} B_c$ and was the actual value calculated by us).

3. Plotting Atomic Positions on Projections. -- The plotting of positions on the {100} projection is straightforward because projection coordinates are simply the atomic coordinates, properly chosen and modified where necessary by the symmetry operations of the projection so as to fall within the calculated unit. For the $(1\bar{1}0)$ projection, however, the procedure is not so direct, and we therefore list in Table XII the coordinates of all atomic positions on the projection and the combinations of parameter values which give rise to these coordinates.

4. Electron Counts and Atomic Shapes. -- Lipson and Cochran (1943, p. 106) have emphasized the desirability of integrating the electron densities derived by Fourier synthesis in order to compare the number of electrons in the calculated atomic peaks with those in the postulated structure. Of course, if the difference map of the final structure is flat, one may say that the postulated and real structures have the same electron distributions, and there is no need for recourse

TABLE XII

COORDINATES OF ATOMIC POSITIONS ON THE (110) PROJECTION

Atom	Multiplicity[2]	Parameter Combinations		σ	z
		σ	z		
Si_{II}	1	2x	x	27.4[1]	13.7[1]
	2	1/2	1/2 - x	60.0	46.3
O_{I}	1	1/2 + 2x	1/2 + x	18.1	39.0
	2	0	- x	0.0	21.0
O_{II}	1	2x	x	43.6	21.8
	2	1/2	1/2 - x	60.0	38.2
O_{III}	1	1/2	1/2 - x	60.0	26.7
	2	x	0	33.3	0.0
	2	1/2 - x	1/2	26.7	60.0
	1	0	0	0.0	33.3
O_{IV}	2	0	1 - z	0.0	54.4
	2	1/2 + x - z	1/2 - x	15.9	38.5
	1	1/2 - 2x	z - 1/2	17.0	5.6
	2	1 - x - z	x	32.9	21.5
O_{V}	2	1/2	1/2 - z	60.0	60.0
	2	x + z	x	16.6	16.6
	2	1/2 + z - x	1/2 - x	43.4	34.4
	1	2x	z	33.2	0.0
Al_{II}	2	0	-z	0.0	28.0
	2	1/2 + z - x	1/2 - x	21.8	49.7
	1	1/2 - 2x	1/2 + x	39.5	32.0
	2	-(x + z)	x	17.8	10.2

1. In units of $a_o/120$.

2. Multiplicity in atoms per two structural units.

to electron counting. It would also seem that deviations in electron density could best be evaluated from the difference map. The difficulty with this method is one of scale: unless one is able to convert reliably from the somewhat arbitrary units in which the calculated electron densities or density differences appear, no counts on the difference maps have any quantitative significance. The only sure way to verify that the scale is taken properly into account is to demonstrate that the correct electron counts can be obtained from the Fourier syntheses. If this is shown, then counts on difference maps can be trusted.

Our interest in perfecting reliable electron counting techniques for the zunyite structure arises from the use of the atomic shapes, peak heights, and other electron density details in the considerations of the next chapter, where it is necessary to have electron densities in absolute units. We have therefore carried out electron counts for a number of atoms in the structure. For ionic crystals the atoms prove to be essentially spherical (projections can show only circular symmetry, of course), and questions of deviation from sphericity due to redistribution of electrons in bonding do not arise. From equation 15 we find that for counts on F_oII, the number of electrons is

$$N = 0.0218 \sum \rho_o(\text{calc.}) \quad \text{electrons,}$$

the sum being over squares 1/120 of the cell edge on a side. Electron counts by this method--summing over densities calculated at specific points in the structure, which is the method mentioned by Lipson and Cochran (1953, p. 106)--does not prove particularly satisfactory for the zunyite projections. For the Al_{II} peak on

F_oII, containing one aluminium ion, it gives a good value of 9.9 electrons, but for the double O^{II}_V peak on the same projection it gives only 8.9 electrons, whereas 20 should be found.

The method that we have found more useful and more illuminating is the "radial sum" method, in which a plot is made of ρ as a function of distance r from the center of a given peak, by compiling all the point-by-point information from the projection onto one plot of $\rho(r)$, and drawing a smooth curve through the points. Such plots of atomic shape are shown in Fig. 26. Electron densities are shown in arbitrary units, but can be converted to electrons $Å^{-2}$ by

$$\rho_o = 1.63\ \rho_o(calc.) \quad .$$

The electron density at the center of an aluminium peak is about 64 e $Å^{-2}$, and at the center of an oxygen peak about 32 e $Å^{-2}$. Fig. 27 shows the shape of the $^2Al_{II}$ peak at (21.8, 49.7) on F_oIII. Here the conversion is

$$\rho_o = 2.12\ \rho_o\ (calc.) \quad e Å^{-2} \quad .$$

The central density is found to be 63 e $Å^{-2}$.

To find the number of electrons in a given peak, the $\rho(r)$ curve is multiplied by r and the resulting radial charge density is integrated graphically. Table XIII shows the results for several atoms in F_o II.

In this table the total charge N (r) is given as a function of the radial distance out to which the integration is carried. It is seen that the total charge depends rather critically on the behavior

FIG. 26

(hk0) Data

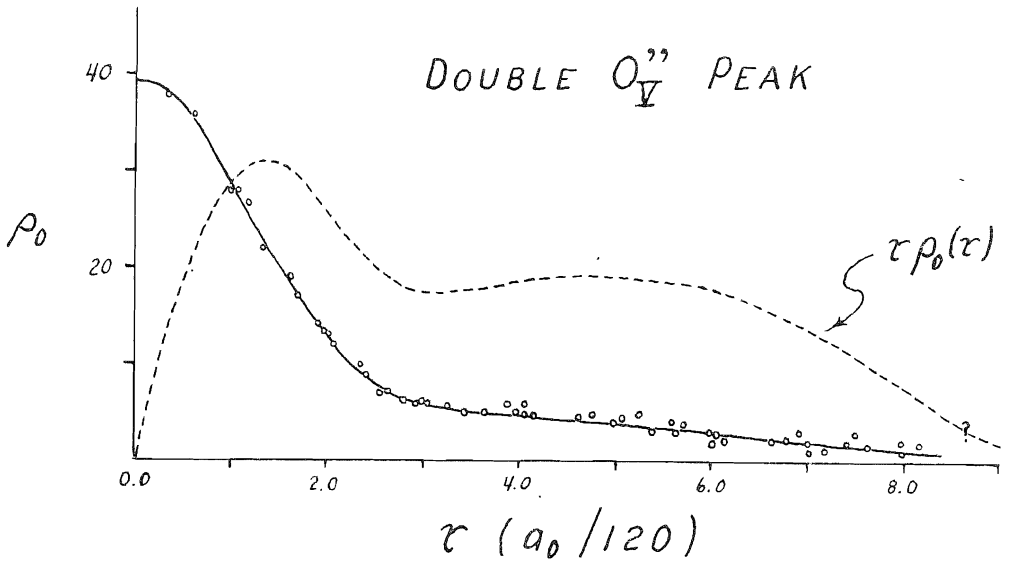

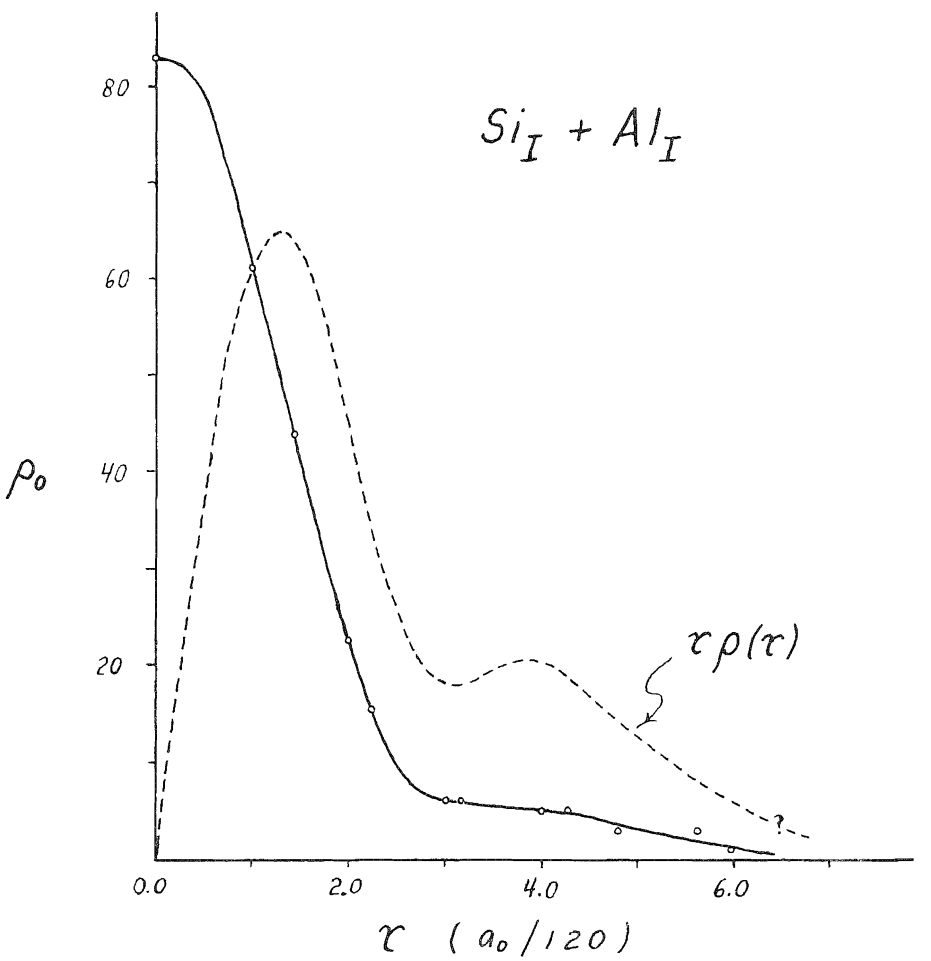

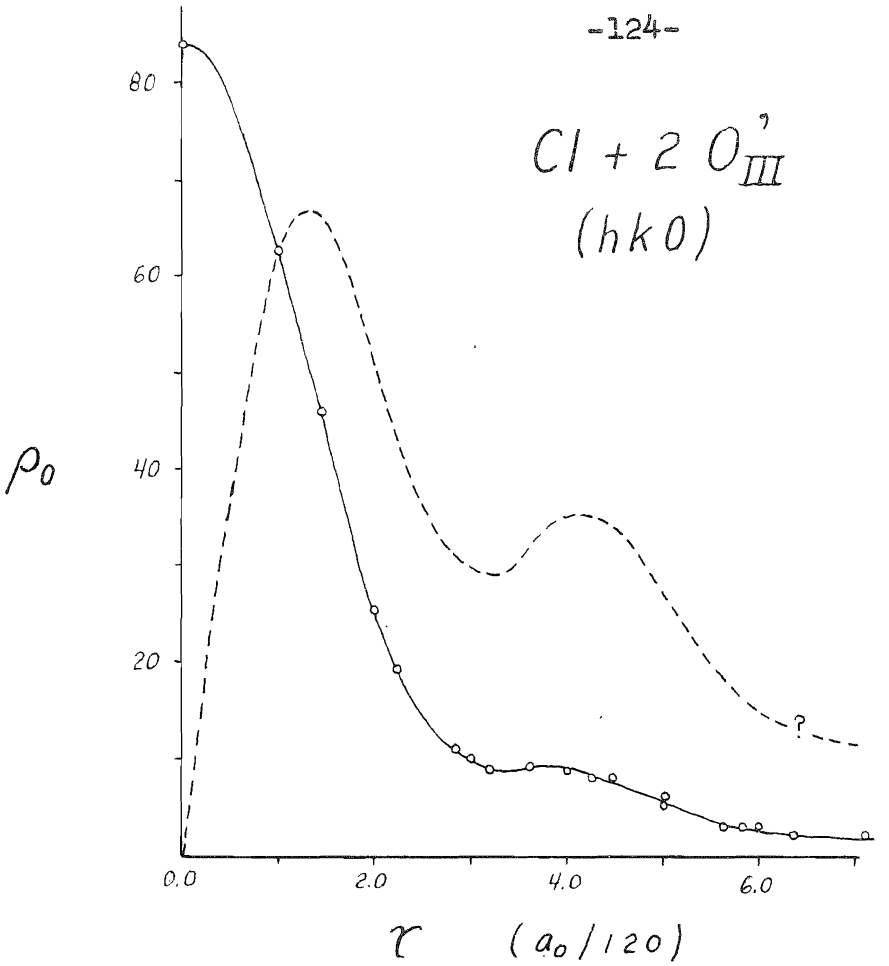
80
60
40
20
ρ_0
Cl + 2 O'_{III}
(hk0)
?
0.0
2.0
4.0
6.0
τ (a_0/120)

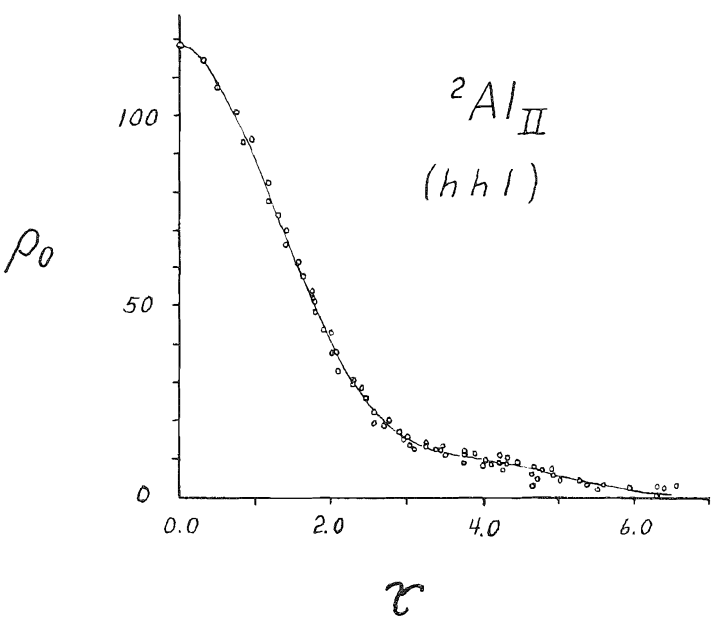
100
50
0
ρ_0
$^2Al_{II}$
(hhl)
0.0
2.0
4.0
6.0
τ

FIG. 27

TABLE XIII

ELECTRON COUNTS FOR F_o II

	$N(r)^2$ for:			
r^1	Al^{I}_{II}	20^{II}_{V}	$Si_I + Al_I$	$Cl + 20^{I}_{III}$
2.8	8.5	8.7		
3.2	9.2		16.6	
3.6	9.8		18.2	
4.0	10.2	11.6	19.3	22.9
4.4	10.5		20.4	
4.8	10.8		21.2	
5.2	11.0			
5.6	11.1			
6.0	11.2	16.8		30.2
6.4	11.3	17.7		
6.8	11.3	18.6	23.2	
7.2		19.4		32.2
7.6		19.9		
8.0		20.4		
8.4		20.8		
8.8		21.0		
9.2		21.1		
9.6		21.1		

1. r = radial distance from center of peak in units of $a_o/120$.

2. N(r) = number of electrons within a cricle of radius r.

of ρ at large values of r, but that, with reasonable sizes for the ions, the expected number of electrons can be accounted for in all cases.

The main feature of the shapes of all peaks is their general resemblance to Gaussian curves, as has been discussed by Booth (1946). They show an additional important feature, however. This is the "apron" of charge density which extends to values of r at which the Gaussian distribution would have dropped practically to zero. The importance of this apron is especially great for oxygen atoms, as can be seen in Fig. 26 and in Table XIII. The central Gaussian core accounts for only half of the electrons in the peak, the rest lying out in the apron. This fact adds to the difficulty of making accurate electron counts, because an accurate scale factor is required if the contribution of the apron to the total charge is to be correct. For cations the central core accounts for about three fourths of the total charge.

The radii of the cations, taken as the radius of the sphere enclosing the expected charge, is 0.50 Å for the Si_I+Al_{II} peak, which agrees tolerably with Pauling's (1948, p. 346) crystal radii for these atoms. But the value for oxygen is conspicuously low, 0.9 Å. The value for Cl cannot be reasonably estimated, because of irregularities in charge density in the outer part of the atom.

Following Booth (1946), we have fitted Gaussian curves to the density profiles of the core:

$$\rho(r) = \rho_0 e^{-pr^2}$$

The simplest ready evaluation of p is from the radius at half maximum:

$$p = \frac{\ln 2}{r_{1/2}^2}$$

Values obtained in this way are in the range 19 - 23 $Å^{-2}$ for all peaks in the structure.

The fact that p for all peaks observed on our Fourier syntheses is close to 20 might be interpreted as indicating the limit of resolution of our X-ray data. That this is not the case is shown by the difference maps, where peaks with half-widths corresponding to values of p up to 60 are observed.

The values of 19 - 23 A^{-2} for p in zunyite are to be compared with Megaw's (1952, p. 484) values 9.7 for Ca, 9.0 for Si, and 8.2 for O in afwillite. In view of the fact that Megaw reports a temperature parameter B = 0.4 A for the afwillite structure, the values of p obtained by her are probably influenced mainly by the resolution of her data.

Cruickshank (1949 a, p. 80) finds values p = 2.9 or 3.4 for carbon peaks in dibenzyl, the different values corresponding to different methods of fitting the Gaussian curve to the peak shape. The value 3.4 corresponds more closely with the method used here. This low value doubtless reflects a high temperature parameter for the structure. Jeffrey (1947), who obtained the data used by Cruickshank, does not report a temperature parameter for dibenzyl, and Robertson (1934), who did the original analysis of dibenzyl, used empirical scattering factors. On the basis of equations 28 and 30 of the next chapter, and assuming (for the

sake of a rough calculation) $\rho_o = 15$ for carbon, we obtain the improbably large value $B = 8.9\ A^{-2}$.

Booth (1946) found that the shapes of peaks due to carbon, nitrogen, oxygen and chlorine in a number of structures could be well accounted for (in their central regions) by taking $p = 4.69$. This circumstance parallels our observation that all peaks in the present study can be accounted for by p near to 20. However, it seems unlikely that the cause is the same in the two cases, as Booth's value was derived from organic structures where the shapes are determined to a considerable extent by the thermal motion alone, the value 4.69 corresponding to a $B = 6.4$, which still seems excessive, in view of the statement by Megaw (1952) that B for organic structures is in the neighborhood of 2.5.

A more accurate treatment has been applied to the peak in Fig. 31, with the result $\rho_o = 114$, $p = 19$. Since the height of the peak is 118, the fit is not perfect, but values of $\rho(r)$ calculated from these parameters are generally in good agreement with observed values for the core, as shown in Table XIV. The table shows that the apron appears at about $r = 3.0$ (120ths) or 0.34 Å.

With the Gaussian density function, electron counts can be carried out easily.

$$N_{Core} = \frac{\pi \rho_o}{p}$$

For the $^2Al_{II}$ peak, which contains 4 aluminium atoms, the result is 40.5 electrons. This value is puzzling, since it accounts

TABLE XIV

$\rho(r)$ FOR $^{2}Al_{II}$ IN F_o III

r	ρ calculated	ρ observed
0.0	114	118
0.5	107	108
1.0	89	89
1.5	65	64
2.0	41.5	41
2.5	24	24
3.0	12	15.5
3.5	5	12
4.0	2	9.5
4.5	0.7	6.5

TABLE XV

TEMPERATURE PARAMETER CORRECTION
DERIVED FROM ΔF I

Equation	Si_I-Al_I Peak		Cl-20_{III} Peak	
	$\Delta B_{Si, Al}$	$\varkappa$	ΔB_{Cl}	$\varkappa$
33	-0.18	---	+0.24	---
36, 37	-0.16	-0.015	+0.17	-0.022
56	-0.41	-0.083	+0.31	-0.034

entirely for the number of electrons in the peak without considering the contribution of the apron, which is estimated to amount to at least 10 electrons. A similar result is obtained by this method for other cations, the core accounting for the full number of electrons.

We have not pinned down the explanation for this and for a few other discrepancies, but it is seen that the electron counts indicate a general consistency and correctness for the atomic shapes derived from the projections.

X. REFINEMENT OF THE STRUCTURE BY MEANS OF DIFFERENCE SYNTHESES

1. Positional Parameters. -- Following the discussion by Lipson and Cochran (1953, pp. 300-301), we have calculated positional parameter changes from the relation

$$\Delta x_i = \frac{\left(\frac{\partial D}{\partial x}\right)_i}{\left(\frac{\partial^2 \rho}{\partial x^2}\right)_i} = \frac{\left(\frac{\partial D}{\partial x}\right)_i}{2p\rho_o}$$

where D represents the density on the difference map. This equation can be applied quite satisfactorily, and even small positional parameter errors cause a distinct gradient on the difference map.

Our chief concern in the use of difference maps has been with the correction of temperature parameters, and we therefore devote the remainder of the chapter to that problem.

2. Temperature Parameters. -- The evaluation and correction of temperature parameters from information obtained from difference syntheses was first discussed fully by Cochran (1951 b). It had been shown (Cruickshank, 1949, p. 155) that difference synthesis refinement is equivalent to least squares refinement with weighting factors $W = 1/f_i$, where f_i is the atomic scattering factor for the atom whose coordinates are to be refined. Cochran made use of this analogy to derive normal equations for least squares refinement of temperature factors using the weighting $w = 1/f_i$. These equations, although applied to anisotropic temperature factors, are entirely analogous to the equations we employed (Chapter VIII, sec. 5) in numerical calculations for correction of isotropic temperature factors. Cochran showed that

these normal equations reduce to a simple expression in terms of the Fourier and difference map densities. His result for two dimensional data (equation 4.8 of the paper cited) reads, when reduced to the isotropic case and written in our notation:

$$\Delta B_i = 12\pi^2 \frac{\left(\frac{\partial^2 D}{\partial r^2}\right)_i}{\left(\frac{\partial^4 \rho_c}{\partial r^4}\right)_i} \tag{20}$$

where the derivatives are evaluated at the center of the i'th atom. For purposes of calculation Cochran gave an expression for $\partial^4 \rho_c / \partial r^4$ derived from the Fourier synthesis formula, with the usual trigonometric averaging:

$$\left(\frac{\partial^4 \rho_c}{\partial r^4}\right)_i = \frac{6\pi^4}{A} \sum_h f_i e^{-\frac{1}{4} B_i s^2} s^4 \tag{21}$$

where the sum is over all reciprocal lattice points for which structure factors were used in making the projection on which D is measured, and $s = 2 \sin\theta/\lambda$.

Cochran's results suffer from two drawbacks: (1) the presence of the fourth derivative in equation 20 is difficult to understand intuitively; and (2) the fact that this derivative cannot be evaluated from the Fourier synthesis directly requires calculation of the sum in equation 21. The disadvantage of using large sums is, first, that it reduces the method to a crank-like numerical operation similar to the least squares or differential synthesis methods. The use of difference maps and Fourier synthesis should enable one to get away from these purely numerical methods, and to evaluate the parameter shifts from

the distribution of electron density itself as seen in the maps. Second, the use of formulae such as equation 21 is always attended by the need for a re-examination for special space groups.

These disadvantages appeared the more acute to us because of the fact that Cochran's method is based on a least squares calculation, whereas we had gone to difference synthesis methods for the express purpose of avoiding the uncertainties and contradictions which had arisen in our least squares refinement of the temperature parameters (Chapter IV). When, therefore, the ΔB_i's calculated by Cochran's method came out absurdly large (due to an error in the use of equation 21, as we subsequently discovered), we were ready to look for other approaches. In the following pages we describe our approach, and then discuss the temperature factor question from a more general standpoint, from which it is possible to show the relationships between the various methods.

The effect of thermal motion is to broaden the apparent shapes of the atomic peaks. Let $\bar{R} = \bar{\imath}x + \bar{\jmath}y + \bar{k}z$ be the displacement of an atom from its equilibrium position, and let $P(\bar{R})$ be the probability density of displacement due to thermal motion. Then the apparent electron density $\rho(R)$ is related to the atomic electron density $\rho_o(R)$ by

$$\rho(\bar{R}) = \int \rho_o(\bar{R}-\bar{S})\, P(\bar{S})\, dv_{\bar{S}} \qquad (22)$$

the integral extending over all of space. The "apparent" density is of course the time average for a given atom, or the instantaneous average for all equivalent atoms in the crystal. The probability $P(\bar{R})$ is given

by Boltzmann's principle (Fowler, 1929, p. 48)

$$P(\bar{R}) = C e^{-\frac{U(\bar{R})}{kT}} \tag{23}$$

where $U(\bar{R})$ is the difference between the potential energy of the atom at $\bar{R}$ and at its equilibrium position, $\bar{R} = 0$. Without a more detailed analysis we will regard this as an approximation, justified by the time-averaging of the potential distribution due to the surrounding atoms. We take the environment to be isotropic; and we suppose that the displacements $\bar{R}$ are small enough that the atom behaves as though bound by Hooke's Law forces, an approximation satisfactory for describing the thermal properties of most substances at ordinary temperatures (Seitz, 1940, p. 100). Then

$$U(\bar{R}) = \tfrac{1}{2} a R^2 \tag{24}$$

where a is a force constant. Writing $a/2kT = \gamma$,

$$\rho(\bar{R}) = \left(\frac{\gamma}{\pi}\right)^{\frac{3}{2}} \int \rho_o(\bar{R} - \bar{S})\, e^{-\gamma S^2}\, dv_{\bar{S}} \quad . \tag{25}$$

We now assume that $\rho_o(\bar{R})$ is a Gaussian distribution of electron density. This assumption has been criticized by Cruickshank (1949 a, pp. 81-82) and by Professor Schomaker (in conversation). But we support its use for the following reasons: 1. It does approximate the observed atomic shape in the main part of the peak quite closely. 2. Even if the observed shape is conditioned more by X-ray resolution than by the true electron distribution, the Gaussian peak still approxi-

mates the general shape of the central part of the real peak, which for our purpose will be at least roughly satisfactory, since we work with the general shape of the peak rather than with such details as may be determined by high-order derivatives. 3. Use of the Gaussian distribution makes simple a calculation which would otherwise involve tedious numerical integrations for each application, a feature which, like the evaluation of $\sum f e^{-\frac{1}{4}Bs^2} s^4$, we expressly wish to avoid.

We therefore take

$$\rho_o(\bar{R}) = \check{\rho}_o(o)\, e^{-p_o R^2} \quad . \tag{26}$$

Performing the integration in equation 24, we obtain

$$\rho(\bar{R}) = \check{\rho}(o)\, e^{-pR^2} \tag{27}$$

where

$$p = \frac{p_o \gamma}{p_o + \gamma} \tag{28}$$

and $\check{\rho}(o)$ is a constant. The density $\rho(\bar{R})$ can now be projected on the x, y plane. If $\bar{r} = \bar{i}x + \bar{j}y$, then

$$\rho(\bar{r}) = \rho(0)\, e^{-pr^2} \tag{29}$$

the simplicity of the projected density being another happy consequence of the use of the Gaussian form.

From this result the effect of thermal motion on the observed peak shape is seen directly. For large thermal motion ($\gamma < p_o$), the

shape is determined largely by the statistical distribution of the atomic centers, while for small motion ($\gamma > p_o$), the thermal effect is only a small modification of the electron distribution for the atom at rest. The parameter γ can be interpreted directly in terms of the temperature parameter B (James, 1950, p. 23) by using equations 23 and 24:

$$B = 8\pi^2 \overline{x^2} = \frac{4\pi^2}{\gamma} \tag{30}$$

For zunyite, and for hard crystals generally, the observed values of B (around 0.5) lead to $\gamma > p_o$, whereas for organic crystals, with values of B up to 5 or more, the situation is $\gamma < p_o$.

The required method for correcting temperature parameters is then clear. From the shape of the difference map peak we evaluate the error Δp in the assumed dispersion parameter p. From equation 28 we interpret Δp in terms of $\Delta\gamma$, and from equation 30 we derive ΔB. The result is simply

$$\Delta B = -4\pi^2 \frac{\Delta p}{p} \tag{31}$$

The problem then is how best to determine Δp. For the most satisfactory determination, one would wish to make use of the shape of the entire difference map peak. We will, however, be concerned mainly with the so-called "paracentric" methods, as they are more adaptable to application and more capable of precise analysis.

It can be shown that to first order the width of the difference map peak or trough is independent of Δp:

$$r_o = \frac{1}{\sqrt{p}} \tag{32}$$

r_o being the radius of the O-contour on the difference map. The only satisfactory readily determined measures of Δp are

$$\Delta p = \frac{\pi D(0)}{Z} \tag{33}$$

where Z is the number of electrons in the atom and D(0) is the difference map density at the center of the peak, and

$$\Delta p = -\frac{\pi}{4pZ}\left(\frac{\partial^2 D}{\partial r^2}\right)_{r=0} . \tag{34}$$

Equation 33 is the more simple and direct to apply, but its use is endangered by the possibility of scale factor error, which gives rise to simple peaks at all atomic positions on the difference map. This difficulty can be avoided by introducing the scale factor as a parameter and solving equations corresponding to 33 and 34 simultaneously. If we let

$$D = \frac{Z}{\pi}(p+\Delta p)\, e^{-(p+\Delta p)r^2} - (1-\varkappa)\frac{Z}{\pi} p\, e^{-pr^2} \tag{35}$$

where $\varkappa$ is the fractional error in the scale factor, then the result is

$$\Delta p = -\frac{\pi}{Z}\left(\frac{D''}{2p} + D\right) \tag{36}$$

$$\varkappa = \frac{\pi}{pZ}\left(\frac{D''}{2p} + 2D\right) \tag{37}$$

where $D'' = (\partial^2 D/\partial r^2)_i$ and $D = D(0)$. Equation 36 corresponds to an equation used by W. C. Hamilton (1954, p. 20) for refining temperature parameters. He arrived at the result in a more formal way which did not show explicitly the manner in which it corrects for scale factor error. And he derived constants for the atomic shapes by means of numerical integration rather than directly from Fourier syntheses, as done here.

In practice, equation 36 gives results little different from equation 33, if the scale factor correction is small, as was the case here. That scale factor error leads to noticeable effects can be seen, however, from the peaks on ΔF I, which do not satisfy equation 32, but have r_o values displaced from the predicted ones in accordance with a negative value of $\varkappa$, an effect which can be calculated from equation 40 (above). Equation 37 can be used to compare the results from different peaks. Results and comparisions are given in the next section.

A simple non-paracentric method which takes into account the general shape of the difference map peak may be derived by using the central density, D(0), the density at the stationary points in the trough surrounding the central peak or the crater lip surrounding the central crater, D(1), and the radius of the smallest 0-contour, r_o. The resulting equations are

$$\Delta p = \frac{1}{2}\frac{\pi}{Z}\left[\, D(0) - e^{2pr_o^2} D(1) \right] \tag{38}$$

$$\varkappa = \frac{1}{2}\frac{\pi}{Zp}\left[D(0) + e^{2pr_o^2} D(1)\right] \tag{39}$$

The three data are not independent, because r_o should be given by

$$r_o^2 = \frac{1}{p}\left(1 + \frac{\varkappa p}{\Delta p}\right) \tag{40}$$

This method has the advantage that it avoids calculation of the second derivative on the difference map. It is not practicable, however, and we present it only as an illustration of a basic difficulty inherent in non-pracentric methods. The factor pr_o^2 can be greater or less than one, but if peaks with $\Delta p > 0$ and others with $\Delta p < 0$ are both present, it will be greater than one for one group or the other (equation 40). If the scale factor error is small, $pr_o^2 = 1$. In any case, the factor $e^{2pr_o^2} \approx e^2 = 7.4$ multiplying D (1) in equation 38 and 39 makes the probable error of Δp large, because D (1) is known to no greater accuracy than D (0). The result is that local irregularities in the outer part of the difference map peak can have large effects on Δp. These local irregularities may be largely spurious.

Thus the main objection to non-paracentric methods is that they are forced to use information from the low-density outer parts of the difference map peaks, where the percentage error of the density is much greater than at the center. A similar effect tends to enter in the calculation of derivatives, but it can be shown that the standard derviation of the term $D''/2p$ in equation 36 is only twice that of D, so that the effect is not too serious for paracentric methods.

We turn now to a more general discussion in which we will use an approach suggested by Professor Hughes (in conversation). The atomic scattering factor and the electron density are Fourier transforms of one another (James, 1950, p. 96):

$$f(\bar{q}) = \int \rho_o(\bar{R})\, e^{2\pi i\, \bar{R}\cdot\bar{q}}\, dv_{\bar{R}} \tag{41a}$$

and the inverse

$$\rho_o(\bar{R}) = \int f(\bar{q})\, e^{-2\pi i\, \bar{q}\cdot\bar{R}}\, dv_{\bar{q}} \tag{41b}$$

where q is a vector in reciprocal space ($|q| = 2\sin\theta/\lambda$). The result of introducing the Debye temperature factor $\exp(-\frac{1}{4}Bq^2)$ is a transformed density (apparent density) given by the (three-dimensional) folding theorem (Waser and Schomaker, 1953, p. 684):

$$\rho(\bar{R}) = \int \rho_o(\bar{R}-\bar{S})\, T(\bar{S})\, dv_{\bar{S}} \tag{42}$$

where $T(\bar{S})$ is the transform of the temperature factor:

$$T(\bar{S}) = \int e^{-\frac{1}{4}Bq^2}\, e^{-2\pi i\, \bar{q}\cdot\bar{S}}\, dv_{\bar{q}} = \left(\frac{\gamma}{\pi}\right)^{\frac{3}{2}} e^{-\gamma S^2} \tag{43}$$

where

$$\gamma = \frac{4\pi^2}{B} \quad ,$$

the integral in equation 42 being evaluated by standard methods. Hence equation 41 reads

$$\rho(\bar{R}) = \left(\frac{\gamma}{\pi}\right)^{\frac{3}{2}} \int \rho_0(\bar{R}-\bar{S})\, e^{-\gamma S^2}\, dv_{\bar{S}} \tag{44}$$

This is identical with equation 25, derived from a quite different standpoint, and shows the close connection between the Debye temperature parameter B and the interatomic force constant a.

Instead of specifying the shape of $\rho(\bar{R} - \bar{S})$, we now derive paracentric relationships for determining changes in γ for any radially symmetrical distribution of electron density. Since we are interested in two-dimensional data here, we note that the projection

$$\rho(\bar{r}) = \int_{-\infty}^{\infty} \rho(\bar{R})\, dz$$

can be carried out explicity in equation 44:

$$\rho(\bar{r}) = \left(\frac{\gamma}{\pi}\right) \int \rho_0(\bar{r}-\bar{s})\, e^{-\gamma s^2}\, dv_{\bar{s}} \tag{45}$$

Now differentiate and set $\bar{r} = o$. Because of the radial symmetry,

$$\left.\frac{\partial \rho}{\partial \gamma}\right|_0 = -\frac{\gamma}{\pi} \int_0^{\infty} e^{-\gamma s^2} s^2 \rho_0(s)\, 2\pi s\, ds + \frac{1}{\pi}\rho(o)$$

$$= -\frac{1}{4\gamma^2}\,\frac{\gamma}{\pi} \int_0^{\infty} e^{-\gamma s^2}\, \frac{1}{s}\,\frac{\partial}{\partial s}\left(s\,\frac{\partial \rho_0}{\partial s}\right) 2\pi s\, ds \tag{46}$$

after integrating twice by parts. Now for $\bar{r} = o$,

$$\nabla^2_{\bar{r}}\ \rho_o(\bar{r}-\bar{s})\Big|_{\bar{r}=0} = \nabla^2_{\bar{s}}\ \rho_o(\bar{r}-\bar{s})\Big|_{\bar{r}=0}$$

and in cylindrical coordinates, for radially symmetric $\rho(\bar{s})$,

$$\nabla^2\rho_o(s) = \frac{1}{s}\frac{\partial}{\partial s}\left(s\,\frac{\partial\rho_o}{\partial s}\right) \quad .$$

Hence by interchanging the order of integration and differentiation in equation 46,

$$\frac{\partial\rho}{\partial\gamma}\Big|_o = -\frac{1}{4\gamma^2}\,\nabla^2\rho\,\Big|_o \tag{47}$$

and since

$$\nabla^2\rho\,\Big|_o = \frac{\partial^2\rho}{\partial x^2}\Big|_o + \frac{\partial^2\rho}{\partial y^2}\Big|_o = 2\,\frac{\partial^2\rho}{\partial r^2}\Big|_o$$

we obtain

$$\frac{\partial\rho}{\partial\gamma}\Big|_o = -\frac{1}{2\gamma^2}\,\frac{\partial^2\rho}{\partial r^2}\Big|_o \tag{48}$$

By the same procedure we derive

$$\frac{\partial}{\partial\gamma}\,\nabla^2\rho\,\Big|_o = -\frac{1}{4\gamma^2}\,\nabla^4\rho\,\Big|_o \tag{49}$$

and since

$$\nabla^4\rho\,\Big|_o = \frac{8}{3}\,\frac{\partial^4\rho}{\partial r^4}\Big|_o$$

this results in

$$\frac{\partial}{\partial\gamma}\,\frac{\partial^2\rho}{\partial r^2}\Big|_o = -\frac{1}{3\gamma^2}\,\frac{\partial^4\rho}{\partial r^4}\Big|_o \tag{50}$$

Equation 50 describes Cochran's method of temperature parameter correction for the case of no scale factor error:

$$\Delta B = -4\pi \frac{\Delta\gamma}{\gamma^2} = 12\pi^2 \frac{\frac{\partial}{\partial\gamma}\frac{\partial^2\rho}{\partial r^2}\Big|_0 \Delta\gamma}{\frac{\partial^4\rho}{\partial r^4}\Big|_0} = 12\pi^2 \frac{\frac{\partial^2 D}{\partial r^2}\Big|_0}{\frac{\partial^4\rho}{\partial r^4}\Big|_0} \qquad (51)$$

Since this result is entirely equivalent, through equation 44, to the simple methods previously discussed, one can understand the (at first) puzzling fact that equations 31 and 33, which involve no derivatives at all, give the same result as is obtained by introducing a Gaussian density into Cochran's equation, which involves the fourth derivative of ρ . This seemed remarkable at first because there was no particular reason to expect the fourth derivative of the Gaussian density to bear much relation to the fourth derivative of the actual density.

From equation 48 a second correction formula is obtained:

$$\Delta B = 8\pi^2 \frac{D(0)}{\frac{\partial^2\rho}{\partial r^2}\Big|_0} \qquad (52)$$

This result expresses the physics of the situation more understandably than equation 51, and obviates the need for the fourth derivative and hence for the sum in equation 21, regardless of the shape of the density profile.

Equation 52 describes a parameter refinement procedure which was given in essence in an earlier paper by Cochran (1951 a, p. 84). Equation 8 of that paper can be reduced exactly to our equation 52 by taking advantage of the circular symmetry at the center of the atomic peak.

The results derived above can be used to construct a paracentric refinement method which takes into account a possible error in scale. If we write

$$\rho_{obs} = (1+\varkappa)\,\rho_{calc} + \frac{\partial \rho_{calc}}{\partial \gamma}\,\Delta\gamma \tag{53}$$

and use equations 48 and 50, which are valid irrespective of scale factor error, the result analogous to equation 36 is

$$\left(\frac{\rho''}{\rho} - \frac{2}{3}\,\frac{\rho^{IV}}{\rho''}\right)\frac{\Delta B}{8\pi^2} = \frac{D}{\rho} - \frac{D''}{\rho''} \tag{54}$$

where all densities and derivatives are to be evaluated at the center of the peak. The coefficient of ΔB in equation 54 involves ρ^{IV}, and is therefore unsuited to evaluation from electron density maps. This difficulty can, however, be avoided by what seems to us a justifiable approximation. The critical feature in equation 54 is the right hand side, because it determines what portion of the observed peak height is due to scale factor error and what portion to temperature factor error. The coefficient of ΔB is unrelated to these effects and would be expected to be the same from peak to peak for a given atom. The fourth derivative evaluates the "first order" departure of the peak from parabolic shape, and is therefore the term which causes the peak to have

the shape of a Gaussian curve rather than a parabola. In this sense it is an intrinsic feature of the Gaussian shape in the central part of the peak, and we may therefore expect to evaluate the coefficient in equation 54 by making use of this observed shape. On this basis

$$\frac{\rho''}{\rho} - \frac{2}{3}\frac{\rho^{IV}}{\rho''} = 2p \tag{55}$$

where p is the parameter in equation 29. The suggested refinement procedure is then simply

$$\Delta B = \frac{4\pi^2}{p}\left(\frac{D}{\rho} - \frac{D''}{\rho''}\right) \cdot \tag{56}$$

The scale factor error can be determined from

$$\kappa = \frac{D}{\rho} - \frac{\rho''}{\rho}\frac{\Delta B}{8\pi^2} \cdot \tag{57}$$

We regard equation 56 as inherently the most satisfactory means of isotropic temperature factor refinement using data derived directly from Fourier and difference syntheses. Unfortunately we have not had opportunity to test it out thoroughly in practice for purposes of comparison with other methods, because it was developed after the refinement was completed, using the methods given by the Gaussian approximation. Equation 56 makes use of that approximation, but only as a multiplying factor whose value is not critical. The basic feature of equation 54, the difference of the ratios of densities and derivatives, is retained in equation 56.

The foregoing considerations have taken no notice of the fact that the electron densities obtained in practice are affected by the finite termination of the Fourier series. Thus in equation 41b the integration is represented as extending over all of reciprocal space. But the effect of termination is readily taken into consideration. We rewrite equation 41b by including the cutoff function:

$$1(\bar{q}\,;q_o) = \begin{cases} 1 & |q| \leq q_o \\ 0 & |q| > q_o \end{cases} \tag{58}$$

$$\rho_o^I(\bar{R}) = \int f(\bar{q})\, 1(\bar{q}\,;q_o)\, e^{-2\pi i\, \bar{q}\cdot\bar{R}}\, dv_{\bar{q}} \tag{59}$$

The density ρ_o^I could be evaluated by using the folding theorem, but for our purposes there is no need to do this, because $\rho_o^I(\bar{R})$ is the density distribution which would replace $\rho_o(\bar{R})$ in equation 42 and the ensuing discussion, and hence it is seen that the results we have obtained apply directly to the densities calculated with series termination.

The above discussion leads, we believe, to a more unified approach to the problem of isotropic temperature parameter correction than has hitherto been given, and allows the formulation of an improved method for direct application, equation 56.

3. Results. -- The zunyite structural refinement did not have the benefit of the comprehensive point of view developed in the preceding section. Instead we were obliged to rely more on rule-of-thumb methods,

and particularly on equation 33, which is the most readily applicable refinement method but neglects the effect of errors of scale. In practice it was found that parameter shifts derived from equation 33 do not converge to the final parameters as rapidly as might be expected. This fact was conspicuous for the chlorine atom, as shown in Table VI, which was all the more puzzling because the estimated scale factor error ($\varkappa$ negative) should have caused an overestimation of the parameter change ΔB_{Cl}. Probably the first order theory is at fault here, and the parameter changes should have been computed directly from equation 28.

The scale factor error seen in the difference maps is of course ficticious in the sense that it represents only the weighting system of the Fourier refinement, because the scale factor had been refined by least squares methods to a final value before the difference syntheses were calculated. In the refined difference map (F_o IV), the effects of scale factor error with $\varkappa < 0$ are visible at the Cl, Si_I, and Al''_{II} positions. At the other positions there is no definite evidence of scale factor error, but, in fact, perhaps even evidence for $\varkappa > 0$. Hence it is debatable whether the error at the former positions is truly a scale factor error in the sense of the preceding section or is due to some other effect.

The present study does not provide an adequately rich sampling of temperature parameter corrections to allow a satisfactory comparison of the relative merits of the various refinement methods discussed in the previous section. As an illustration of the type of comparison that should be made, we show in Table XV the results of the various refinement methods applied to the two peaks Cl + $2O'_{III}$ and Si_I + Al_I. The

comparison is interesting because the effects of scale factor error should work in the opposite direction for the two peaks. However, without a greater number of examples, and particularly peaks at non-special positions, we do not feel justified in discussing the results in detail.

XI. THE TETRAHEDRAL TEMPERATURE FACTOR

The observed electron distribution around the Si_I - Al_I position, as found in the difference maps, leads to the suspicion that these atoms may have thermal motions corresponding to a tetrahedral temperature factor, that is, a temperature factor that is the transform of an electron density modification having tetrahedral symmetry. At first this idea appears absurd, because the (100) projection was chosen for the specific purpose of projecting out the effects of tetrahedral symmetry. However, the projection can show such effects — as, for example, if the atom should move solely on lines directed toward the vertices of a tetrahedron.

The main feature of the observed difference density is a strong negative anomaly projected onto the main diagonal [110] at a distance of 0.32 Å from the Si_I - Al_I position. If the isotropic temperature factor were completely corrected, as well as real or spurious errors in scale, the difference map density in the neighborhood of this position would appear as shown in Fig. 28a.

Unfortunately it is not possible to make a least squares calculation to see whether a small displacement of the average position of the atoms in tetrahedral directions would improve the F_o, F_c agreement, a displacement corresponding to dividing each atom into "fourths" and putting each part in point position 16e. The calculation cannot be done because all the required derivatives vanish. The necessary experimental approach is first to place the "fourths" at a small arbitrary displacement and make a structure factor calculation with these positions.

Due to the fact that the tetrahedral temperature factor has not hitherto been discussed, we deemed it advisable before carrying out the

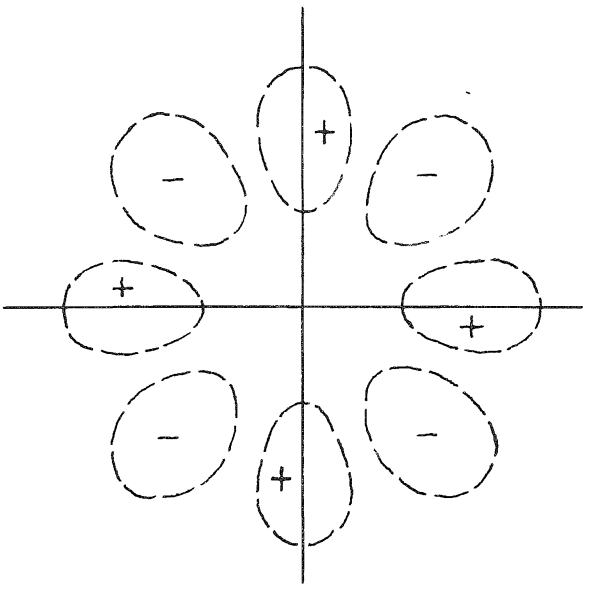

a

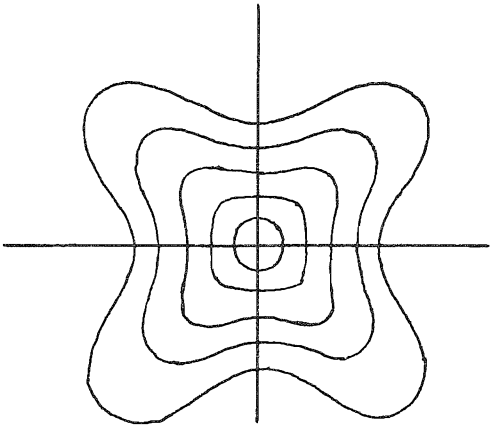

b

FIG. 28

suggested experimental approach to study its formulation from a theoretical standpoint. This study, which we now describe, showed that the observed electron density defects could not be accounted for with any reasonable thermal motions of the atoms, and the experimental calculations have therefore not been attempted, though it might still be of interest to do so.

We approach the problem from the standpoint of equations 22 and 23 of the previous chapter, and investigate the probability distribution of the center of a cation moving in the potential of four anions surrounding it at the vertices of a regular tetrahedron. For the interatomic potential we employ the simple Coulomb-Born model which has been used by Pauling (1939, p. 337 ff.) in treating ionic crystals:

$$U(\bar{r}) = -\frac{z_1 z_2}{r}\left(1 - \frac{1}{n}\frac{a^{n-1}}{r^{n-1}}\right) \tag{60}$$

In this equation a is the equilibrium cation-anion distance, and z_1 and z_2 are the respective charges on the ions.

Choosing a cartesian coordinate system with the equilibrium position of the cation at the origin, we place the anions at (x^1, y^1, z^1) = (a, a, a), (-a, -a, a), (a, -a, -a), and (-a, a, -a). Now we expand the potential, due to the four anions, in powers of the displacement (x, y, z) of the cation from its rest position. The calculation is cumbersome but straightforward, and we simply state the result:

$$U = \frac{e^2 z_1 z_2}{a}\left\{-\left(1-\frac{1}{n}\right) + (n-1)\frac{2}{3}\frac{x^2+y^2+z^2}{a^2} + \frac{4(n+7)(n-1)}{3\sqrt{3}}\frac{xyz}{a^3}\right\} \tag{61}$$

where all terms of third order have been retained.

The xyz term is the only third order term that appears, and it is just what is required to describe a potential distribution of tetrahedral symmetry. The coefficient of this term is positive, meaning that the cation tends to move toward the tetrahedral faces rather than toward the anions.

We now ask what kind of probability distribution of the cation results when the system is projected onto the x, y plane. The projection of equation 23, introducing U from equation 61, is easily carried out. Writing U in the form

$$\frac{U}{kT} = -a + \frac{1}{2} b (x^2+y^2+z^2) + c(xyz)$$

where all constants are positive, we find

$$P(x,y) = K \exp \left\{ -\frac{1}{2} b (x^2+y^2) + \frac{c^2}{2b} x^2y^2 \right\} \qquad (62)$$

It is not possible to normalize this density, but we ignore this fact because we work with small displacements. The electron density which would result from equation 62 is shown in Fig. 28b. The resulting difference map would have the plus and minus signs of Fig. 28a interchanged. This is true regardless of the sign of C, as seen from equation 62. Hence, motions with tetrahedral symmetry cannot account for the observed electron density.

We have overlooked something, however. Because of the projection, a potential of octahedral symmetry would be expected to project to give an x^2y^2 term to add to equation 62, and this term might

correspond to preferred motion of the cation toward the tetrahedral edges, which might reverse the sign of the x^2y^2 term.

This proves to be a definite possibility. It requires an expansion of the potential to fourth order, and results in a new projected probability density:

$$P(x,y) = K' \exp \left\{ -\tfrac{1}{2} b (x^2+y^2) + (\theta - d) x^2y^2 \right\} \tag{63}$$

where

$$\theta = \frac{c^2}{2\left[b + 2d(x^2+y^2)\right]} \tag{64}$$

and

$$d = \frac{e^2 z_1 z_2}{a^5} \left\{ \frac{5}{18}(n-1) + \frac{1}{9}(n+4)(n-1) + \frac{1}{54}(n-1)(n^2+7n+8) \right\} \tag{65}$$

d is the coefficient of the fourth order term in the expansion. It has not been reduced to simplest form, but evidently d is much less than b since the motion is mainly isotropic, and so we obtain

$$\theta \approx \frac{c^2}{2b} \tag{66}$$

A conclusion as to the sign of the x^2y^2 term depends on the relative size of θ and d. We have evaluated these numerically using n = 9, and find (in arbitrary units)

$$\theta = 455$$

$$d = 36.2$$

There seems therefore to be no possibility of $d > \theta$, and hence inclusion of the octahedral terms does not modify the previous conclusions. The calculations admit of easy error due to their complication, however, and have not been thoroughly checked.

XII. STATISTICAL EVALUATION

Cruickshank (1949a, 1949b, 1950) has given methods for estimating standard deviations of parameters derived from difference syntheses. We have used his approach and have estimated standard deviations of positional parameters for comparison with standard deviations estimated in the standard way (Mood, 1950, pp. 301 - 303) from the least squares calculations. The results are given in Table XVI.

The main difficulty in applying Cruickshank's method is that the formulae have to be revised for the high symmetry of T_d^2. If this is not done properly, the formulae may lead to a doubling of the electron density curvatures for atoms at special positions. Curvatures derived by Cruickshank's methods are found to agree roughly (to within about 5 %) with curvatures derived directly from the Fourier syntheses using the Gaussian approximation.

A peculiar feature of the standard deviations given in Table XVI is the high value for z_6 derived from the least squares calculations. The reason for this is the fact that z_6 was taken almost zero (actually 0.001). This causes all derivatives $\partial F / \partial z_6$ to be small (they would vanish strictly for $z_6 = 0$), so that the coefficient of the diagonal term for z_6 in the normal equation matrix is very small. Evidently a second order theory would be required to estimate correctly the z_6 variance.

The estimated standard deviation for the electron density is 1.3 electrons Å^{-2} by Cruickshank's method. Cruickshank's method takes as the estimate of σ for a given reflection the value of $(F_o - F_c)$. An alternative approach was proposed by Booth (1946) and Booth and

TABLE XVI

ESTIMATED STANDARD DEVIATIONS FOR POSITIONAL PARAMETERS

Atom	Coordinate	Least Squares Estimate	Fourier Estimate
Si_{II}	x_1	0.00022	0.00016
O_I	x_2	0.00066	0.00042
O_{II}	x_3	0.00077	-----
O_{III}	x_4	0.00085	0.00046
O_{IV}	x_5	0.00059	-----
	z_5	0.00060	-----
O_V	x_6	0.00033	0.00042
	z_6	0.0103	-----
Al_{II}	x_7	0.00017	0.00018
	z_7	0.00023	0.00018

Britten (1948), and later revised by Lipson and Cochran (1953, p. 288). In this method, σ is estimated from the intensity measurement errors. Taking $\sigma(F_o) = 0.1\,|F_o|$ for a single structure factor estimate, which is an outside limit on the basis of the information given in Chapter III, we calculate on this basis

$$\hat{\sigma}(\rho) = 2.1\ e\text{Å}^{-2}$$

$$\hat{\sigma}(x) = .0004 = .0055\ \text{Å}$$

$\hat{\sigma}(x)$ is the estimated variance of an atomic coordinate. There is seen to be rough general agreement between these estimates and the values quoted previously, suggesting that random measurement errors contribute a large share of the final discrepancy between calculated and observed structure factors.

The values of $\hat{\sigma}(\rho)$ merit special comment, in view of the desirability of attempting to locate the hydrogen atoms in the structure by means of difference syntheses. Mc Connell (1955) found the heights of the hydrogen peaks in a difference synthesis of diphenyl napthacene to be slightly under $0.5\ \text{Å}^{-2}$. Projections given by Cochran (1951a, p. 87) of adenine hydrochloride show hydrogen peaks of height $1.0\ e\text{Å}^{-2}$. If these values are representative, it is evidently out of the question to locate the hydrogen atoms in zunyite by this method, because the electron density around the proton is less than in organic molecules, owing to the large electronegativity difference between oxygen and hydrogen. The above authors did not quote standard deviations for their electron densities, but it is evident that the values must have been $0.2\ e\text{Å}^{-2}$ or lower. One wonders why the standard deviation for the

zunyite projection is so much higher. The reason is that the peak heights in the Fourier synthesis are much higher in zunyite, because of the heavier atoms present. Booth (1946) has shown that $\sigma(\rho)$ is proportional to the root mean square electron density in the Fourier synthesis, which increases with the total number of electrons per square Angstrom in the projection and also with the sharpness of the Fourier peaks. Thus high density and low temperature factor lead to high values of $\sigma(\rho)$, and it therefore seems unlikely that protons can be located in silicate structures by difference synthesis methods.

Accuracy of temperature parameters could be estimated from the estimated standard deviation of the electron density. The temperature parameter s.d. estimate would be rather beside the point, it would seem, in view of the large discrepancy between the temperature parameters for the (h k 0) and the (h h l) data.

XIII. DISCUSSION OF THE STRUCTURE

The present study verifies the structure proposed for zunyite by Pauling (1933). The main features of Pauling's structure, and the features making the structure unique, as described in Chapter III, are entirely retained. The atomic positions in the refined structure differ by significant but not large amounts from the positions chosen by Pauling for the trial structure. The differences are such as to give interatomic distances and shapes of coordination polyhedra in good agreement with those found in related ionic structures. In this chapter these detailed features of the refined structure will be discussed. The availability of accurate interatomic distances makes possible the prediction of the proton positions in the structure, and this will be attempted. Finally, a theoretical treatment of the shapes of coordination polyhedra in zunyite will be mentioned.

1. Interatomic Distances and Accuracy. --- Final atomic parameters, obtained in the way described in Chapter VI, and listed in Table V, have been used to calculate interatomic distances given in Table XVII. Values derived from the trial structure are given for comparison. For these, values given in Pauling's paper (1933, p. 452) have been used where available.

The accuracy of all interatomic distances derived from this study is taken as + 0.02 Å. This figure is arrived at as follows. By using the parameter standard deviation estimates given in Chapter XII, standard deviation estimates can be calculated separately for each interatomic distance by considering the combination of parameters by which it is derived. The resulting estimates are less than 0.01 Å for

TABLE XVII

INTERATOMIC DISTANCES AND BOND ANGLES

Tetrahedra:

Atoms	Trial	Final
Si_I-O_{II}	1.59 Å	1.64 Å
Si_{II}-O_{II}	1.59	1.62_5
Si_{II}-O_V	1.59	1.65
Al_I-O_I	1.74	1.82

Octahedra:

Atoms	Trial	Final
Al_{II}-O_I	1.86	1.92
Al_{II}-O_{III}	1.85	1.79
Al_{II}-O_{IV}	1.89	1.85_5
Al_{II}-O_V	1.93	1.92

Chlorine:

Atoms	Trial	Final
Cl-O_{III}	3.14	3.07
Cl-O_{IV}	3.59	3.58

TABLE XVII (Continued)

INTERATOMIC DISTANCES AND BOND ANGLES

Tetrahedron Edges:

Atoms	Trial	Final
O_{II}-O_{II}	2.60	2.67
O_{II}-O_{V}	2.60	2.66
O_{V}-O_{V}	2.60	2.72
O_{I}-O_{I}	2.84	2.97

Octahedron Edges:

Unshared:

Atoms	Trial	Final
O_{I}-O_{IV}	2.68	2.69
O_{III}-O_{IV}	2.67	2.63_5
O_{III}-O_{V}	2.67	2.74
O_{IV}-O_{IV}	2.67	2.60
O_{IV}-O_{V}	2.64	2.67
O_{V}-O_{V}	2.84	2.67_6
Average	2.68	2.67_6

Shared:

Atoms	Trial	Final
O_{I}-O_{V}	2.64	2.51

TABLE XVII (Continued)

INTERATOMIC DISTANCES AND BOND ANGLES

"Non-bonded" Contact:

Atoms	Trial	Final
O_{IV}-O'_{IV}	2.71	2.77

Cation-Cation:

Atoms	Trial	Final
Si_I-Si_{II}	3.18	3.26
Si_{II}-Al_{II}	3.27	3.24
Al_{II}-Al_{II}		
Sharing edge	2.72	2.90
Sharing O_{III} corner	3.49	3.34
Sharing O_{IV} corner	3.58	3.56
Al_I-Al_{II}	3.17	3.24
Cl-Al_{II}	4.16	4.06

Angles:

Atoms	Trial	Final
Al_{II}-O_{III}-Al_{II}	142°	137° ± 1.6°
Al_{II}-O_{IV}-Al_{II}	142°	147°

cation-oxygen distances and are from 0.008 to 0.016 Å for oxygen-oxygen distances. However, the separate calculation of estimates for each interatomic distance is not justified by the limited significance that can be attached to the individual parameter standard deviations. We therefore adopt as an inclusive parameter s.d. estimate the value ± 0.001, from a consideration of Table XVI. This estimate harmonizes with a comparison of the results of the (h k 0) and (h h l) refinements, as discussed in Chapter VI. The resulting interatomic distance accuracy, ± 0.02 Å, can be regarded therefore as an outside limiting estimate. Further refinement of the (h h l) data, after correction of the contrast effect, would perhaps justify a claim to greater accuracy.

Using the estimate ± 0.02 Å for the bond length accuracy, the estimated bond-angle accuracy is ± 1°.6.

2. Discussion of Distances. -- The refined structure differs significantly from the trial structure in the following ways: (1) enlargement of the SiO_4 tetrahedra; (2) enlargement of the AlO_4 tetrahedron; (3) increased separation of Al_{II} atoms in octahedra sharing edges; (4) distortion of the AlO_6 octahedra, with prounounced shortening of shared edges; (5) decrease of the $Cl\text{-}O_{III}$ bond distance. All of these features can be given a satisfactory interpretation.

Enlargement of the SiO_4 tetrahedra is due to partial replacement of silicon by aluminium. J. V. Smith (1954) has surveyed bond distances for tetrahedrally coordinated Si and Al in various compounds showing differing degrees of replacement of Si by Al. He finds the distance 1.60 ± 0.01 Å for the pure Si positions and 1.78 ± 0.02 Å

for the pure Al positions, and he postulates a linear dependence of the mean bond length on composition, for random replacement. The observed distance in zunyite, 1.64 $\pm$ 0.013 Å, corresponds to replacement of 1.1 $\pm$ 0.4 out of 5 silicon atoms by aluminium. This rough measure is in rough agreement with the observed composition (Appendix I) of crystals from the Zuni Mine, in which the silicon percentage is 7 °/o below the ideal composition corresponding to 5 silicon atoms in the structural unit.

Inasmuch as the Si-0 distances are equal within the accuracy of measurement at the Si_{II} and Si_{I} positions, substitution of Al for Si must be at random within the Si_5O_{16} group. This random substitution should have the interesting effect of imposing an apparently increased temperature parameter on the atoms of the Si_5O_{16} group. Supposing that the largest displacement of any atom from its unsubstituted (pure Si_5O_{16}) position is half the difference between the pure Si-0 and pure Al-0 distances, 0.09 Å, the root mean square displacement of such an atom is 0.041 Å for 20 °/o substitution. The temperature parameter B = 0.24 corresponds to a root mean square displacement of 0.056 Å. Thus the thermal effect and the random substitution effect are of the same order of magnitude. The difference between B = 0.25 and B = 0.50 being strongly apparent on difference maps, it might be expected that the random substitution effect could be detected. There is no evidence for it in zunyite, but it is not possible to draw any substantial conclusions from the observed temperature parameters, because of the likelihood of systematic error due to

contrast errors. To our knowledge, such an effect has never been reported in careful studies of structures with random substitution (for example, in the feldspars: Bailey and Taylor, 1955).

The increased size of the SiO_4 tetrahedra allows the O_V atom to pull back into the xy, yz, and zx planes, and increases O-O distances throughout the Si_5O_{16} group. The O_V-O_V distance increases by a significantly greater amount, 0.06 Å, producing a distortion in the outer four tetrahedra of the group, by enlarging the outward-directed faces of these tetrahedra. This distortion is caused by the effects of repulsion between the Al_{II} atoms.

The effects of this repulsion are probably the most striking features that distinguish the trial and final structures. The Al_{II} atoms occur in groups of three at the centers of three octahedrally coordinated groups of oxygen atoms, sharing edges to form an Al_3O_{13} group (see description and diagrams in Chapter III). In the trial structure, the octahedra are nearly regular in shape, and the aluminium atoms located nearly centrally in them, the distance Al_{II}-O_V being elongated somewhat by the pulling in of the oxygen atoms toward silicon. In the refined structure, the aluminium atoms increase in separation by 0.18 Å, and the octahedral groups become markedly distorted. The shared edges contract to a length of 2.51 Å. There is a general rearrangement of the other O-O distances, but the average length of the unshared edges does not change significantly. The increased separation of Al_{II} atoms is facilitated by the increase in the O_V-O_V octahedral edge length, the distance Al_{II}-O_V remaining practically unchanged. The Al_{II} atoms move away from the centers of the distorted octahedral groups, and

toward the O_{III} atoms. This effect is strikingly shown in the $(1\bar{1}0)$ projection of the structure (Fig. 20), in which the Al_{II} peak is noticeably offset from the geometrical center of the projected $O_I - O_{III} - {}^2O_{IV} - {}^2O_V$ octahedron. The average Al-O distance, 1.88 Å, remains in close agreement with the radius sum, 1.90 Å (Pauling, 1939, p. 346).

The contraction of the shared edges to 2.51 Å is in harmony with shared-edge lengths in aluminium octahedra found in other structures: 2.50 Å in diaspore (Ewing, 1935) and 2.49 ± 0.03 Å (average value) in gibbsite (Megaw, 1934). The usual comparison with corundum (Struktunbericht, 1931, p. 242), for which a value 2.49 Å is quoted, does not seem entirely justified, inasmuch as the value 2.49 Å refers to the edge of a face shared between two octahedra, while the lengths of single edges shared between octahedra is 2.61 Å. It would be desirable to compare the shared-edge length with values found in the chemically related structures of topaz, andalusite, sillimanite, and kyanite, but the early determinations of these structures have not been systematically refined. The available values (Strukturbericht, 1937, pp. 110 - 117) are scattered: 2.59, 2.83, and 2.47 Å.

Another effect of the shortening of shared edges in the Al_3O_{13} group is the enlargement of the coordination tetrahedron around Al_I. The value 1.82 Å for the Al_I-O_I distance is greater than the Al-O distance of 1.78 Å for pure aluminium tetrahedral sites given by Smith (1954), though the difference is on the margin of significance. To the extent that the difference is significant, it disputes Smith's contention that the surrounding cationic environment has no effect on bond distances at tetrahedral positions.

3. Location of the Protons. -- Of the 38 oxygen atoms in the zunyite structural unit, 18 must have protons attached in order to satisfy the electrostatic valence rule, or must be substituted by fluorine (see Chapter III). Because it has proved impossible to locate these protons by X-ray means, we propose to assign their positions on the basis of structural arguments.

Pauling's reasoning (Chapter III) shows that the protons are associated with the O_{III} and O_{IV} atoms. We first consider O_{III}. If the oxygen and chlorine ions were simply in contact, the expected interatomic distance would be the sum of the crystal radii or 3.21 Å, well in excess of the observed value 3.07 Å. This shows that the proton on O_{III} forms a hydroxyl bond (Bernal and Megaw, 1934) with the chlorine. The observed distance may be accounted for in the following way. The non-bonding radius of the hydroxyl ion has values ranging from 1.6 to 1.8 Å (loc. cit.). To be specific we take the contact radius 1.60 Å shown in brucite (Strukturbericht, 1931, p. 193). The non-bonded Cl-OH distance is then 3.41 Å. The shortening of this bond due to hydroxyl bond formation may be estimated from comparison of the OH-OH distances in brucite and gibbsite: 3.19 Å and 2.79 Å, respectively, giving a shortening of 0.40 Å. This shortening implies a hydroxyl-bonded Cl-OH distance of 3.01 Å, which, while short, is a considerable improvement over the non-bonded distance.

The above calculation is open to attack, of course. Another approach, due to Professor Pauling (in conversation), is as follows. The equilibrium positions of the proton between two oxygen atoms in ice are 0.8 Å apart. Thus, in the Cl---H-O bond, the distance

expected is the sum of the proton-anion distances in HCl and in H_2O, lengthened by 0.8 Å. This results in 3.08 Å, in excellent agreement with the observed value of 3.07 Å.

These considerations indicate that the proton lies along the line of centers of the Cl and O_{III} atoms, a location that is supported by the bond angles at O_{III}. Bernal and Megaw (1935) have pointed out that the proton in hydroxyl bonding tends to assume a tetrahedral orientation with respect to the surrounding cations, as seen from the oxygen ion to which the proton is attached. Professor Pauling suggests (in conversation) that the acceptable proton positions be found by the intersection of cones of apex angle $360^\circ - 2(109^\circ 28')$, the apices located at the oxygen ion and the cone axes directed toward the surrounding cations. For two cations subtending the tetrahedral angle at the oxygen ion, this construction gives, of course, two possible proton positions in regular tetrahedral orientation. As the cation-oxygen-cation angle is increased, the possible proton positions approach one another, and when this angle reaches 141° the cones become tangent and the single possible proton position is coplanar with the two cations and the oxygen ion. This is very nearly the situation at O_{III}, because the Al_{II}-O_{III}-Al_{II} angle is 137°. The symmetry then places the proton along the O_{III}-Cl line.

Fluorine probably does not substitute for O_{III}, because the sum of the fluorine and chlorine crystal radii is 3.17 Å, and there would be no hydroxyl bonding.

We now turn to the O_{IV} atoms, of which there are 12 in the structural unit. These atoms are arranged at the corners of a truncated regular tetrahedron, shown in Fig. 29, at the center of which is

the Al_I atom. The O_I atoms lie at the centers of the four large faces of the truncated tetrahedron. Each of these large faces forms the face of an Al_3O_{13} group (better, $Al_3O_4(OH)_9$) which attaches on the outside.

Now the bond angle Al_{II}-O_{IV}-Al_{II} is 147°. If this is interpreted to require that the protons occupy the coplanar positions, as in O_{III}, then they must stick out perpendicular to the long edges of the truncated tetrahedron, as shown in Fig. 29a. This places the atoms O_{IV} and O'_{IV} (Fig. 30a) in a non-bonding arrangement, an arrangement which seems to us unlikely in view of its expected effect on the O_{IV}-O'_{IV} distance. The O_{IV} and O'_{IV} atoms are not bonded together by forces from within the truncated tetrahedron. Instead, they form one edge of a tetrahedral group of oxygen atoms with no cation at the center. Neither are the O_{IV} and O'_{IV} atoms bonded together by forces from the Al_3O_{13} group outside. There again they form part of a tetrahedron with no central cation, as can be seen in Fig. 30. We therefore have reason to expect the O_{IV}-O'_{IV} distance to approach the non-bonded hydroxyl distance of 3.2 Å or greater. This expectation is substantiated in gibbsite, in which the octahedral groups distort in such a way that the oxygen atoms equivalent to O_{IV} and O'_{IV} are placed at an average distance of 3.20 ± 0.20 Å, (see Megaw, 1934). The actual O_{IV}-O'_{IV} distance is only 2.77 Å. Although this is notably the longest O-O distance in the Al_3O_{13} group, it falls far short of the expected non-bonded distance, and is instead a typical hydroxyl-bonded distance.

We therefore introduce hydroxyl bonds between the O_{IV} and O'_{IV} atoms by rearranging the protons according to a scheme such as shown in Fig. 29b, in which one proton is assigned to each long edge of the

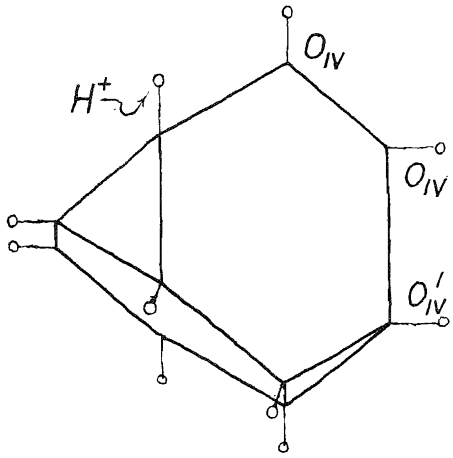

a

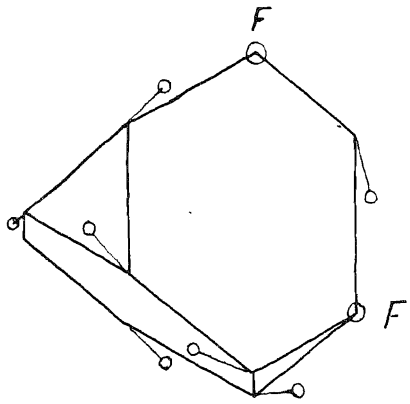

b

Fig. 29

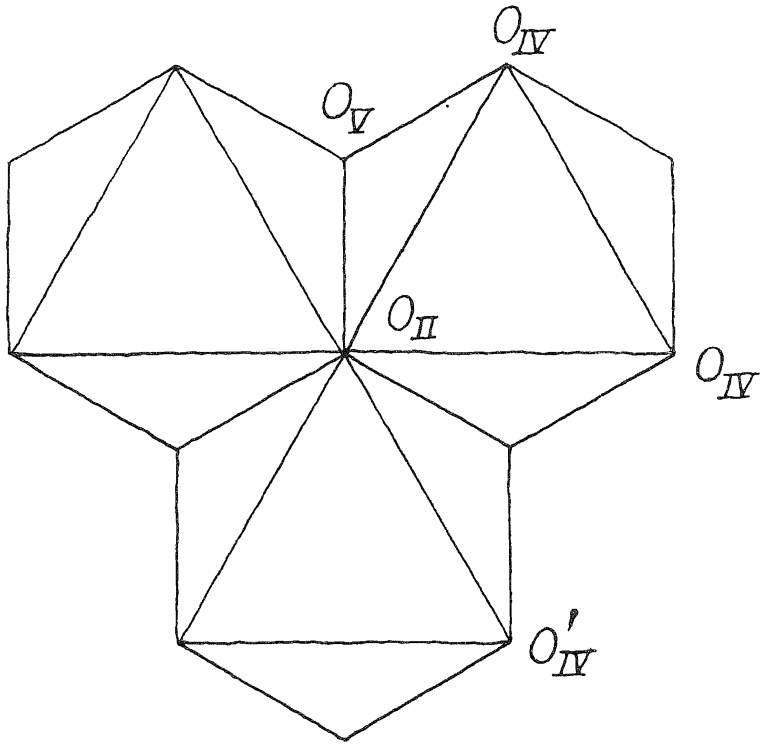

Fig. 30

truncated tetrahedron, and one to each truncation, sticking out toward the chlorine atom. In disregarding the requirement of coplanarity we make use of the fact that the angle Al_{II}-O_{IV}-Al_{II} is greater than 141°, so that in the strict sense of Professor Pauling's construction the protons no longer have a preferred position. This interpretation is of course specious as long as the bond angle is not strictly 180°, but serves to emphasize the fact that the more nearly 180° is approached, the less determinative is the tetrahedral orientation, so that the protons become free to adopt positions most favorable electrostatically. It seems clear that the configuration proposed by us is more favorable in this way than the configuration required by coplanarity, because it reduces the repulsive potential between the O_{IV} and O'_{IV} atoms. But in any case the proposed arrangement is required by the interatomic distances, in our opinion.

It may be worthwhile to note that tetrahedral proton orientation is not a rigid requirement, because in many structures it is impossible to satisfy. In diaspore, for example, where three aluminium cations are associated with the proton-bearing oxygen ions, the most acceptable position for the proton would (due to symmetry) be in the b direction from the O_{II} oxygen ion (see Ewing, 1935), at an angle of 112° to the aluminium atoms. Although this angle differs by only 2°.5 from the tetrahedral, interatomic distances show that the proton moves around so as to form a smaller angle with two of the aluminium atoms and a larger angle with the third. With the positions proposed by Ewing we calculate angles of 104°.4 and 143°.5 respectively, for the proton attached to the O_{II} atom (Ewing's notation). Likewise for the proton on

O_I in diaspore we find two aluminium atoms at 109.°8 and one at 82.°3. It seems more likely that the protons adopt intermediate positions as suggested in the diagram of Bernal and Megaw (1935), but in any case it is clear that the requirement of tetrahedral proton orientation is mitigated by features peculiar to each individual structure.

The proton arrangement proposed for the O_{IV} atoms of zunyite allows only 10 of the 12 protons to be placed in the truncated tetrahedral group. Two more could be added, of course, by introducing two protons into positions on two of the truncated corners. This would make the O_{IV} atoms non-bonding on these corners, but inasmuch as these atoms are held directly to the same aluminium cations no conspicuous distance effects would be expected. However, such an arrangement is bound to have higher energy (lower binding energy) than the 10-proton arrangement, and it can be avoided by replacing two of the O_{IV} atoms by fluorine. This, indeed, may be the true role of fluorine in the structure. That fluorine does have a special role is suggested in a striking way by the synthesis of presumed zunyite by Niggli, as discussed in Chapter XIV. The mineral has been synthesized under hydrothermal conditions in the presence of a small amount of fluorine, but not without. The Zuñi Mine crystals contain consistently about 3-3.5 atoms of F out of the 18 (OH + F), which accords with our expectations. The same is true for the new analyses of crystals from Uaxactum and from Kazakhstan (see Appendix I). For the Postmasburg material values of only 0.3 - 0.5 for F are reported, but for two of the three analyses the sum OH + F is low by about 2.0 and the third was considered untrustworthy by Pauling for other reasons. Hence there seems to be support for the

proposed special role of fluorine in the zunyite structure, a role which can be expressed by reformulating the composition thus:

$$(OH,F)_{16}\ F_2\ Al_{13}\ Si_5\ O_{20}\ Cl$$

It should be mentioned in conclusion that the proposed proton-fluorine arrangement is of course statistical, the configuration shown in Fig. 29b being only one of many equally likely configurations.

4. Relationships to Other Structures. -- Zunyite is classified by Dana (1932, p. 591) with helvite and the ultramarines, probably on the basis of morphological similarity. There is no basic relationship, however, the only feature in common being the inclusion of chlorine or other large ions in the structures. There is no counterpart in any other known structure for the Si_5O_{16} group in zunyite, whose existence conflicts with the well-known rule that silicon tetrahedra do not share corners unless the ratio O:Si is less than 4:1 (Bragg, 1937, p. 140). The closest structural relative of zunyite is diaspore, $AlHO_2$, which is built by linking together $Al_3(OH)_{13}$ groups of the kind found in zunyite. The groups link together by sharing edges to form endless ribbons through the structure (the double rutile strings of Ewing), and the ribbons are linked together by sharing corners of aluminium octahedra and by hydroxyl bonds. The linking is such that no "non-bonded" oxygen atoms equivalent to O_{IV}-O'_{IV} in the Al_3O_{13} group occur, because every pair of oxygen atoms is common to at least one octahedral group around an aluminium atom. The nearest equivalent in diaspore of the O_{IV}-O'_{IV} pair in zunyite is a pair of hydroxyls which are an unshared edge with respect to one ribbon and a "non-bonded" pair with respect to

the adjoining one. The interatomic distance of this pair is 2.84 Å, which is accurately known because it is the C-axis repeat distance of the crystal. This distance is significantly larger than the O_{IV}-O'_{IV} distance of 2.77 Å in zunyite, and provides additional support for the expected repulsion between non-bonded hydroxyl ions.

In böhmite the ribbons are linked together in a different way, with the result that OH^- and $O^=$ positions are distinguished in the structure, a point of similarity with zunyite.

The aluminosilicate minerals andalusite, sillimanite, kyanite, topaz, and zunyite all have ratios Al:Si $\cong$ 2:1, and it would be desirable to give a structural interpretation of the conditions required for the stability of each. This cannot be adequately done, but we may remark that a basic hydrothermal environment leads to topaz, $[Al(OH,F)]_2 SiO_4$, and the additional requirement of including chlorine atoms would favor the zunyite structure.

5. Other Properties. -- Ordinary X-ray data cannot distinguish between the two possible orientations of the zunyite structure relative to the external morphology of the crystals, owing to Friedel's Law. We therefore predict the orientation, by considering the growth process of the crystal. The basis of the argument is that the structure builds up by a packing together of Si_5O_{16} groups and of large aluminium-oxygen groups, $Al_{13}O_{16}(OH)_{24}$, formed by addition of four Al_3O_{13} groups to the truncated tetrahedron of Section 3. The oxygens in these large Al-O groups are approximately in closest packing, and because of the resulting compactness it may be expected that such a group could build up

relatively readily on a crystal face of any orientation, especially with the help of the hydroxyl bonding scheme proposed in Section 3. The same is not true of the relatively spindly Si_5O_{16} group. For growth of the (111) face in Pauling's orientation, which is described by the coordinates we have used (Chapter III), it is necessary for Si_5O_{16} groups to build out from the crystal face into the surrounding medium in order that growth can continue, whereas on the $(1\bar{1}1)$ face the Si_5O_{16} group builds up in accommodating niches between the large Al-O groups. We regard the formation of the Si_5O_{16} group as the rate-limiting process, and hence predict that Pauling's orientation is in accord with the external morphology, the (111) face being the positive tetrahedral face (large, i.e., slow-growing) and the $(1\bar{1}1)$ face being the small negative tetrahedral truncation.

The observed octahedral cleavage (Spencer, 1930) of zunyite can be explained by planes of weakness similar to the basal planes of topaz. Twinning is observed (Spencer, 1930) with [111] as twinning axis and (211) as composition plane. We have been unable to find a satisfactory structural interpretation of this.

6. Shapes of coordination polyhedra: theoretical. -- Pauling (1937) has shown that it is possible to account satisfactorily for the shapes of coordination octahedra in rutile and anatase by making use of the Born-Madelung theory of the energy of ionic crystals. We have been interested in carrying out similar calculations for the shape of the Al_3O_{13} group in zunyite. The calculations are too involved to report here in detail, and have

not led to satisfactory quantitative results, but we wish to mention one feature of special interest. For small displacements of the atoms from the undistorted configuration for the three octahedra in the Al_3O_{13} group, the change in potential energy takes the form

$$\Delta U = \Delta U_{K-K} + \frac{1}{2}\sum_{i,j}{}' \Psi_{ij}\frac{\delta_{ij}^2}{r_{ij}^2} + 3\Phi_{15}\frac{\delta_{15}}{r_{15}} - 3\Phi_{44'}\frac{\delta_{44'}}{r_{44'}} \qquad (67)$$

where the δ_{ij} are the changes in interatomic distances from the undistorted configuration, atoms being labelled as shown in Fig. 31, and Φ_{ij} and Ψ_{ij} are the coefficients of the first and second order terms in the expansion of the interatomic potentials for small displacements from equilibrium. The ΔU_{K-K} term is the change of mutual (Coulomb) energy of the cations. Because of the fact that an undistorted octahedron is separately in equilibrium, the sum of the first-order energy terms vanishes, leaving the second order term in equation 67. When the octahedra share edges, however, a linear term appears for the shared edges (the 1-5 term), in addition to a term due to repulsion in the "non-bonded" O_{IV}-O'_{IV} contact. This linear term for the shared edges is responsible for the pronounced shortening of these edges, and the form of equation 67 shows that the shortening would be expected irrespective of whether or not it leads to a decrease in the mutual coulomb energy of the cations. The effect of the latter would be distributed among all O-O bond distances, more or less. These qualitative considerations are in accord with the observed distortion of the octahedra in zunyite, as described in Section 2.

XIV. GEOLOGIC OCCURRENCE AND SIGNIFICANCE OF ZUNYITE

1. Natural Occurrence. -- Zunyite has been found at five localities in the world: the Zuñi Mine and the Charter Oak Mine, near Silverton, in the San Juan Mountains, Colorado; Uaxactum, Guatemala; Postmasburg, South Africa; near Lake Balkash, in Kazakhstan; and recently reported from Afn, Algeria.

The Zuñi Mine locality, where the mineral was discovered, apparently was never visited by Hillebrand (1885). The following statement is quoted from the Proceedings of the Colorado Scientific Society (1885, p. 131): "Mr. Guiterman, in reference to the occurrence of the zunyite in the Zuñi Mine, mentioned that there seemed to be no indication of a fissure vein, but that the ore appeared to occur in a pipe enlarged in places. The ore is a heavy lead ore containing arsenic and a little silver, and much altered at the surface." A more illuminating report was given by Penfield (1893), who visited both the Charter Oak and Zuñi Mines. At the Charter Oak Mine the mineral occurs only in the wall rock, which is described as an "altered porphyrite". The rock is "very hard, fine grained, grayish white ... and very much altered by stream and fumarolic action so that only remnants of the original minerals are left." The zunyite crystals in the rock are fresh and clear. It is unfortunate that an adequate petrological description and chemical analysis of the "porphyrite" are not available.

Penfield found that zunyite crystals also occur in the wall rock of the Zuñi Mine. The wall rock is this same "porphyrite", and the two localities are closely related, being only 5 miles apart. Penfield states: "At both localities zunyite is plainly secondary and formed by

fumarolic action on the silicates of the rock." The associated minerals at the Zuñi Mine are guitermanite, and, in the oxidized zone, anglesite. At the Charter Oak Mine they are enargite, pyrite, scorodite, and sulfur.

The most illuminating occurrence of zunyite so far reported is the locality near Postmasburg, South Africa, described in detail by Nel (1930). The zunyite occurs in small patches in a diaspore-bearing highly aluminous shale of the Gamargara Series (probably younger pre-Cambrian in age). The shales are red, purplish, and gray, occur at the base of a thick quartzite section, and overlie a coarse, ferruginous, basal breccia. Chemical analysis of a sample of the Gamargara shale is quoted in Appendix III, with typical analyses of zunyite and common shale for comparison. Nel considers the shales to be a lateritic residue derived from the weathering of a large mass of older limestones and dolomites.

Nel finds the alteration to zunyite difficult to explain as hydrothermal, because no igneous rocks of age as young as the shales or younger are found in the area. Instead, he regards it as due to "changes set up by circulating waters or some other process without the conditions of high temperature and mechanical force".

The intimate association of zunyite and diaspore is noteworthy, in view of the similarity of the two structures.

Palache (1932) reported the bizarre discovery of zunyite in powder contained in pots from graves in the ruined Mayan city of Uaxactum, in the plains of northern Guatemala. The powder is red and contains an abundance of fine hematite scales, typical of fumarole

deposits. Palache interprets the powder as a pigment brought by the natives from the volcanic highlands of San Salvador to the south. The zunyite presumably was formed in place with the hematite, as a superficial deposit.

Astashenko and Moleva (1939) described zunyite from near Lake Balkash as occurring in a vein in "secondary quartzite", derived from grandodiorite porphyry. The crystals occur in a green matrix of mimetite and anglesite, an environment resembling that of the Silverton occurrences.

The most recent report is by Turco (personal letter, 1956) who has discovered a mineral resembling zunyite at Afn in Algeria. It occurs in a kaolinite-montmorillonite gangue, but unfortunately the locality is no longer accessible, for political reasons.

2. Synthesis. -- Schlaepfer and Niggli (1914) carried out hydrothermal mineral syntheses in the system SiO_2-Al_2O_3-K_2O, and found that when K_2O was absent, a zunyite-like mineral was formed under a range of mole ratios SiO_2:Al_2O_3 from 6:4 to 3:7, spanning the composition of the Gamargara shales. The mineral was isotropic, tetrahedral, insoluble in HCl (as is zunyite), and had index of refraction 1.545-1.547. For natural zunyite are reported indices of 1.589 (Larsen, 1921), 1.602 (Albis, 1921), 1.595 (Gossner and Mussgnug, 1925), 1.600 (Spencer, 1930), 1.590-1.594 (Astashenko and Moleva, 1939). The average value is n = 1.596. The difference between the index of natural zunyite and of Niggli's synthetic crystals is nicely accounted for by the lack of chlorine in the latter. We make use of Fajan's and Joss's treatment of the Lorenz-Lorentz equation (see Seitz, 1940, p. 660), and

calculate $\Delta n = 0.049$ for the contribution of the chlorine atom to the index (assuming no change of density). This gives a predicted $n = 1.547$ for the chlorine-free synthetic crystals.

The amount of synthetic material obtained was microscopic, but the above facts confirm its identification as zunyite. The syntheses were carried out in a closed bomb with water in excess, heated to 470°C for 8 to 10 hours. The remarkable fact is that in no subsequent phase studies of the system SiO_2-Al_2O_3-H_2O has zunyite been synthesized. In the recent study by Roy, Rustum, and Osborn (1954), a wide range of conditions was explored, with controlled pressures of H_2O up to 25,000 p.s.i. The phases stable in the temperature range 420°-575° are reported to be pyrophyllite, hydralsite (hydrous aluminosilicate related to pyrophyllite), mullite, corundum, andalusite, quartz, and water.

The conditions of Schlaepfer and Niggli's synthesis differed in only one tangible way from conditions covered in the more recent study: the presence of fluorine. Schlaepfer and Niggli used silicic acid which they prepared themselves from SiF_4, and they state that the product contained a little HF. There is strong suggestion that the presence of fluorine is required for formation of zunyite.

Chlorine does not seem essential to the zunyite structure, to judge from the chlorine-free synthetic crystals. Nel (1930) reports that the chlorine is expelled from natural zunyite on heating. It is difficult to see how chlorine moves through the structure, but perhaps under the influence of large thermal motions it is able to squeeze past the Si_5O_{16} group. But in any case, chlorine appears to be necessary for the stable mineral as formed in nature.

In the syntheses of Schlaepfer and Niggli, the addition of 10 mol percent. K_2O (the lowest non-zero K_2O composition reported) inhibited the formation of zunyite in every case, and resulted in phases such as kalinepheline, orthoclase, and phyrophyllite.

3. Conclusion. -- From the various lines of evidence presented, the geologic role of zunyite becomes distinct: it is formed at moderate pressures and temperatures, under hydrothermal conditions, from rocks containing roughly equal proportions of alumina and silica (e.g. aluminous shales), in the presence of solutions containing fluorine and chlorine. Nel's objections to a hydrothermal origin is based only on negative evidence, and seems premature in consideration of the heavy ferruginous alteration of the basal Gamargara breccia and the presence of extensive manganese deposits at the same horizon (psilomelane, braunite, and manganese-bearing mica: see Nel, 1929). The presence of diaspore also indicates hydrothermal conditions at moderately high pressures ($>$ 2000 p.s.i., see Roy, Rustum, and Osborn, 1954). Palsche's evidence for surficial origin of the zunyite from Uaxactum seems insubstantial.

Aside from these diverging interpretations, all evidence points to a well-defined and special geologic meaning for zunyite. If the present structural study has helped to clarify this meaning, it has been in pointing out and offering an explanation for the special role of fluorine in the structure.

APPENDIX I

ANALYSES OF ZUNYITE *

	1	2	3	4	5	6	7	8
Si	4.66	4.62	4.63	4.65	4.62	5.58	4.82	4.85
Al	13.21	13.05	13.17	12.97	13.00	12.39	12.90	12.94
Fe	0.03	0.09	0.03	0.19	0.21	0.07	0.23	0.01
P	0.10	0.11	0.09	0.04	0.04	0.03	0.08	0.09
Ca	---	0.02	---	0.07	0.04	---	---	0.02
Mg	---	---	---	0.12	0.09	---	---	0.01
Na	0.09	0.18	0.12	0.62	0.55	---	0.05	0.05
K	0.02	---	0.04	---	---	---	---	0.02
Cl	0.96	0.86	0.96	1.15	1.58	0.81	0.89	0.83
F	3.44	3.56	3.17	0.31	0.25	0.49	3.29	3.34
OH	14.04	14.37	14.37	14.71	15.05	17.39	13.54	13.18
O	20.28	20.45	20.08	21.54	21.11	20.57		

1. Hillebrand (1885)
2. Penfield (1893)
3. Gossner and Mussgnug (1926)
4. Nel (1930)
5. Nel (1930)
6. Nel (1930)
7. Palache (1932)
8. Astashenko and Moleva (1939)

*Composition given in atoms per structural unit (1/4 of the unit cell). Columns 1 - 6 were calculated by Pauling (1933) from the published analyses.

APPENDIX II

STRUCTURE FACTOR AND INTENSITY TABLES

Unobserved reflections marked with an asterisk (see p. 25)

(h k 0) DATA

h	k		$\|F_o\|$	F_c	ΔF	h	k		$\|F_o\|$	F_c	ΔF
0	2		3.6	-3.6	0.0	4	8		2.5	-2.5	0.0
0	4		2.5	-2.2	0.3	4	10		2.0	-1.8	0.2
0	6		4.5	3.3	1.2	4	12		8.0	8.2	0.2
0	8		6.3	8.5	2.2	4	14		5.0	5.1	0.1
0	10		9.0	9.0	0.0	4	16		0.7	-0.4	0.3
0	12		18.0	18.0	0.0	4	18		5.6	-6.0	0.4
0	14		3.6	-3.1	0.5	4	20		2.8	3.0	0.2
0	16		7.0	6.3	0.7	4	22		1.8	1.7	0.1
0	18		1.2	-0.3	0.9	4	24		2.8	3.2	0.4
0	20		2.2	-2.1	0.1	4	26		3.6	-3.3	0.3
0	22		10.0	10.2	0.2	4	28		1.0	1.0	0.0
0	24		4.0	4.6	0.6	4	30	*	0.7	-0.5	0.2
0	26		2.2	2.7	0.5	4	32		2.8	2.7	0.1
0	28		3.2	3.0	0.2	4	34		2.2	-1.9	0.3
0	30		2.5	-3.4	0.9	4	36		0.9	0.8	0.1
0	32		1.8	-2.0	0.2	4	38	*	0.4	-0.4	0.0
0	34		3.2	4.8	1.6	6	6		35.0	36.3	1.3
0	36		2.8	3.1	0.3	6	8		5.0	-5.9	0.9
0	38	*	0.6	0.7	0.1	6	10		2.2	-1.7	0.5
2	2		2.8	-2.8	0.0	6	12		9.0	-9.3	0.3
2	4		1.0	0.1	0.9	6	14		2.8	2.4	0.4
2	6		3.2	3.5	0.3	6	16		7.0	5.9	1.1
2	8		9.0	9.7	0.7	6	18		7.0	6.8	0.2
2	10		1.8	1.7	0.1	6	20		0.9	1.4	0.5
2	12		5.0	-5.9	0.9	6	22		4.0	3.7	0.3
2	14		5.6	6.6	1.0	6	24		2.0	-2.2	0.2
2	16		1.1	-1.1	0.0	6	26		2.8	-3.0	0.2
2	18		4.5	4.2	0.3	6	28		5.6	5.6	0.0
2	20		1.8	-1.4	0.4	6	30		2.5	2.1	0.4
2	22		1.2	1.0	0.2	6	32	*	0.8	0.5	0.3
2	24		3.2	-3.3	0.1	6	34		1.2	-1.8	0.1
2	26		2.0	2.0	0.0	6	36		1.2	-1.3	0.1
2	28		1.0	-0.6	0.4	8	8		22.0	22.2	0.2
2	30		2.5	2.7	0.2	8	10		4.5	4.1	0.4
2	32		1.1	-1.0	0.1	8	12		0.9	-0.6	0.3
2	34		0.9	0.5	0.4	8	14		8.0	6.8	1.2
2	36	*	0.6	-0.3	0.3	8	16		3.2	2.9	0.3
2	38		0.6	0.5	0.1	8	18		0.8	-0.3	0.5
4	4		11.0	10.4	0.6	8	20		5.0	5.3	0.3
4	6		0.8	-0.2	0.6	8	22		3.2	-3.3	0.1

8	24		3.6	3.1	0.5	14	34 *	0.5	0.2	0.3
8	26		1.6	1.6	0.0	14	36 *	0.4	1.5	1.1
8	28		2.0	2.0	0.0	16	16	5.0	5.1	0.1
8	30	*	0.8	0.2	0.6	16	18	1.8	1.6	0.2
8	32		1.8	1.3	0.5	16	20	1.8	1.6	0.2
8	34		1.0	-0.5	0.5	16	22 *	0.7	-0.1	0.6
8	36		4.5	4.5	0.0	16	24 *	0.9	0.3	0.6
10	10		4.0	4.2	0.2	16	26	1.8	-0.7	0.1
10	12		3.6	-3.5	0.1	16	28	5.0	4.2	0.8
10	14		2.2	1.8	0.4	16	30	1.6	-1.5	0.1
10	16		1.4	-1.1	0.3	16	32 *	0.6	0.7	0.1
10	18		4.5	4.5	0.0	16	34	1.2	-1.2	0.0
10	20		2.2	-1.8	0.4	18	18	5.0	5.2	0.2
10	22		1.8	1.5	0.3	18	20	1.0	-0.9	0.1
10	24		1.8	-1.6	0.2	18	22	1.4	-1.4	0.0
10	26		3.2	3.4	0.2	18	24 *	0.9	-0.4	0.5
10	28		1.4	-1.2	0.2	18	26 *	0.8	0.3	0.5
10	30		0.9	0.5	0.4	18	28	2.8	2.2	0.6
10	32		1.6	-1.6	0.0	18	30	1.0	-1.1	0.1
10	34		1.2	1.3	0.1	18	32 *	0.5	-0.2	0.3
10	36	*	0.5	-0.0	0.5	18	34 *	0.4	0.0	0.4
12	12		9.0	9.8	0.8	20	20	2.2	2.4	0.2
12	14		2.0	1.7	0.3	20	22	1.2	-1.5	0.3
12	16		2.5	-1.9	0.6	20	24 *	0.8	-0.3	0.5
12	18		5.0	-4.7	0.3	20	26	0.9	-1.2	0.3
12	20	*	0.6	-0.7	0.1	20	28	1.6	1.8	0.2
12	22		5.6	5.4	0.2	20	30	0.6	1.0	0.4
12	24		2.0	2.1	0.1	20	32	1.4	1.4	0.0
12	26		1.1	-0.8	0.3	22	22	7.0	9.1	2.1
12	28		1.2	-1.6	0.4	22	24	0.9	0.7	0.2
12	30	*	0.8	-0.4	0.4	22	26 *	0.7	-0.0	0.7
12	32	*	0.7	-0.7	0.0	22	28 *	0.6	-0.1	0.5
12	34	*	0.6	0.7	0.1	22	30	1.4	0.9	0.5
12	36	*	0.4	0.4	0.0	24	24 *	0.9	-0.1	0.8
14	14		14.0	14.3	0.3	24	26 *	0.6	-0.1	0.5
14	16		2.5	-2.7	0.2	24	28 *	0.5	-0.1	0.4
14	18		1.4	-1.3	0.1	24	30 *	0.4	0.6	0.2
14	20		3.2	2.7	0.5	26	26	2.0	2.2	0.2
14	22		4.0	4.0	0.0	26	28	1.2	-1.4	0.2
14	24	*	0.7	0.2	0.5					
14	26		1.4	1.3	0.1					
14	28		0.9	-1.2	0.3					
14	30		4.5	4.6	0.1					
14	32		1.0	0.6	0.4					

(h h l) DATA

h	l		I_o	I_c	ΔI	h	l		I_o	I_c	ΔI
0	2		17.1	16.0	1.1	2	18		7.9	8.5	0.6
0	4		9.4	7.5	1.9	2	20		28.9	32.0	3.1
0	6		31.8	1.1	30.7	2	22		6.6	9.6	3.0
0	8		86.4	88.9	2.5	2	24		1.1	1.9	0.8
0	10		99.8	85.4	14.4	2	26		2.2	6.4	4.2
0	12		441.0	377.9	63.1	2	28		5.6	9.0	3.4
0	14		17.0	10.8	6.2	2	30		1.0	1.6	0.6
0	16		51.7	48.3	3.4	2	32	*	0.8	3.2	2.4
0	18		1.0	0.0	1.0	2	34		2.1	4.2	2.1
0	20		4.0	4.8	0.8	2	36	*	0.5	0.5	0.0
0	22		129.6	123.2	6.4	3	1		73.2	49.5	23.7
0	24		20.5	23.5	3.0	3	3		1726.2	964.7	761.5
0	26		5.5	8.1	2.6	3	5		348.0	164.3	183.7
0	28		14.1	6.7	7.4	3	7		50.0	46.8	3.2
0	30		9.5	11.7	2.2	3	9		393.4	292.9	100.5
0	32		3.4	5.5	2.1	3	11		343.0	269.6	73.4
0	34		30.2	28.4	1.8	3	13		46.6	56.8	10.2
0	36		10.6	12.5	1.9	3	15		28.2	30.7	2.5
0	38		0.6	0.5	0.1	3	17		52.7	54.4	1.7
1	1		110.4	182.5	72.1	3	19		8.7	10.9	2.2
1	3		147.7	207.1	59.4	3	21		7.9	13.5	5.6
1	5		386.3	230.6	155.7	3	23		8.9	17.6	8.7
1	7		21.3	11.6	9.7	3	25		6.1	12.0	5.9
1	9		112.8	93.6	19.2	3	27		2.8	6.9	4.1
1	11		112.9	112.2	0.7	3	29		9.8	14.0	4.2
1	13		15.6	13.7	1.9	3	31		11.2	17.0	5.8
1	15		23.8	36.5	12.7	3	33		8.3	12.9	4.6
1	17		1.8	3.3	1.5	3	35	*	0.6	1.4	0.8
1	19		15.0	15.3	0.3	3	37		4.8	10.5	5.7
1	21		27.3	23.2	4.1	4	0		131.9	130.2	1.7
1	23		5.5	8.0	2.5	4	2		1.3	0.4	0.9
1	25		6.0	13.8	7.8	4	4		1302.7	820.9	481.8
1	27		1.4	3.8	2.4	4	6		14.1	15.0	0.9
1	29	*	1.0	1.0	0.0	4	8		308.0	282.4	25.6
1	31	*	0.9	1.3	0.4	4	10		26.5	34.1	7.6
1	33		2.1	3.9	1.8	4	12		1.0	2.4	1.4
1	35		2.0	3.4	1.4	4	14		38.0	51.9	13.9
1	37	*	0.4	0.1	0.3	4	16		126.1	112.5	13.6
2	0		11.1	10.0	1.1	4	18		185.6	167.2	18.4
2	2		225.9	318.3	92.4	4	20		9.6	11.2	1.6
2	4		289.0	189.5	99.5	4	22		12.1	21.9	9.8
2	6		55.9	50.0	5.9	4	24	*	0.8	1.6	0.8
2	8		93.5	63.2	30.3	4	26		14.0	22.8	8.8
2	10		93.2	88.4	4.8	4	28		9.9	14.4	4.5
2	12		129.2	118.6	10.6	4	30	*	0.9	1.5	0.6
2	14		155.8	135.4	20.4	4	32		2.6	4.6	2.0
2	16		18.8	24.1	5.3	4	34	*	0.6	0.4	0.2

4	36	1.0	1.6	0.6	7	33	0.9	1.5	0.6
5	1	119.9	74.1	45.8	7	35	5.5	8.3	2.8
5	3	328.6	185.9	142.7	8	0	782.4	592.4	190.0
5	5	67.7	53.1	14.6	8	2	66.6	75.2	8.6
5	7	27.9	20.3	7.6	8	4	22.1	22.4	0.3
5	9	11.8	17.5	5.7	8	6	60.2	57.9	2.3
5	11	39.2	44.4	5.2	8	8	189.1	134.5	54.6
5	13	41.4	58.7	17.3	8	10	6.7	9.0	2.3
5	15	61.2	74.4	13.2	8	12	10.8	14.3	3.5
5	17	79.9	69.7	10.2	8	14	97.0	101.8	4.8
5	19	6.5	7.4	0.9	8	16	62.0	72.4	10.4
5	21	8.3	14.5	6.2	8	18	8.8	17.8	9.0
5	23	23.0	42.8	19.8	8	20	21.8	29.4	7.6
5	25	1.8	3.1	1.3	8	22	5.3	6.7	1.4
5	27	2.8	5.5	2.7	8	24 *	1.2	0.1	1.1
5	29 *	1.0	1.9	0.9	8	26	5.0	10.5	5.5
5	31 *	0.9	1.3	0.4	8	28	16.8	22.3	5.5
5	33	1.0	1.0	0.0	8	30	1.2	2.0	0.8
5	35 *	0.5	0.2	0.3	8	32	1.0	1.1	0.1
5	37	1.3	3.4	2.1	8	34 *	0.5	1.9	1.4
6	0	2244.3	1983.8	260.5	8	36	0.8	2.0	1.2
6	2	190.8	152.4	38.4	9	1 *	0.2	0.1	0.1
6	4	5.2	4.8	0.4	9	3	196.4	155.6	40.8
6	6	295.0	263.7	31.3	9	5	165.6	127.5	38.1
6	8	13.5	14.9	1.4	9	7	0.9	1.6	0.7
6	10	2.0	4.8	2.8	9	9	112.2	90.1	22.1
6	12	183.1	148.3	34.8	9	11	0.6	1.0	0.4
6	14	4.2	7.1	2.9	9	13	39.2	43.6	4.4
6	16	12.4	19.6	7.2	9	15	8.8	16.5	7.7
6	18	14.2	20.1	5.9	9	17	3.9	7.7	3.8
6	20	2.0	4.8	2.8	9	19	4.3	7.0	2.7
6	22	17.9	33.6	15.7	9	21	11.8	21.1	9.3
6	24	7.6	9.1	1.5	9	25	5.6	7.2	1.6
6	26 *	1.0	1.1	0.1	9	37 *	1.0	0.4	0.6
6	28	1.8	6.2	4.4	9	29	3.9	5.6	1.7
6	30	2.5	4.7	2.2	9	31	8.0	12.2	4.2
6	32	2.4	6.8	4.4	9	32	4.5	7.3	2.8
6	34	2.9	4.3	1.4	9	33 *	0.5	0.2	0.3
6	36	2.1	4.0	1.9	9	35 *	0.3	1.7	1.4
7	1	312.5	249.3	63.2	10	0	17.3	17.4	0.1
7	3	9.2	7.0	2.2	10	2	88.0	91.2	3.2
7	5	56.8	56.3	0.5	10	4	258.5	200.2	58.3
7	7	71.0	59.5	11.5	10	6	15.5	14.3	1.2
7	9	80.0	60.0	20.8	10	8	66.9	73.7	6.8
7	11	93.0	80.4	12.6	10	10	3.7	12.0	8.3
7	13	75.2	79.9	4.7	10	12	10.1	19.1	9.0
7	15	8.6	17.6	9.0	10	14	5.0	9.2	4.2
7	17	1.1	1.1	0.0	10	16	14.0	21.2	7.2
7	19	12.5	23.5	11.0	10	18	30.6	31.6	1.0
7	21	55.5	58.6	3.1	10	20	3.7	5.1	1.4
7	23	9.5	14.1	4.6	10	22	4.4	9.2	4.8
7	25	14.0	20.1	6.1	10	24 *	1.0	0.6	0.4
7	27 *	1.0	0.2	0.8	10	26	5.4	7.6	2.2
7	29	1.3	1.9	0.6	10	28	7.8	14.1	6.3
7	31 *	0.8	0.6	0.2	10	30	1.3	0.3	1.0

10	32		2.9	8.9	6.0	14	2		20.1	22.1	2.0
10	34	*	0.4	0.6	0.2	14	4		5.7	12.2	6.5
11	1		31.6	31.7	0.1	14	6		13.4	17.3	3.9
11	3		14.4	18.4	4.0	14	8		44.2	58.7	14.5
11	5		299.5	236.3	63.2	14	10		5.9	7.6	1.7
11	7		20.1	28.8	8.7	14	12		4.4	7.7	3.3
11	9		1.5	3.7	2.2	14	14		46.4	45.9	0.5
11	11		26.6	32.1	5.5	14	16		21.6	32.1	10.5
11	13		3.7	6.0	2.3	14	18		3.5	5.2	1.7
11	15		14.3	25.4	11.1	14	20		17.7	25.8	8.1
11	17		97.7	137.1	39.4	14	22		8.6	10.6	2.0
11	19		4.7	4.8	0.1	14	24		3.1	1.6	1.5
11	21		4.4	6.6	2.2	14	26		4.9	9.5	4.6
11	23		4.5	8.3	3.8	14	28		11.5	12.8	1.3
11	25		2.1	3.9	1.8	14	30		0.7	1.5	0.8
11	27		3.6	5.3	1.7	15	1		7.8	13.9	6.1
11	29		8.7	12.8	4.1	15	3		15.8	23.4	7.6
11	31	*	0.6	1.7	1.1	15	5		9.1	13.7	4.6
11	33		3.0	4.1	1.1	15	7		10.5	15.9	5.4
12	0		126.1	122.5	3.6	15	9	*	0.9	0.4	0.5
12	2		20.2	27.1	6.9	15	11		10.2	16.8	6.6
12	4		41.6	33.2	8.4	15	13		1.9	2.6	0.7
12	6		77.4	69.5	7.9	15	15		3.4	3.4	0.0
12	8		16.4	22.3	5.9	15	17	*	1.0	0.4	0.6
12	10		0.7	1.3	0.6	15	19	*	1.0	1.2	0.2
12	12		9.6	17.9	8.3	15	21		9.6	9.8	0.2
12	14		4.1	8.2	4.1	15	23		5.0	9.3	4.3
12	16	*	0.7	1.3	0.6	15	25	*	0.8	0.7	0.1
12	18		2.1	3.1	1.0	15	27	*	0.6	0.1	0.5
12	20		1.4	0.3	1.1	15	29		1.7	4.7	3.0
12	22		1.4	0.1	1.3	15	31	*	0.3	2.3	2.0
12	24		2.1	2.5	0.4	16	0		30.1	32.6	2.5
12	26		4.5	4.4	0.1	16	2		34.1	49.9	15.8
12	28		3.5	5.0	1.5	16	4		8.6	18.6	9.9
12	30		1.1	0.6	0.5	16	6		7.0	10.1	3.1
12	32	*	0.5	1.3	0.8	16	8		5.8	10.6	4.8
13	1		44.9	34.7	10.2	16	10		3.8	9.7	5.9
13	3		25.7	28.6	2.9	16	12		7.7	13.5	5.8
13	5		105.5	103.5	2.0	16	14		2.2	3.9	1.7
13	7		9.9	21.9	12.0	16	16		2.2	1.8	0.4
13	9		11.7	16.0	4.3	16	18	*	1.0	0.5	0.5
13	11		1.4	1.7	0.3	16	20	*	0.9	1.0	0.1
13	13	*	1.0	0.3	0.7	16	22		1.6	3.2	1.6
13	15		7.1	10.1	3.0	16	24	*	0.8	0.3	0.5
13	17		2.7	4.8	2.1	16	26	*	0.6	0.7	0.1
13	19		4.5	12.9	8.4	16	28		4.2	8.1	3.9
13	21	*	1.0	0.7	0.3	16	30	*	0.3	1.2	0.9
13	23	*	1.0	0.7	0.3	17	1		5.8	12.3	6.5
13	25		2.5	5.5	3.0	17	3		3.7	5.4	1.7
13	27		1.1	2.3	1.2	17	5		5.9	8.5	2.6
13	29		1.8	5.9	4.1	17	7		1.9	4.2	2.3
13	31		4.2	7.6	3.4	17	9		2.1	6.1	4.0
14	0		281.4	225.9	55.5	17	11		1.6	6.1	4.5

17	13		6.3	11.8	5.5	21	1	10.8	11.3	0.5
17	15		3.5	7.0	3.5	21	3 *	1.0	2.1	1.1
17	17		30.7	40.8	10.1	21	5	7.5	10.6	3.1
17	19	*	0.9	1.3	0.4	21	7	2.0	4.2	2.2
17	21		3.0	4.4	1.4	21	9	2.5	1.5	1.0
17	23		10.4	20.2	9.8	21	11	2.4	4.1	1.7
17	25	*	0.6	0.0	0.6	21	13	2.3	0.5	1.8
17	27	*	0.5	1.3	0.8	21	15	2.1	4.1	2.0
17	29		1.3	3.4	0.8	21	17 *	0.7	0.4	0.3
18	0		24.2	31.8	7.6	21	19 *	0.6	1.0	0.4
18	2	*	1.0	2.9	1.9	21	21	3.9	4.2	0.3
18	4		30.8	37.2	6.4	22	0	79.7	96.4	16.7
18	6		1.0	0.3	0.7	22	2 *	0.9	0.6	0.3
18	8		14.0	23.6	9.6	22	4	4.0	5.5	1.5
18	10		3.2	4.0	0.8	22	6 *	0.9	0.4	0.5
18	12		2.8	4.8	2.0	22	8	1.8	6.5	4.7
18	14		4.4	7.3	2.9	22	10 *	0.8	2.3	1.5
18	16		7.5	10.6	3.1	22	12	1.3	4.1	2.8
18	18		22.4	29.5	7.1	22	14	0.9	0.9	0.0
18	20	*	0.8	0.7	0.1	22	16	5.8	9.5	3.7
18	22	*	0.7	1.2	0.5	22	18 *	0.5	1.4	0.9
18	24		1.0	0.3	0.7	22	20 *	0.4	0.4	0.0
18	26		6.9	8.4	1.5	23	1	0.8	2.1	1.3
18	28		1.2	1.8	0.6	23	3	2.2	4.1	1.9
19	1		1.8	4.3	2.5	23	5	0.9	0.5	0.4
19	3		7.1	12.5	5.4	23	7	2.1	2.7	0.6
19	5	*	1.0	1.3	0.3	23	9 *	0.7	0.9	0.2
19	7		10.0	13.7	3.7	23	11	6.5	8.9	2.4
19	9	*	1.0	1.5	0.5	23	13 *	0.6	1.1	0.5
19	11		13.9	24.2	10.3	23	15 *	0.5	1.2	0.7
19	13		1.7	0.8	0.9	23	17	1.8	5.2	3.4
19	15		4.1	5.5	1.4	23	19 *	0.3	0.0	0.3
19	17		1.5	1.0	0.5	24	0	1.1	0.0	1.1
19	19		3.5	7.2	3.7	24	2	6.0	14.2	8.2
19	21	*	0.7	0.2	0.5	24	4	6.6	11.5	4.9
19	23	*	0.5	2.0	1.5	24	6 *	0.6	0.3	0.3
19	25	*	0.4	1.4	1.0	24	8	2.7	3.0	0.3
20	0		4.0	5.4	1.4	24	10	1.9	3.4	1.5
20	2	*	1.0	1.0	0.0	24	12	0.7	2.6	1.9
20	4	*	1.0	3.1	2.1	24	14	1.4	3.6	2.2
20	6		3.5	7.6	4.1	24	16	0.9	3.2	2.3
20	8		5.5	8.7	3.2	25	1 *	0.5	1.3	0.8
20	10		1.9	5.5	3.6	25	3	3.0	7.7	4.7
20	12		4.1	6.5	2.4	25	5	0.9	0.5	0.4
20	14		12.2	21.9	9.7	25	7	2.4	2.8	0.4
20	16		3.6	4.7	1.1	25	9	1.5	3.4	1.9
20	18	*	0.7	0.4	0.3	25	11	5.8	9.0	3.2
20	20		8.6	14.7	6.1	26	0	4.4	6.9	2.5
20	22	*	0.5	0.3	0.2	26	2 *	0.6	0.8	0.2
20	24		1.0	1.3	0.3					

APPENDIX III

ANALYSES*

	1	2	3
SiO_2	24.25	46.5	60.88
TiO_2	---	1.75	0.62
Al_2O_3	56.75	42.2	17.78
Cr_2O_3	---	0.05	
Fe_2O_3	1.3	0.7	1.94
FeO	---	0.2	4.07
MgO	0.4	nil	3.53
MnO	---	tr	
CaO	0.35	tr	2.77
Na_2O	tr	0.35	2.65
K_2O	1.65		3.16
Cl	3.5	---	
F	0.5	---	
P_2O_5	0.25	0.05	0.29
H_2O^+	11.4	8.35	1.91
H_2O^-	0.4	0.1	0.13
C			1.70
Total (less 0 for Cl, F)	99.75	100.25	101.53

1. Zunyite: Nel (1930): small crystals.

2. Gamagara shale (white or pale grayish): Nel (1930).

3. A "common" shale: Pettijohn (1949) Sedimentary Rocks. Harper and Bros. p. 285.

*Weight percent

REFERENCES

Albis, M., (1921) Indici di rifrazione della cancrinite, della zunyite e della organite: Rend. R. Accad. Lincei, Cl. Sci. Fis., Roma (5) 30, 472. (Min. Abstr. II, 22).

Astashenko, K. L., and Moleva, V. A., (1939) Zunyite and Zunyite Rock of Karabas: Compt. Rend. (Doklady) Acad. Sci. U.S.S.R., 22, 327-330. (Min. Abstr. VII, 462).

Bailey, S. W., and Taylor, W. H., (1955) The Structure of a Triclinic Potassium Feldspar: Acta Cryst. 8, 621-632.

Berghnis, J., Jbertha, I., Haanappel, M., Potters, M., Loopstra, B. O., MacGillavry, C. H., and Veendendaal, A. L., (1955) New Calculations of Atomic Scattering Factors: Acta Cryst. 8, 478-483.

Bernal, J. D., and Megaw, H. D., (1935) The Function of Hydrogen in Intermolecular Forces: Proc. Roy. Soc. A 151, 384-420.

Booth, A. D., (1946) The Accuracy of Atomic Coordinates Derived From Fourier Series in X-Ray Structure Analysis: Proc. Roy. Soc. A 188, 77-92.

Booth, A. D., and Britten, K. H. V., (1948) The Accuracy of Atomic Coordinates Derived From Fourier Series in X-Ray Crystallography, V: Proc. Roy. Soc. A 193, 305-310.

Bragg, W. L., (1937) Atomic Structure of Minerals. Ithaca: Cornell University Press.

Brown, R., (1933) Charge Distributions in Fluorine and Neon: Phys. Rev. 44, 214.

Buerger, M. J., (1941) Numerical Structure Factor Tables. G.S.A. Spec. Paper No. 33.

Buerger, M. J., (1942) X-Ray Crystallography. New York: Wiley.

Clark, G. L., (1955) Applied X-Rays (4th ed.). New York: McGraw-Hill.

Cochran, W., (1948) The Fourier Method of Crystal-Structure Analysis: Acta Cryst. 1, 138-142.

Cochran, W., (1951) The Structures of Pyramidines and Purines. V. The Electron Distribution in Adenine Hydrochloride: Acta Cryst. 4, 81-92.

Cochran, W., (1951) Some Properties of the $(F_o - F_c)$ Synthesis: Acta Cryst. 4, 408-411.

Cramer, H., (1937) Random Variables and Probability Distributions. Cambridge: University Press.

Cruickshank, D. W. J., (1949a) The Accuracy of Electron-Density Maps in X-Ray Analysis With Special Reference to Dibenzyl: Acta Cryst. 2, 65-82.

Cruickshank, D. W. J., (1949b) The Accuracy of Atomic Co-Ordinates Derived by Least-Squares or Fourier Methods: Acta Cryst. 2, 154-157.

Cruickshank, D. W. J., (1950) Convergence of Least-Squares and Fourier Refinement Methods: Acta Cryst. 3, 10-13.

Cruickshank, D. W. J., and Rollett, J., (1953) Electron Desnity Errors at Special Positions: Acta Cryst. 6, 705-707.

Dana, E. S. (rev. Ford, W. E.), (1932) A Textbook of Mineralogy. New York: Wiley.

Ewald, P. P., and Hermann, C., (1931) Strukturbericht, 1913-1928: Z. f. Krist., Ergsbd. 1.

Ewing, F. J., (1935) The Crystal Structure of Diaspore: J. Chem. Phys. 3, 203-207.

Ewing, F. J., (1935b) The Crystal Structure of Lepidocrocite: J. Chem. Phys. 3, 420-424.

Fowler, R. H., (1929) Statistical Mechanics. Cambridge: University Press.

Gossner, B., (1927) Röntgenographische Untersuchungen am Zunyite: N. jb. Min., Abt. A, Beil.-Bd. 55A, 319-332. (Strukturber. (1931) 468).

Gossner, B., and Mussgnug, F., (1926) Die chemische Zusammensetzung von Zunyite: Centralbl. f. Min. Abt. A, 149-155.

Groth, P., (1889) Tabellarische Übersicht der Mineralien, 3rd ed., 104.

Hamilton, W. C., (1954) The Crystal Structure of Dimethyl Phosphinoborine Trimer: Thesis (Part I), C.I.T. 19-27.

Hermann, C., Lohrmann, O., and Phillip, H., (1937) Strukturbericht, Bd. II, 1928-1932: Z.f. Krist., Ergsbd. 2.

Hillebrand, W. F., (1885) On Zunyite and Guitermanite, Two New Minerals From Colorado: Proc. Col. Sci. Soc., 1 (for 1883-4), 124-131.

Hughes, E. W., (1941) The Crystal Structure of Melamine: J. Am. Chem. Soc. 63, 1737-1752.

International Business Machines Corp., (1954) Electronic Calculating Punch, Type 604: Manual of Operation (8th rev.): IBM Corp. Form 22-5279-8.

Internationale Tabellen zur Bestimmung von Kristalstrukturen (1935) Bd. II: Berlin: Gebr. Borntraeger.

International Tables for X-Ray Crystallograph (1952): Birmingham: Int. Union of Cryst.

James, R. W., (1950) The Optical Principles of the Diffraction of X-Rays. London: G. Bell and Sons.

Jeffrey, G. A., (1947) The Structure of Polyisopropenes. VI. An Investigation of the Molecular Structure of Dibenzyl by X-Ray Analysis: Proc. Roy. Soc. A 188, 222-236.

Kempthorne, O., (1952) The Design and Analysis of Experiments. New York: Wiley.

Lipson, H., and Cochran, W., (1953) The Determination of Crystal Structures. London: G. Bell and Sons.

Megaw, H. D., (1934) The Crystal Structure of Hydrargillite, $Al(OH)_3$: Z.f. Krist. 87, 185-204.

Megaw, H. D., (1952) The Structure of Afwillite, $Ca_3(SiO_3OH)_2 \cdot 2H_2O$: Acta Cryst. 5, 477-491.

McConnell, J. F., (1955) A Comparison of Optical Methods and Difference Syntheses in the Location of Hydrogen: Acta Cryst. 8, 308-310.

McCrae, J., (1929): quoted in Nel (1930, p. 215).

Nel, L. T., (1929) The Geology of the Postmasburg Manganese Deposits and the Surrounding Country: Geol. Surv. S. Africa Spec. Pub., Pretoria. (Min. Abstr. IV, 232).

Nel, L. T., (1930) A New Occurrence of Zunyite Near Postmasburg, South Africa: Min. Mag. 22, 207-221.

Palache, C., (1932) Zunyite From Guatemala: Am. Min. 17, 304.

Pasternak, R. A., (1954) A Method of Calculating Electron Density and Patterson Density Functions on IBM Machines: Unpublished.

Pauling, Linus, (1928) The Sizes of Ions and Their Influence on the Properties of Salt-Like Compounds: Z. f. Krist. 67, 377-404.

Pauling, Linus, (1933) The Crystal Structure of Zunyite, $(OH)_{18}Al_{13}Si_5O_{20}Cl$: Z. f. Krist. 84, 442-452.

Pauling, Linus, (1939) The Nature of the Chemical Bond. Ithaca: Cornell University Press.

Pauling, Linus, and Wilson, E. B., (1935) Introduction to Quantum Mechanics. New York: McGraw-Hill.

Penfield, S. L., (1893) Zunyite From Red Mountain, Ouray County, Colorado: Am. J. Sci. (3) 45, 397.

Robertson, J. M., (1934) X-Ray Analysis of the Crystal Structure of Dibenzyl: Proc. Roy. Soc. A 146, 473-482.

Roy, R., and Osborn, E. F. (1954) The System Al_2O_3-SiO_2-H_2O: Am. Min. 39, 853-885.

Schlaepfer, M., and Niggli, P., (1914) Neue Beitrage zur hydrothermaler Silikatbildung: Z. anorg. Chim. 87, 56.

Seitz, F., (1940) The Modern Theory of Solids. New York: McGraw-Hill.

Smith, J. V., (1954) Review of Al-O and Si-O bond distances: Acta Cryst. 7, 479-481.

Spencer, L. J. (1930) Note on the Crystallography of Zunyite: Min. Mag. 22, 217-220.

Waser, J., and Schomaker, V., (1953) The Fourier Inversion of Diffraction Data: Rev. Mod. Phys. 25, 671-690.

Wilson, A. J. C., (1949) The Probability Distribution of X-Ray Intensities: Acta Cryst. 2, 318-321.

Wilson, A. J. C., (1950) Largest Likely Values for the Reliability Index: Acta Cryst. 3, 397.